THE PROPAGATION AND GENERATION OF
TOPOGRAPHIC OSCILLATIONS IN THE OCEAN

by

ALFREDO A. SUAREZ

B.S., Boston College
(1965)

M.S., University of Illinois
(1967)

SUBMITTED IN PARTIAL FULFILLMENT OF THE
REQUIREMENTS FOR THE DEGREE OF
DOCTOR OF PHILOSOPHY

at the

MASSACHUSETTS INSTITUTE OF TECHNOLOGY

and the

WOODS HOLE OCEANOGRAPHIC INSTITUTION

July, 1971

Signature of Author _____
Joint Program in Oceanography,
Massachusetts Institute of Tech-
nology - Woods Hole Oceanographic
Institution, Department of Earth
and Planetary Sciences, and Depart-
ment of Meteorology, Massachusetts
Institute of Technology, July, 1971

Certified by_ _____
Thesis Supervisor

Accepted by _____
Chairman, Joint Oceanography Committee
in the Earth Sciences, Massachusetts
Institute of Technology - Woods Hole
Oceanographic Institution

THE PROPAGATION AND GENERATION OF TOPOGRAPHIC OSCILLATIONS IN THE OCEAN

by

Alfredo A. Suarez

Submitted to the Joint Oceanographic Committee in the Earth Sciences, Massachusetts Institute of Technology and Woods Hole Oceanographic Institution, in July, 1971, in partial fulfillment of the requirements for the degree of Doctor of Philosophy.

ABSTRACT

This thesis is an investigation of the way in which low-frequency topographic oscillations propagate and are generated over ocean topography. In this study we emphasize those topographic oscillations which are affected by the density stratification of the ocean. A simple calculation using the model of topographic oscillations over a constant slope is made to interpret the Aries measurements. It is found that the frequency and length scales predicted by the theory are consistent with deduced values from the data. A calculation of the normal modes of oscillation for a simple one-dimensional corrugated bottom is made. This is done in order to illustrate the possibility of interaction between small-scale topography and long-scale forced motions in the ocean. It is found that when the scale of the corrugations is smaller than NH/f , where N is the Brunt-Vaisala frequency, f the coriolis parameter and H the mean depth, the topographic oscillations are trapped to the bottom.

The excitation of topographic oscillation by Rossby waves is explored. It is found that Rossby waves do not efficiently excite bottom-intensified oscillations, but rather excite topographic modes with a velocity node on the topography. For the period range considered (less than 1 year) these modes were trapped to the edge of the slope. It is suggested that for low-frequencies the edge of the shelf behaves remarkably like an elastic membrane yielding under the influence of the impinging Rossby wave but springing back with little energy lost.

The role of the bottom-intensified oscillations
in the adjustment of initially imposed disturbances on
the topography is investigated. It is found that when
the imposed scales of the disturbance are smaller
than NH/f the resulting motions consist of a steady
current and bottom-intensified oscillations. The
implications of this partition of the motion in the
vertical are discussed.

The generation of bottom-intensified waves by wind
is studied and it is found that wind forces cannot
effectively generate these motions. Finally, a study
of the local interaction of topographic oscillations
with a steady shear current is made. It is found
that the general effect of a shear current is to
intensify the oscillations at the bottom. It is also
found that this process leads to the transfer of wave
energy to the current.

Summarizing, it is suggested that perhaps the
most important role of bottom-intensified waves is to
release the ocean interior from the constraints imposed
by topography.

Thesis Supervisor_____Peter B. Rhines_____
Assistant Professor, Department of
Meteorology, Massachusetts Institute
of Technology

To Kathy and Carolyn

5

Acknowledgements

The author wishes to take this opportunity to
thank Professor Peter Rhines for introducing him to
the very interesting subject of low-frequency motions
in the ocean. He gratefully acknowledges Professor
Rhines' guidance and inspiration throughout this work.
He would also especially like to thank Professor Mollo-
Christensen for his support during the author's stay
at M.I.T. Thanks are also expressed to Dr. Schmitz
for very interesting and helpful discussions, and to
Professor Wunch for his advice in the preparation of
the thesis.

Table of Contents

Table of Contents (cont.)

.List of Figures and Tables

List of Figures and Tables (cont.)

List of Figures and Tables (cont.)

List of Figures and Tables (cont.)

Chapter I Introduction

For several years the Woods Hole Oceanographic Institution has kept an ocean station at a site located at $39° 20'N$, $70°W$. This station known as Site D is situated in a region of gently sloping bottom (slope $\approx 10^{-2}$) which extends some 50 km north to the continental shelf and about 150 km south. The low-frequency current meter data collected at this location have been recently analyzed by Thompson (19). The results of this analysis indicate that variable currents with periods from about a week to a month are on the average depth-independent. This fact has been inferred by Rhines (10) from a comparison of the horizontal kinetic energy spectrum at different depths calculated from the data by Thompson. However, recently collected current meter records occasionally have shown variable currents with periods of order a week to two weeks with speeds decreasing away from the bottom (Schmitz 14). These measurements suggest the presence of a dynamical regime at low frequencies where stratification is important.

The observation of this peculiar baroclinic structure in ocean currents is not isolated to Site D. A series of current measurements using Swallow floats made by the research vessel Aries in the Bermuda rise (1959-1960)

showed the presence of variable currents whose speeds
increased with depth below the main thermocline and
whose periods were of several weeks. Furthermore,
simultaneous measurements of the currents and the
density field showed that the currents were geostrophic
(Swallow 17). One of the most remarkable aspects of
the observations was the magnitude of the velocity
fluctuations. Stommel in his book The Gulf Stream
(16) discusses the implications of these observa-
tions from the point of view of the general circulation
of the oceans. The emphasis here is the clue their
baroclinic structure provides regarding their dynamical
origin.

Theoretical models have been proposed to explain
the observed variability of the currents. Rhines (10)
and Thompson (19) point out that the depth-independent
currents present in the Site D records in the period range
from a week to about a month perhaps can be explained
in terms of depth-independent, topographic Rossby
waves. The use of this model implies that these topographic
waves must have sufficiently long horizontal scales over
the gently sloping bottom for stratification not to
destroy the barotropic mode.

The possibility that low-frequency, quasigeostrophic

currents in the ocean might have larger velocities at
the bottom was suggested by Rhines in a recent paper
(8). In this paper he showed how the effects of
a simple topographic slope (constant slope), rotation
and stratification combined to support wave motions
which have the property of being confined to the bottom
slope decaying exponentially away from it. The paper
demonstrated, for example, that for topographic slopes
of order f/N and smaller, where N is the Brunt -
Väisälä frequency and f the coriolis parameter,
the dynamic scales of the wave motion are given by
keeping the ratio $NH/fL \sim O(1)$, where H is the
penetration scale of the boundary induced motion, and

L is the along-the-slope scale. For slopes ϵ
$\leq f/N$ we can think of L as the horizontal
scale of the imposed motion. For an ocean $4\,km$ deep
and for $f/N \sim O(10^{-1})$ a typical average value, if

$L < 40\,km$, the penetration depth will be less
than the ocean depth and the resulting motion will
appear bottom-trapped. The wave frequency for this
case is essentially dominated by the component of the
basic density gradient along the boundary. If $L > 40\,km$
the penetration depth H will be greater than the ocean
depth and the vertical structure of the motion will show

depth-independence. The frequency of the waves is determined by the well-known vortex stretching effect (topographic β-effect). The paper also shows that introducing the planetary β-effect results in the appearance of a complimentary mode which resembles the baroclinic Rossby wave mode. These complimentary waves tend to have a node in the horizontal velocity at the bottom when the slope, stratification and scales are such that the bottom-trapped waves decay exponentially within the interior of the fluid.

In another recent paper Rhines (7.) briefly reviews the various interpretations of the Aries measurements and introduces another possibility based on the results of this previously mentioned work. His main point is to suggest that the combined effects of stratification, rotation and topographic slope are competitive with the planetary β-effect in the Bermuda rise. We will discuss this suggestion in more detail in the next chapter.

Some indirect evidence of time-dependent, bottom-intensified currents can perhaps be found in the published literature. Since the early 1960's oceanographers using Swallow floats have observed the deep currents Stommel predicted would exist in the western boundaries of the

oceans. Some of these measurements have shown time
variability. Unfortunately most of the measurements
were taken for only enough duration to define the mean
direction of the flow, and not long enough to obtain a
time resolution of the motion. For example, the Swallow
and Worthington (18) measurements of deep currents in
the Labrador Sea show the presence at certain locations
of a deep variable current superimposed on a somewhat
steadier deep flow.

To summarize, there is limited but suggestive
evidence that quasigeostrophic motions in the ocean
show to some extent the peculiar baroclinic structure
of the topographic waves described by Rhines. In view
of this evidence, it is important to understand how
topographic waves propagate and are generated in a
stratified ocean. The general problem of quasigeostrophic
motions which takes into account simultaneously the
real topography of the ocean basins, the planetary
β -effect and the different sources for these motions
is of extreme complexity. The best one can do, at the
present time, is to isolate, model and evaluate the
different elements that make up the general problem. In
the forthcoming chapters we will discuss a variety of
problems which model processes where topography might

lead to observable effects. The goal of this study is to allow us to describe the gross properties of quasigeostrophic motions in different oceanic regions in terms of the physical parameters of the area (topographic slopes, horizontal dimensions, depth, stratification, currents, etc.) and their most likely sources.

In more detail, the thesis will proceed as follows. In Chapter II we will derive the equations for inviscid, linear topographic waves in the small slope approximation. We will discuss the normal mode solutions to these equations over a constant slope and over a one-dimensional continuously corrugated bottom. We will apply the solutions for the constant-slope case in a simple calculation based on the Aries measurements. The calculation of the modes over a corrugated bottom are done to illustrate the interaction of a long-scale barotropic wave with small-scale topography. In Chapter III we will study the excitation of topographic waves by Rossby waves impinging on an abrupt change in the topography. In particular we wish to determine the efficiency of the generation of the bottom-intensified mode. We will also discuss the problem of wave trapping over simple topography.

In Chapter IV we will discuss some aspects of the

local generation of topographic oscillations. In section A we will consider the response of the fluid over topography to an initially imposed geostrophic current. In section B we will discuss some aspects of the excitation of topographic oscillations by wind stress over the surface. In section C we will consider the effects of the local interaction of topographic waves with a mean shear. Finally, a general discussion of the results and conclusions is given in Chapter V.

Chapter II   Derivation of the Basic Equations for

Quasigeostrophic Motions over Topography and Their

Elementary Solutions

The basic concept in this study is geostrophic

balance. The main balance in the momentum equations is

between the horizontal pressure gradient and the coriolis

accelerations, while the vertical pressure gradient remains

in hydrostatic equilibrium. This basic state of motion

may not be consistent with the physical requirement of

zero normal velocity over the sloping bottom. Rhines

(8) found that the stratified fluid could adjust

to such a situation by developing a velocity gradient

strongest at the bottom and executing small amplitude,

time-dependent oscillations which, for small slopes

$\epsilon \ll f/N$, were just small departures from geostrophy.

These results should apply to large areas of the ocean

where the average slopes rarely exceed 10^{-2} .

Larger slopes are found only around some islands, in the

continental rise and perhaps in the roughness scale

of the bottom topography. The quasigeostrophic motions over

the slope are the small slope limit of the trapped modes

which exist for arbitrarily large slopes. The larger

slopes, $\epsilon \gtrsim f/N$, produce ageostrophic motions. When

the vertical scale of the fields comes in contact with

the surface of the ocean, these slopes lead to non-separable solutions in the up-slope and vertical coordinates.

In Fig. 2-1 we see a map of the average slopes found in the western North Atlantic. Over horizontal scales where the motion would appear trapped to the bottom

$$L \leq NH/f$$

(H is the mean depth of the particular region), the planetary β -effect has been compared to the topographic effect $\epsilon f/H$. At Side D, for example, $\epsilon f/H$ is about twenty times larger than β , whereas at the site of the Aries measurements, it is about the same order. Except for the regions with slopes smaller than 10^{-3} the planetary β -effect is comparable or smaller than the topographic effect for horizontal scales less than $N/f H_{DEPTH}$. It is easy to see that, except for the regions in the continental rise, the slopes are consistent with the quasigeostrophic limit.

We will now derive the system of equations for small-amplitude, time-dependent motions in the quasigeostrophic parameter range over small slopes. The implicit assumptions in the derivation are: 1. Boussinesq approximation. We assume incompressibility of the fluid motion. The variations of the fluid density are neglected in the inertial terms but are retained in the buoyancy term. The small density variations in the ocean and small

Fig. 2-1. Map of the average slopes found in the western North Atlantic.

Legend:

(hatched)	$5 \cdot 10^{-2} \leqq \varepsilon$
(diagonal)	$10^{-2} \leqq \varepsilon \leqq 4 \cdot 10^{-2}$
(cross-hatch)	$5 \cdot 10^{-3} \leqq \varepsilon \leqq 8 \cdot 10^{-3}$
(fine dots)	$10^{-3} \leqq \varepsilon \leqq 4 \cdot 10^{-3}$
(light dots)	$\varepsilon < 10^{-3}$
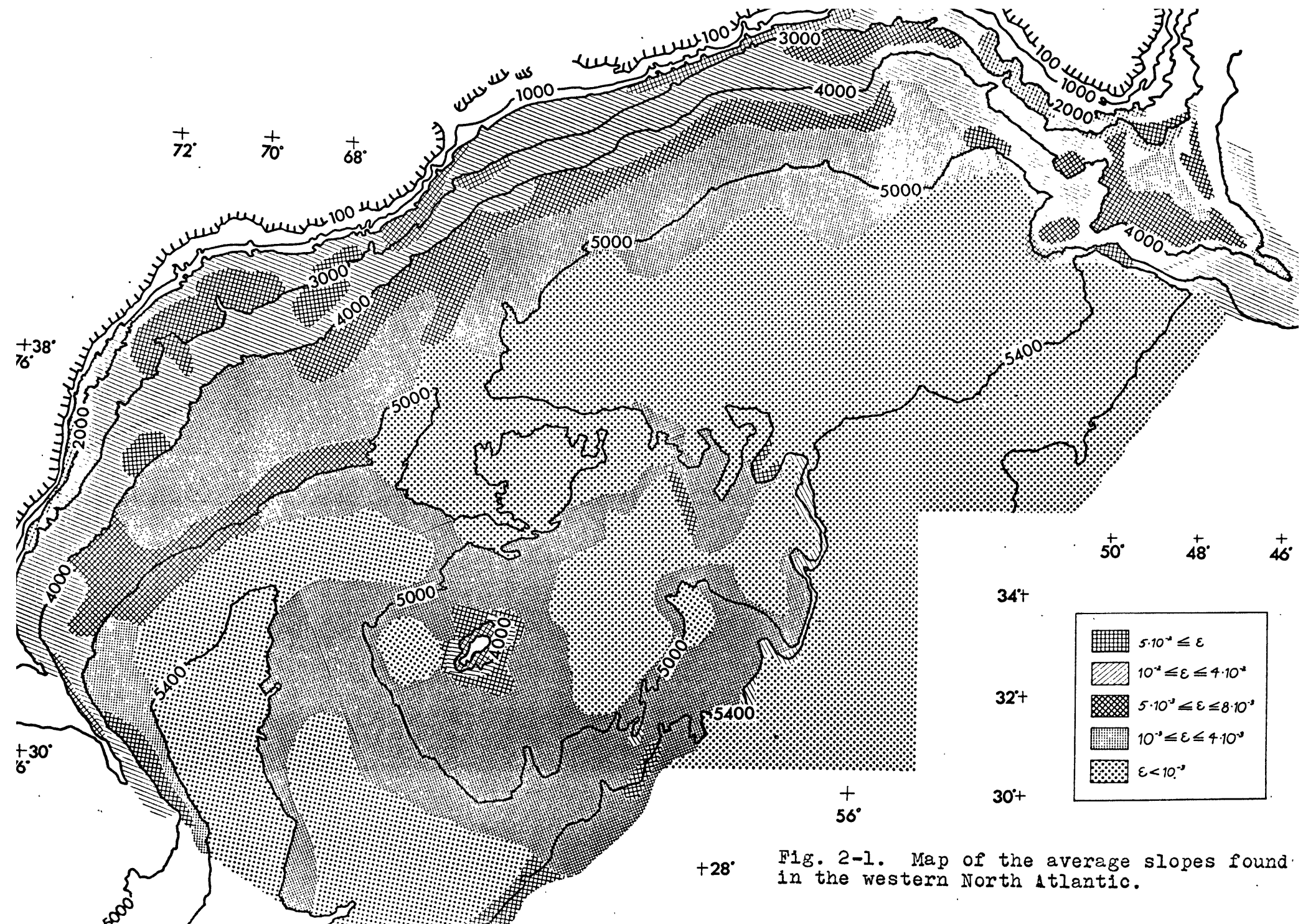
frequencies of the motions justify this approximation.
2. Traditional approximation. We omit the horizontal
components of the rotation vector. The presence of
stratification and large horizontal scales of the motions
make these terms smaller than those retained in the
analysis. 3. β -plane approximation. This approxima-
tion is good for topographic motions because their
horizontal scales are much smaller than f/β ($f/\beta \approx 10^4 km$
at midlatitudes). 4. We restrict our dimensional
time scale (large compared to rotation) to be small
compared to the spin-up. We will comment on this
point after we discuss the solutions. 5. We neglect
free surface displacements. This approximation is valid
except for very long quasigeostrophic waves. The
restriction implied on the wavelength is written as
$f^2 L^2 / g H << 1$. L is the length scale associated
with the wave and H is the depth of the region.

The dimensional, inviscid equations are given by:
x-momentum equation, axis to the east

(II-1)

$$ \frac{\partial}{\partial t^*} u^* + (\vec{u}^* \cdot \nabla) u^* - f^* v^* = -\frac{p_x^*}{\rho_o} $$

y-momentum equation, axis to the north

23

$$\text{(II-2)} \quad \frac{\partial}{\partial t^*} v^* + (\vec{u}^* \cdot \nabla^*) v^* + f^* u^* = - \frac{p_{y^*}^*}{\rho_0}$$

z-momentum equation, z measured upwards from the surface

$$\text{(II-3)} \quad \frac{\partial}{\partial t^*} w^* + (\vec{u}^* \cdot \nabla^*) w^* = - \frac{p_{z^*}^*}{\rho_0} - \frac{\rho^*}{\rho_0} g$$

$$z^* = -H - \alpha f(x^*)$$
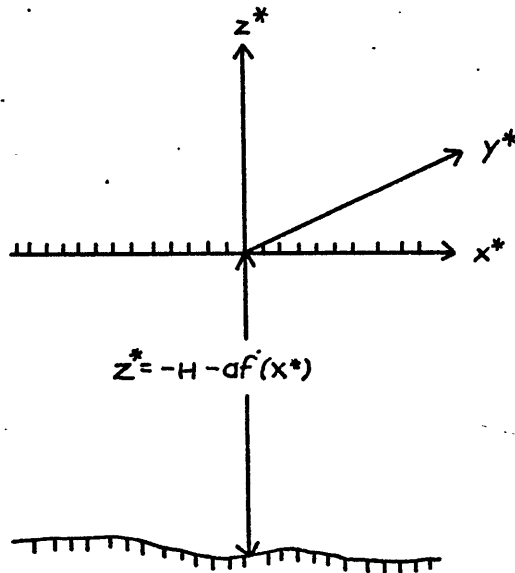
Fig. 2-2. Diagram illustrating the topographic region .

density continuity

(II-4) $\qquad \frac{\partial}{\partial t^*} \rho^* + (\vec{u}^* \cdot \nabla^*) \rho^* = 0$

mass continuity

(II-5) $\qquad \frac{\partial}{\partial x^*} u^* + \frac{\partial}{\partial y^*} v^* + \frac{\partial}{\partial z^*} w^* = 0$

The boundary conditions we use are

(II-6a) $\qquad w^* = 0 \qquad\qquad z^* = 0$

At the bottom we have the condition of no normal flow

leading to

(II-6b) $\qquad w^* = -a \frac{d}{dx^*} f(x^*) u^* \qquad z^* = -H - a f(x^*)$

The constant slope case, $\qquad w^* = -\epsilon u^*$ at $z^* = -H - \epsilon x^*$,

will be treated first because it leads to the simplest

and most transparent results. In section B of this chapter,

we will discuss another model of bottom topography.

We decompose the field variables of the above equations

as follows

24

(II-7) $\qquad p^* = P^*(z^*) + p^*(x^*, y^*, z^*, t^*)$

and

(II-8) $\qquad \rho^* = \rho_o \left(1 + \dfrac{\bar{\rho}(z^*)}{\rho_o} + \dfrac{\rho^*(x^*, y^*, z^*, t^*)}{\rho_o} \right)$

We let

(II-9) $\qquad P_{z^*}^* = -g\left(\rho_o + \bar{\rho}(z^*)\right)$

We scale

(II-10a) $\qquad (u^*, v^*) \rightarrow V_o(u, v)$

(II-10b) $\qquad w^* \longrightarrow W_o\, w \qquad W_o = \lambda V_o$

(II-10c) $\qquad (x^*, y^*) \rightarrow L(x, y)$

(II-10d) $\qquad z^* \rightarrow H z$

(II-10e) $\qquad t^* \rightarrow \delta^{-1} f_0^{-1} T$

(II-10f) $\qquad p^* \rightarrow \rho_0 f_0 L V_0 \, p$

(II-10g) $\qquad \rho^* \longrightarrow \rho_0 \dfrac{f L V_0}{g H} \rho$

and let

(II-10h) $\qquad f^* = f_0 f \quad , \quad f = 1 + \alpha y$

where $\qquad \alpha = \beta/_{f_0} L \qquad - \beta\text{-effect}.$

The scaling for $p^*,\ \rho^*$ implies that our basic state is geostrophic and satisfies the thermal wind balance. Substituting eqs. II-7,8 in eqs. II-1, 6, and using the scales defined above, we find the following non-dimensional set of equations

(II-11a) $\qquad \delta \dfrac{\partial}{\partial T} u + R_0 (\vec{u} \cdot \nabla) u - f v = -p_x$

(II-11b) $$\delta \frac{\partial v}{\partial T} + R_0 (\vec{u}\cdot\nabla) v + f u = -p_y$$

(II-11c) $$\lambda^2 \left(\delta \frac{\partial}{\partial T} w + R_0 (\vec{u}\cdot\nabla) w \right) = -p_z - \rho$$

(II-11d) $$\delta \frac{\partial \rho}{\partial T} + R_0 (\vec{u}\cdot\nabla)\rho - (\Gamma\lambda)^2 w = 0$$

(II-11e) $$\frac{\partial}{\partial x} u + \frac{\partial}{\partial y} v + \frac{\partial}{\partial z} w = 0$$

(II-11f) $$w = 0 \qquad z = 0$$

and on the slope

(II-11g) $$w = -\delta u \qquad z = -1 - \delta x$$

The non-dimensional number appearing on the equations measures the relative importance of each term.

(II-12a) $\qquad \delta \equiv \in L/H \qquad$ is the slope parameter which measures the size of the fractional change of depth over a length scale L.

(II-12b) $\lambda \equiv H/L$ is the aspect ratio.

(II-12c) $\Gamma \equiv N/f$ where $N = \sqrt{-\frac{1}{\rho_o} g \frac{\partial \rho}{\partial z}}$

is the Brunt-Vaisala frequency which we take, for

simplicity, to be a constant. If, for $N(z)$, we use

the lowest value of the distribution of N in a column

of fluid, our results, frequencies, penetration depths,

etc. are a lower bound to any realistic dependence of

$N(z)$ with depth. Finally,

(II-12d) $R_o \equiv V_o/f_o L$ is the Rossby number.

We consider $\delta \ll 1$. The nonlinear terms may be

neglected compared to the local time derivative if

$R_o \ll \delta$. This assumption is not always valid for

bottom-trapped waves because their horizontal scales

are not large. In the case of the Swallow eddies, for

example, $R_o \sim O(\delta)$. We will neglect the effects of

nonlinearities in order to formulate the problem of

topographic motions in the simplest possible manner.

Rhines recently has shown in a numerical study of

two-dimensional, quasigeostrophic turbulence that the

motion behaves remarkable like waves when the topographic

parameter is of order the Rossby number.

Since the topographic parameter is much less than

one ($\delta \ll 1$), we can linearize the bottom boundary

condition by making a Taylor expansion about $z = -1$.

Eq. II-11g becomes

(II-13)

$$w\Big|_{z=-1} - \delta\,dx\,\frac{\partial w}{\partial z}\Big|_{z=-1} + \cdots = -\delta\left(u\Big|_{z=-1} - \delta\,dx\,\frac{\partial u}{\partial z}\Big|_{z=-1} + \cdots\right)$$

We expand all the dependent variables in terms of δ .
This expansion guarantees that the lowest order balance
will be geostrophic and hydrostatic.

(II-14)

$$\begin{Bmatrix} u \\ v \\ w \\ p \\ \rho \end{Bmatrix} = \begin{Bmatrix} u^{(0)} \\ v^{(0)} \\ w^{(0)} \\ p^{(0)} \\ \rho^{(0)} \end{Bmatrix} + \delta \begin{Bmatrix} u^{(1)} \\ v^{(1)} \\ w^{(1)} \\ p^{(1)} \\ \rho^{(1)} \end{Bmatrix} + O(\delta^2) + \cdots$$

To order δ^0 we find

(II-15a)

$$-v^{(0)} = -p_x^{(0)}$$

(II-15b)

$$u^{(0)} = -p_y^{(0)}$$

$$(\text{II-15c}) \qquad 0 = -p_z^{(0)} - \rho^{(0)}$$

$$(\text{II-15d}) \qquad (\Gamma\lambda)^2 \, w^{(0)} = 0$$

$$(\text{II-15e}) \qquad u_x^{(0)} + v_y^{(0)} = 0$$

The δ^0 equations are consistent with the geostrophic and hydrostatic approximation.

To order δ^1 we find

$$(\text{II-16a}) \qquad \frac{\partial}{\partial\tau} u^{(0)} - v^{(1)} - \left(\frac{\alpha}{\delta}\right) y \, v^{(0)} = -p_x^{(1)} \quad , \quad \frac{\alpha}{\delta} \leq 0(1)$$

$$(\text{II-16b}) \qquad \frac{\partial}{\partial\tau} v^{(0)} + u^{(1)} + \left(\frac{\alpha}{\delta}\right) y \, u^{(0)} = -p_y^{(1)}$$

$$(\text{II-16c}) \qquad 0 = -p_z^{(1)} - \rho^{(1)}$$

$$(\text{II-16d}) \qquad \frac{\partial}{\partial\tau} \rho^{(0)} - (\Gamma\lambda)^2 \, w^{(1)} = 0$$

(II-16e) $\quad \dfrac{\partial}{\partial x} u^{(1)} + \dfrac{\partial}{\partial y} v^{(1)} + \dfrac{\partial}{\partial z} w^{(1)} = 0$

To the first two orders, the boundary condition at the top is

(II-16f)
$$w^{(1)} = 0$$

at $\quad z = 0$

Using the linearized bottom boundary condition eq. II-13, we find

(II-16g) $\quad w^{(1)} = - u^{(0)}$

at $\quad z = -1$

The first order equations remove the degeneracy of the fields through the coupling imposed on the velocities at the bottom. From eqs. II-16a, b, we construct a vorticity equation which eliminates the first order fields except for the vertical velocity. This velocity is coupled to the zeroth fields by mass continuity and the vertical hydrostatic equation.

(II-17a) $\quad \dfrac{\partial}{\partial \tau} (v_x^{(0)} - u_y^{(0)}) - w_z^{(1)} + \left(\dfrac{\alpha}{\delta}\right) v^{(0)} = 0$

From eqs. II-15c and II-16d, we find

(II-17b)
$$w^{(1)} = \frac{1}{(\Gamma\lambda)^2} \frac{\partial}{\partial T} \zeta^{(0)} = -\frac{1}{(\Gamma\lambda)^2} \frac{\partial}{\partial T} p_z^{(0)}$$

Using the geostrophic equations to relate $u^{(0)}, v^{(0)}$ in terms of the pressure $p^{(0)}$, we obtain an equation in the lowest order pressure field

(II-18)
$$\frac{\partial}{\partial T}\left(\nabla_1^2 p^{(0)} + \frac{1}{(\Gamma\lambda)^2} p_{zz}^{(0)} \right) + \left(\frac{\alpha}{\delta}\right) p_x^{(0)} = 0$$

This equation is usually called the linearized potential vorticity equation. It may be derived directly from Ertel's theorem. The term $\frac{\alpha}{\delta} p_x^{(0)}$ denotes the meridional divergence due to the planetary β-effect. The boundary conditions can also be simply expressed in terms of $p^{(0)}$. Eq. II-16f becomes

(II-19a)
$$\frac{1}{(\Gamma\lambda)^2} \frac{\partial}{\partial T} p_z^{(0)} = 0 \qquad \text{at } z = 0$$

and eq. II-16g becomes

(II-19b)
$$\frac{1}{(\Gamma\lambda)^2} \frac{\partial}{\partial T} p_z^{(0)} = -p_y^{(0)} \qquad \text{at } z = -1$$

We emphasize that the relatively simple form of the
lower boundary condition, eq. II-19b, depends strongly
on the geostrophic scaling, which in turn depends on the
smallness of the slope. For topographic waves with time
scales of order of the rotation (slopes of order f/N),
the cross-slope gradient of the field becomes equally
important to the along-the-slope gradients, and has to
be included.

When the β -effect ($\alpha = \beta L/f_0$) is comparable to
the topographic effect δ , $\alpha/\delta \approx O(1)$, the equations
derived above take up a particular geometric orientation.
They represent the case in which the slope is oriented
east-west. If $\alpha = 0$, the x-coordinate refers to the
up-slope direction and the y-coordinate to the along-
the-slope direction. Fig. 2-1 tells us the importance
of the β -effect compared to the topography for bottom-
trapped motions.

It is not difficult to derive the general form of
the boundary condition for an arbitrary orientation of
the slope with respect to north. Let us consider that
the slope is oriented at angle φ with respect to north
(see Fig. 2-3).
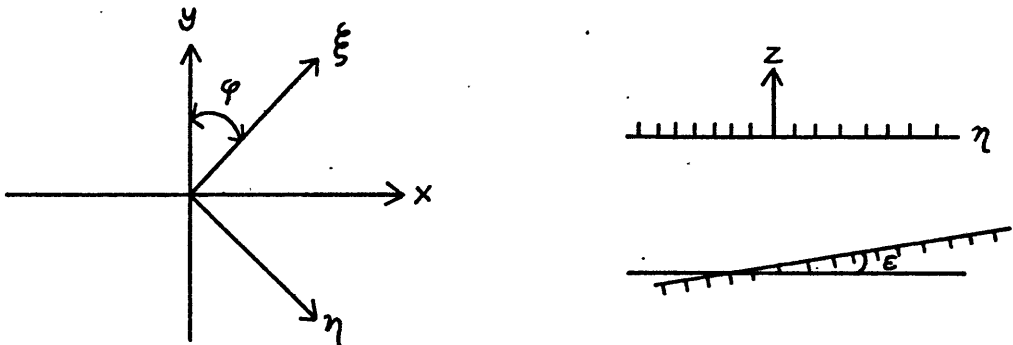
Fig. 2-3. Diagram defining the angles for general form of the boundary condition for an arbitrary orientation of the slope.

The simplest way to formulate the problem is to write the bottom boundary condition in terms of the north-south and east-west coordinates. The potential vorticity equation II-18 and the surface boundary condition II-19a remain unchanged. The bottom boundary condition II-19b becomes

$$(II-20) \qquad \frac{1}{(\Gamma\lambda)^2} \frac{\partial}{\partial T} p_z^{(0)} = \left(\cos\varphi \frac{\partial}{\partial y} + \sin\varphi \frac{\partial}{\partial x} \right) p^{(0)}, \quad z = -1$$

In the next section we will use this equation in a simple calculation.

Section A. 1. Normal Modes

In this section we will briefly review some of the

main results found by Rhines (8). We will also

discuss some aspects of the Aries measurements. Eq. II-18,

the potential vorticity equation for $\alpha = 0$ (no planetary

β -effect), will admit solutions of the form

(II. A-1)
$$p^{(0)} = A \, e^{i \vec{K} \cdot \vec{x} - i \omega T} \cosh \Gamma \lambda K z$$

where
$$K = \sqrt{k^2 + l^2}$$

$\not{p}^{(0)}$ represents the bottom-intensified mode. We note

that the vertical scale is solely determined by the

horizontal wavenumbers. The lower boundary condition

yields the dispersion relation

(II. A-2)
$$\omega = -\frac{l}{K} \frac{\Gamma \lambda}{\tanh \Gamma \lambda K}$$

where l is the along-the-slope wavenumber and $\Gamma \lambda$

is the parameter β which appears in Rhines' work. The

dispersion relation states that the wave propagates with

phase velocity to the left when an observer looks up the

slope. The unscaled form of eq. I. A-2 is

(II. A-2a)
$$\frac{\sigma}{f} = \omega = \frac{\epsilon \Gamma |l|}{K \tanh \Gamma K H}$$

For $\Gamma KH \to 0$ ($H = 4Km$, $\Gamma = 10$ if $L = 1/K >> 40Km$), frequency given by $\omega = \epsilon/H \, |\mathcal{R}|/K^2$ independent of stratification. For $\Gamma K H >> 1$, we have strong trapping and $\omega = \epsilon \Gamma |\mathcal{R}|/K$. This solution represents a buoyancy oscillation with its frequency given by $\epsilon \Gamma$ times the angle made by the wavenumber with respect to the depth contours. The maximum frequency $\omega = \epsilon \Gamma$ corresponds to the case in which the fluid velocities oscillate up and down the slope. In regions (see Fig. 2-1) where the slope effect is appreciably stronger than the

β -effect for distances as large as a few wave scales, we might expect to find these trapped motions.

In Fig. 2-4 we show the constant-frequency curves of the dispersion relation eq. II-2a. The curves are symmetrical about the $\Gamma H |\mathcal{R}|$ axis. For convenience we have only drawn half of the curves. α_1 is the ratio of the buoyancy frequency ($\Gamma \epsilon$) to the frequency of the waves $\omega = \sigma/f$. The lines of constant $\Gamma H K$ (circles) denote the penetration scale of the bottom-intensified mode into the fluid interior. These curves are non-dimensionalized by the depth H . For example, $\Gamma K H = 2$ denotes a penetration scale of one-half the depth of the region.

Consider a line determined by the projection of the
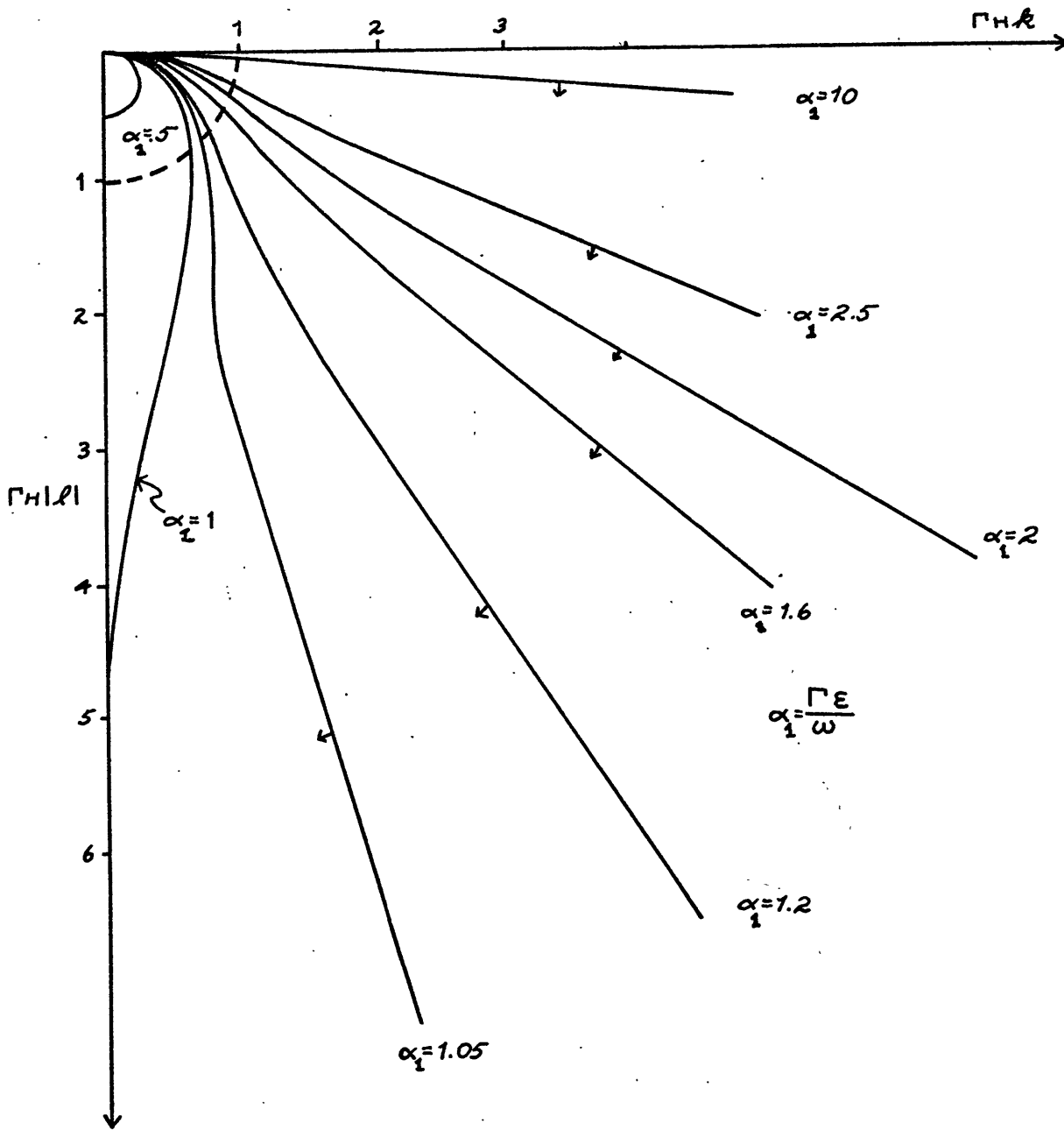
Fig. 2-4. Constant-frequency curves of the dispersion relation for topographic waves.

wavenumber vector along the slope. For large $\Gamma H K$,

this line corresponds to a constant-frequency curve. The

oscillations are not affected by the surface. As

$\Gamma H K$ decreases below a certain value, the frequency

curve no longer coincides with the constant-angle curve.

This separation occurs roughly as the penetration scale

of the wave reaches the surface, $\Gamma H K \sim 1$. For longer

wavelengths the frequency of the wave increases. For

$K < (\Gamma H)^{-1}$, the frequency is dominated by the restor-

ing force associated with the fractional change of depth

over a wavelength ($\in L/H$), rather than by the buoyancy

effect ($\Gamma \in$). The constant-frequency curves resemble

those obtained in the homogeneous limit of topographic

waves.

The group velocity vector is perpendicular to the

constant-frequency curve and points in the direction of

the increasing-frequency curves. In Fig. 2-4 the direction

of the group velocity vector is denoted by arrows.

Fig. 2-4 can be used to simply describe the ray trajectories

of topographic wave packets.

In Fig. 2-5 we show a geographical distribution of

the buoyancy period (the minimum period of the waves)

over the slope regions of Fig. 2-1. The period of the

trapped oscillations could be considerably larger
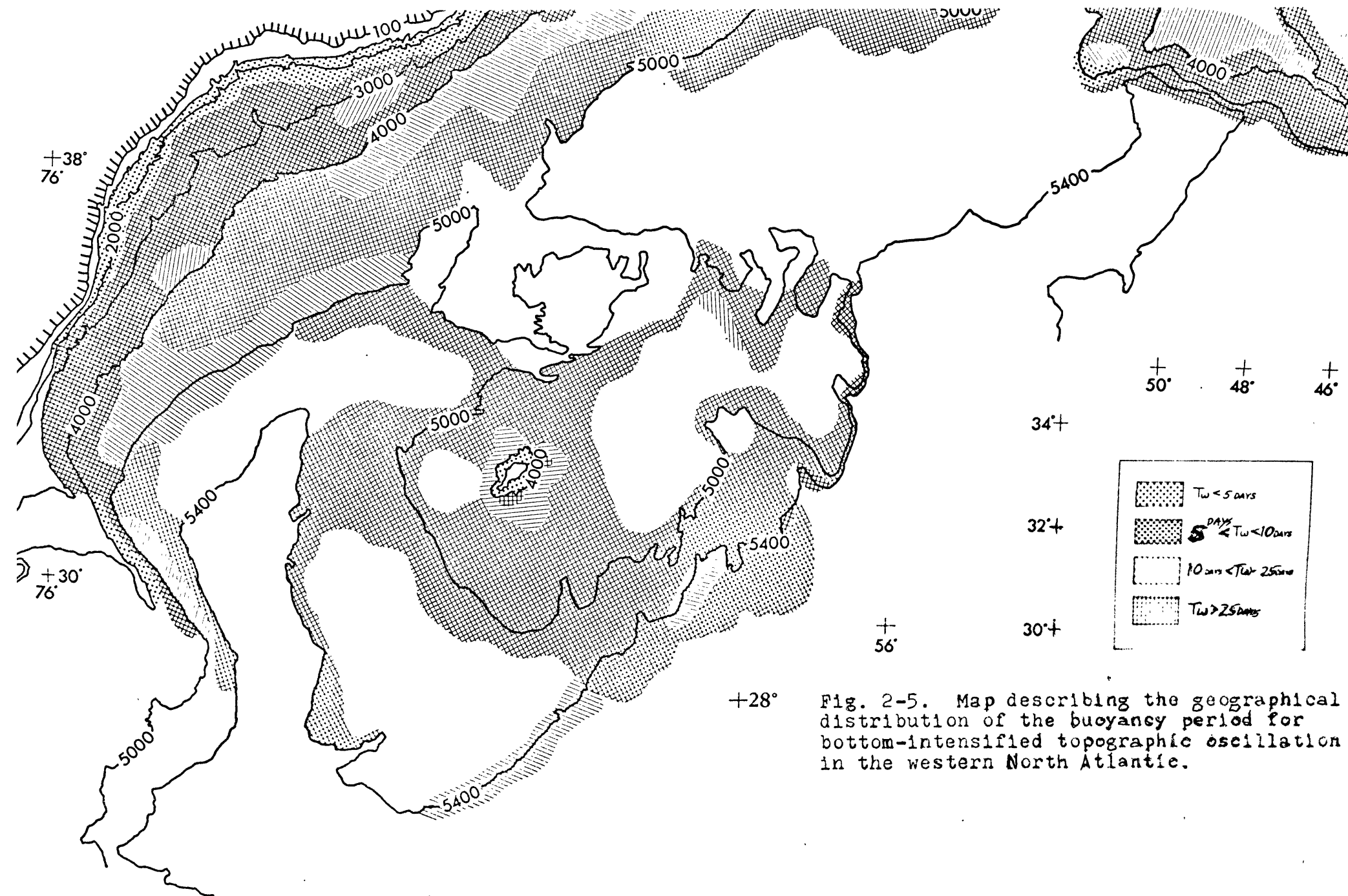
Fig. 2-5. Map describing the geographical
distribution of the buoyancy period for
bottom-intensified topographic oscillation
in the western North Atlantic.

depending on the inclination of the motion with respect
to the depth contours. Fig. 2-5, however, provides a mini-
mum period estimate of the time one should remain in a
particular location to resolve the motion. For this
chart we have used an average value of $N(z)$ for the
column, weighted by the vertical structure of the bottom-
intensified mode $NH/s_L \sim 1$. At Side D where
$\epsilon/\mu \simeq 20 \, \beta/f$, $T_\omega \sim 5-10 \, days$. At the site of the Aries
observations, where $\epsilon/\mu \simeq \beta/f$ $T_\omega \gtrsim 25 \, days$.
The unshaded regions in Fig. 2-5 represent areas where
the topographic map shows the β -effect to be dominant.
The topographic maps, however, do not show the fine
structure of the bottom. In the next section we will
show how this fine structure, with scales of order tens
of kilometers, supports trapped oscillations.

2. Inclusion of the Planetary β -Effect

If $\alpha \neq 0$, eq. II-18 will admit normal mode
solutions of the following form

(II. A-3a) $\qquad \phi_1^{(0)} = e^{i \vec{K} \cdot \vec{x}} \, e^{-i \omega_1 T} \, \cosh m z$

and

(II. A-3b) $\quad p_2^{(o)} = e^{i \overline{K} \cdot \overline{X}} \, e^{-i \omega_2 T} \, \cos r z$

where $p_1^{(o)}$ again represents the bottom-intensified mode, and $p_2^{(o)}$ is the Modified Baroclinic Rossby Wave (MBRW). If the slope is zero $\delta = 0$, $p_1^{(o)}$ reduces to the usual barotropic wave and $p_2^{(o)}$ becomes a baroclinic Rossby wave with roots $r = n\pi$.

Substituting the solutions in eq. II-18, we obtain

(II. A-4a)

$$\omega_1 = -\left(\frac{\alpha}{\delta}\right) \frac{K \sin \theta}{K^2 - \dfrac{m^2}{(r\lambda)^2}}$$

and

(II. A-4b)

$$\omega_2 = -\left(\frac{\alpha}{\delta}\right) \frac{K \sin \theta}{K^2 + r^2/(r\lambda)^2}$$

where θ is measured with respect to north. The orientation of the slope with respect to north is now important, and we use eq. II-20 for the bottom boundary condition to completely determine the modes (Fig. 2-6). These yield

(II. A-5a)
$$m \tanh m = \frac{(\Gamma\lambda)^2 K}{\omega_1} \cos(\theta - \varphi)$$

and

(II. A-5b)
$$r \tan r = -\frac{(\Gamma\lambda)^2 K}{\omega_2} \cos(\theta - \varphi)$$
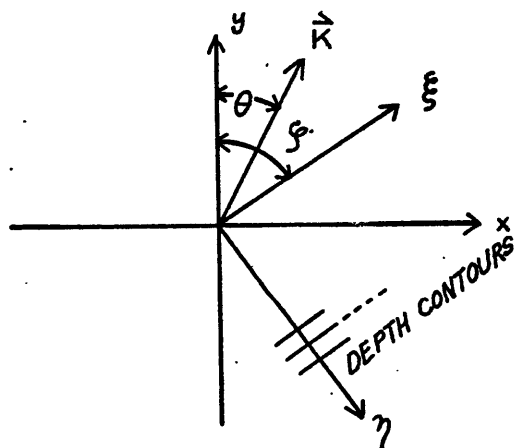
Fig. 2-6. Illustration of the angles appearing in eqs. II. A-5a and II. A-5b.

We solve eqs. II. A-4a, 5a simultaneously, eliminating the frequency to obtain m as a function of K for a given angle. We can do the same for eqs. II. A-4b, 5b. The reader is referred to Rhines (8) for detailed solutions of these equations for the case $\varphi = \pi/2$ (when the slope effect $\in f/\mu$ counteracts β) and $\varphi = 3\pi/2$ (when it reinforces it). We emphasize that the mode structure is quantitatively different for different slope orientations. There are some general qualitative statements one can deduce from eqs. II. A-4a, 4b and II. A-5a, 5b. The bottom-intensified wave solutions exist only for angles $\theta - \varphi$ such that $-\pi/2 < \theta - \varphi < \pi/2$, that is, when the wave's phase velocity is to the left when looking up-slope. If β opposes $\in f/\mu$ and is larger (the least favorable case), then there is a wavelength cut-off above which the bottom-intensified wave cannot exist. The MBRW always have a component of phase velocity to the west regardless of the orientation of the slope. As the slope becomes stronger, the MBRW develop a node in the horizontal topography at the bottom.

It is of interest to apply these results to the Aries measurements. These current observations were done in a region occupying one degree square west of Bermuda

(68°-67° Longitude and 32°-31° Latitude). In Fig. 2-1
we see a large scale view of the topography of the
region. The average slope ϵ is $\simeq 3 \cdot 10^{-3}$,
and is oriented at an angle of about $60°$ east of
north. The average depth is 5 km. so that $\epsilon/H \simeq 6 \, 10^{-4} \, Km^{-1}$.
In this location $\beta/f = 2.7 \, 10^{-4} \, Km^{-1}$. The current
measurements were made for short intervals of time
(1 week - 2 weeks) with Swallow floats at nominal depths
of 2000 m. and 4000 m. for a period of five months
(Crease 2). A dynamic section was performed for
one set of measurements showing that the observed currents
were geostrophic and had a baroclinic structure similar
to the bottom-intensified mode, Swallow (17). The
observed speeds were quite high, of order $10 \, cm/sec$.
Crease estimated from the observations that the apparent
length scales associated with the motion were of order
tens of kilometers ($\simeq 60km$.). The dynamical Rossby
number R_o is of order 10^{-2} -- of the same order as
$\delta = \epsilon L/H$. From the point of view of our topographic
model, nonlinearities should be included. However, to
obtain a rough estimate of the frequency and length
scales implied by the observed vertical structure and
orientation of the velocity vector with respect to the
slope, we will simply use our linear equations. Using

eqs. II. A-3a, 4a in dimensional form, we find for $p = e^{(o)} e^{i(\vec{K} \cdot \vec{x} - \omega T)} \cosh m z$

$$\omega = - \beta/f_0 \frac{K \sin \theta}{K^2 - m^2/\Gamma^2}$$

and

$$m H \tanh m H = \epsilon \frac{\Gamma^2}{\omega} H K \cos(\theta - \varphi)$$

where $H = 5 \, km$ is the mean depth, ϵ the slope and $\Gamma = N/f$. From the observations described by Swallow, we fit $\cosh m z$ to the vertical structure of the current and find that $m H \simeq 1.5$. We use $\Gamma \doteq 12$ which implies $T_N = 2\pi/N \simeq 120 \, MINUTES$. For plane quasigeostrophic waves, the angle α (the direction of the velocity with respect to north) is related to θ (the wavenumber vector angle) by the relation $\tan \alpha = - \frac{1}{\tan \theta}$.
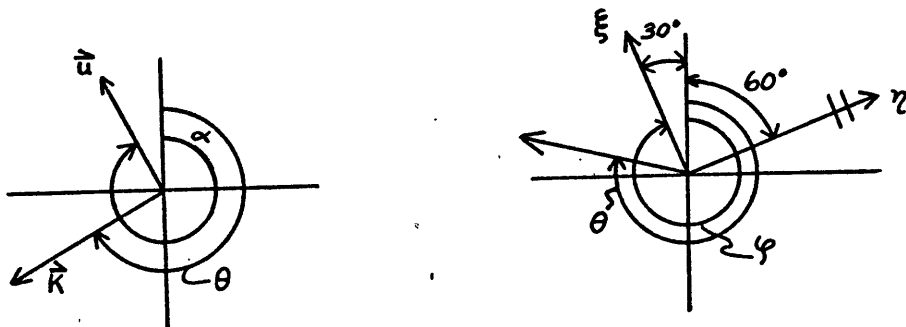
Fig. 2-7. Illustration of angles used to calculate Table 1.

From α, mH and the parameters which define the region, we can compute the frequency and wavenumber (Table 2-1).

	$T\omega$	$(K)^{-1}$
$\alpha = 360°$	40 days	37 km
$\alpha = 340°$	90 days	30 km
$\alpha = 60°$	26 days	40 km

Table 2-1. Periods and wavenumbers calculated from the Aries data.

In the data, the most typical value for α is $360°$ (meridional direction). $\alpha = 60°$ is a hypothetical case for the minimum period, i.e. the velocities point in an up-slope, down-slope direction. The value of the periods and wave scales in Table 1 for $\alpha = 360°$, $\alpha = 340°$ are within the observational estimates. We must be

cautious about these results because the nonlinearities
seem to be important. The wave steepness, for example,

$$\frac{V_o k}{\omega} = \frac{R_o}{\delta}$$ is of order 1 . The phase velocity

for $\alpha = 360°$ to the west is about $6.7 \ cm/sec$. It is of

the same order as the estimate of the mean flow over the

14-month observation period. Fig. 2-8 shows a rough

sketch of the wave for the case $\alpha = 360°$.
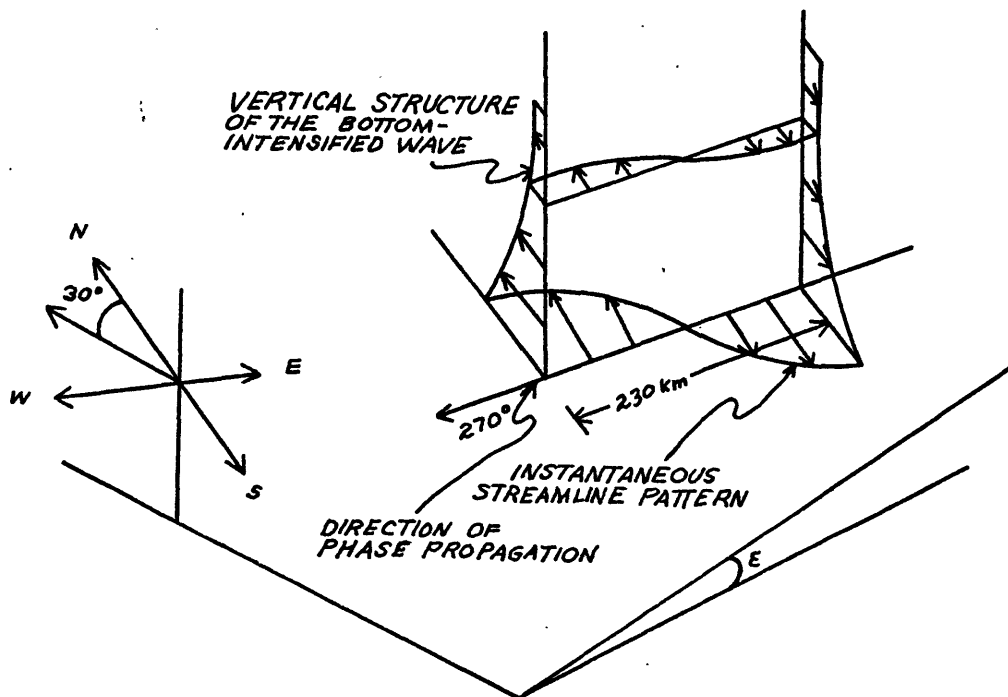
Fig. 2-8. Sketch of bottom-intensified wave calculated
in Table 2-1.

We note that if we had a vertical array of sensors
at a given location determining the vertical structure
and the frequency of the oscillations, eqs. II. A-3a,
4a would determine the horizontal scales and directionality
of the field. On the other hand, measuring purely baro-
tropic, topographic ($\epsilon s/H$) and/or planetary (β) waves
at a single location does not provide enough information
to determine the field. There are many possible wavenumbers
and directions for a given frequency. However, in the
absence of a continuous source of bottom-intensified
modes at given frequency range, dispersion at low fre-
quencies limits the persistence time of the wave group
around the sensor area to about one period of oscillation.
This duration of the signal would not be long enough to
use spectral techniques. The best one can expect is to
search for events in the records.

3. Viscous Effects

For small bottom slopes the effects of viscous
dissipation on the wave motion can be introduced with the
application of the quasisteady Ekman theory. One finds
that the time-dependence of the topographic oscillations
is given by

$$(\text{II. A-6}) \quad \exp{-i\frac{\ell}{k}\frac{NE}{\tanh\frac{NKH}{f}}t} \cdot \exp{-\frac{(\nu s)^{\frac{1}{2}}}{H}\frac{NKH}{f\tanh\frac{NKH}{f}}t}$$

where ϵ is the bottom slope, ν the eddy viscosity coefficient, κ the horizontal scale of the motion and H the mean depth. For long scale wave motion $\frac{N}{f}\kappa H \ll 1$ the damping becomes independent of stratification and horizontal scales. The spin-down time is given by $H/(\nu f)^{\frac{1}{2}}$. Depending on the assumed values of ν we can get various estimates ranging from a month to a hundred days. For bottom intensification scales of topographic oscillations $\frac{N}{f}\kappa H > 1$ the decay time decreases. It is given by the spin-down time above, but with H replaced by the vertical penetration scale $N\kappa/f$ (Walin 20). The relative importance of the viscous effects with respect to the topographic effect is measured by the ratio

(II. A-7)
$$(\nu f)^{\frac{1}{2}} \kappa/\epsilon$$

This ratio can be rewritten as $\left(\frac{\nu}{f H^2}\right)^{\frac{1}{2}} \frac{\kappa H}{\epsilon}$. The ratio of the Ekman number to the one half to the topographic parameter $\delta = \epsilon/\kappa H$. For $E^{\frac{1}{2}} \doteq 10^{-2}$ corresponding to an Ekman layer one hundredth of the depth H , a sloping bottom $\epsilon \doteq 10^{-2}$ and $\kappa H \sim 1/10$ the ratio $\left(\frac{\nu}{f H^2}\right)^{\frac{1}{2}} \left(\frac{\kappa H}{\epsilon}\right)$ is about one-tenth. This implies that the oscillations will decay in about ten buoyancy periods ($2\pi/N\epsilon$).

However, little is known about the actual dissipating mechanism in the ocean's lower boundary. Perhaps the effects of small-scale irregularities in the ocean floor are more important in the dissipation of the energy of the topographic waves.

Section B. Topographic Modes over a Corrugated Bottom

In the previous section we saw that over a constant sloping bottom, topographic oscillations show bottom-intensification when the horizontal scales of the waves are smaller than $N/_f H_{DEPTH}$. For example, if $N/_f$ $\sim O(10)$, $H_D = 5000\ m \longrightarrow L \leq 50\ km$. This implies that sources of these motions must contain the above scales and come in contact with the slope to excite the bottom-intensified modes. For example, sources at the ocean surface with scales $L < \frac{N}{f} H_{DEPTH}$ will not effectively excite the oscillations because their effects will not penetrate to the bottom topography. If their scales are longer than the penetration scale $L > \frac{N}{f} H_{DEPTH}$, the direct topographic response will be essentially depth-independent.

On the other hand, if the bottom topography possesses its own intrinsic scales, the response of the fluid to a long-scale generating disturbance will contain motions with horizontal scales directly induced by the topography.

If the topographic scales are baroclinic, i.e.

$$\frac{N}{f} \frac{H_{DEPTH}}{L_T} \geqslant 1$$ (where L_T is the characteristic

topographic scale), the structure of the modes over

the topography will show bottom-intensification. In

this way, long-scale barotropic motion can generate

bottom-intensified, topographic oscillation. It is

interesting to note that the baroclinic scales of

bottom-intensified waves are comparable to scales quite

commonly found in the topography of the ocean basins.

For example, Swallow (17) reported bottom undulations

of order 50 m in amplitude, and length scales of

order tens of kilometers superimposed on the relatively

smooth rise to the west of Bermuda. These kinds of

scales are evident in the topographic charts of the

IGY (4).

It is possible to determine quasigeostrophic

topographic modes over a small-amplitude, one-

dimensional corrugated bottom. These modes will be

excited to adjust to a long-scale, directly-forced

barotropic disturbance to the topography. Since the

small-scale topography in the ocean is clearly not one-

dimensional, the value of this calculation lies in

illustrating the mechanism of energy transfer from

long scales to small topographic scales, particularly

those scales which support bottom-intensified motions.
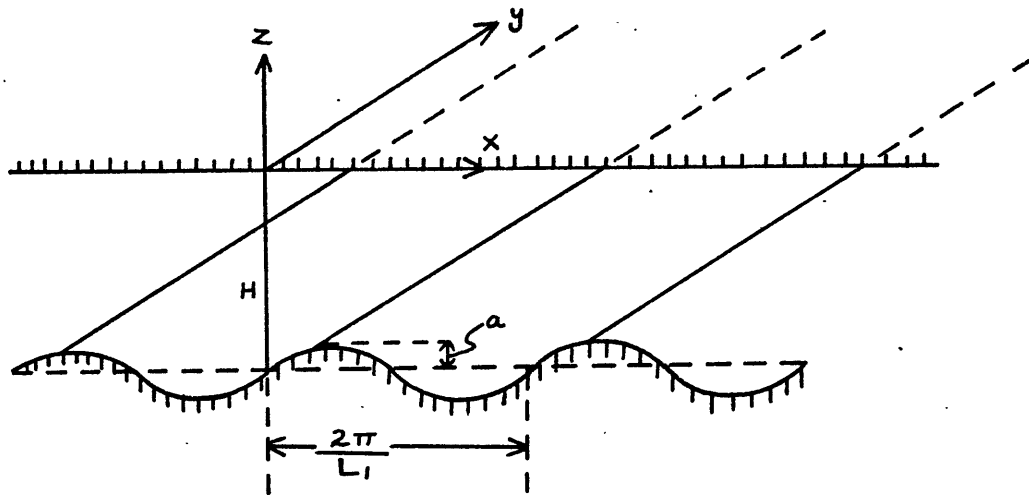
Fig. 2-9. Diagram illustrating the one-dimensional bottom corrugations.

Consider the bottom corrugations to be given by

(II. B-1)

$$Z = -H - a \sin x/L_1$$

where a is the amplitude of the topographic undulation, L_1 is the topographic scale and H is the mean depth. We take $a/H \ll 1$, the amplitude of the undulations is very small compared to the mean depth. This assumption is realistic for small-scale topographic roughness.

In order to obtain the equations that will describe

the topographic motions, we use eqs. II-1 to II-5, with the Rossby number R_o set equal to zero. We also set the β -effect equal to zero. At the end of this section we will comment on the restrictions imposed on the solution by the assumption $R_o = o$.

In the scaling of the equations we formally make a distinction between the along-the-slope scale L and the scale of the corrugation L_1 . We will later take the limit of the ratio L_1/L to be smaller than one. We scale the velocities by the condition of maximum divergence in the continuity equation. The vertical velocities will actually be smaller when we expand the fields in terms of the topographic height a/H . The scales are:

(II. B-2a) $\qquad x \rightarrow L_1 x$

(II. B-2b) $\qquad y \rightarrow L y$

(II. B-2c) $\qquad z \rightarrow H z$

(II. B-2d) $\qquad \dfrac{\partial}{\partial t} \rightarrow -i f \omega$

ω is the frequency

(II. B-2e) $\qquad u \rightarrow \dfrac{L_1}{L} V_o u$

$\overset{\cdot}{u}$ is the velocity in the direction of corrugations,

and where V_0 is the magnitude of the velocity in the

y-direction

(II. B2-f) $\qquad v \rightarrow V_0\, v$

v : the along-the-slope velocity

(II. B-2g) $\qquad w \rightarrow H/_L\, V_0$

w : the vertical velocity

(II. B-2h) $\qquad \Delta p \rightarrow f_0\, L_1\, V_0\, f_0\, ,$

the pressure scale

(II. B-2i) $\qquad \Delta \rho \rightarrow \dfrac{f_0\, L_1\, V_0\, f_0}{g H}$

perturbation density scale.

We define the following symbols

(II. B-3a) $\qquad \dfrac{L_1}{L} \equiv \gamma$

the ratio of the topographic scale to the along-the-slope

scale

(II. B-3b) $\qquad \dfrac{a}{H} \equiv \epsilon$

the topographic height, $\epsilon \ll 1$.

(II. B-3c) $\qquad \dfrac{H}{L_1} \equiv \lambda_1$

the aspect ratio of the topographic scale to the depth.

Substituting the above scales in the eqs. II-1 to II-5,

we obtain a set of non-dimensional scaled equations

(II. B-4a)

$$-i\omega \gamma u - v = -p_x \qquad \text{x-momentum}$$

(II. B-4b)

$$-i\omega v + \gamma u = -\gamma p_y \qquad \text{y-momentum}$$

(II. B-4c)

$$-i\omega \lambda_1^2 \gamma w = -p_z - \rho \qquad \text{z-momentum}$$

(II. B-4d)

$$-i\omega \rho - (\Gamma \lambda_1)^2 \gamma w = 0 \qquad \text{density continuity}$$

(II. B-4e)

$$u_x + v_y + w_z = 0 \qquad \text{continuity.}$$

$(\Gamma \lambda_1)$ in eq. II. B-4d is equal to $\dfrac{N H}{f L_1}$ which we

take to be order $O(1)$. At the bottom boundary we

have

(II. B-5a) $w = -\epsilon \cos x \, u$ on $z = -1 - \epsilon \sin x$

and at the rigid top boundary we have

(II. B-5b) $w = 0$ $z = 0$

Since the topographic height ϵ is much less

than one, we can linearize the bottom boundary condition

by making a Taylor expansion about $z = -1$. Eq. II. B-5a

becomes

(II. B-6) $\left. w \right|_{z=-1} - \epsilon \cos \varkappa \, dx \left. w_z \right|_{z=-1} + \cdots = -\epsilon \cos \varkappa \left(\left. u \right|_{z=-1} + \epsilon \cos \varkappa \, dx \left. u_z \right|_{z=-1} + \cdots \right)$

Since we are interested in quasigeostrophic oscillations

induced by small-amplitude bottom corrugations, we

expand the fields and the frequency in powers of ϵ .

The implicit assumption is that $\epsilon \ll \gamma$.

(II. B-7)
$$\left\{ \begin{array}{c} \vec{u} \\ p \\ \varsigma \end{array} \right\} = \left\{ \begin{array}{c} \vec{u}^{(0)} \\ p^{(0)} \\ \rho^{(0)} \end{array} \right\} + \epsilon^0 \left\{ \begin{array}{c} \vec{u}^{(1)} \\ p^{(1)} \\ \rho^{(1)} \end{array} \right\} + \cdots$$

and the frequency

(II. B-8) $\quad \omega = \epsilon \omega^{(1)} + \cdots$

The details of the expansion of the equations are similar

to the calculations of page   . We will not reproduce

them here. We will simply write the resulting equation

for the lowest-order (in ϵ) quasigeostrophic pressure

field $p^{(0)}$. The interior equation is

(II. B-9)
$$p^{(0)}_{xx} + \gamma^2 p^{(0)}_{yy} + \frac{1}{(r\lambda_1)^2} p^{(0)}_{zz} = 0$$

and the boundary condition

(II. B-10a) $\qquad p_z^{(0)} = 0$

at the top $z = 0$, and

(II. B-10b) $\qquad p_z^{(0)} = (r\lambda_1)^2 \dfrac{\gamma \cos x}{i \omega^{(1)}} p_y^{(0)}$

at the bottom $z = -1$.

γ is the parameter L_1/L which measures the ratio of the topographic scale to the along-the-slope scale.

1. Normal Mode Solutions

We expect that the solutions to the above equations will contain the scales of the topography. We expand $p^{(0)}$ in terms of elementary exponential functions.

(II. B-11) $\qquad p^{(0)} = e^{i\ell y} \displaystyle\sum_{n=-\infty}^{\infty} f_n(z) e^{inx}$

where ℓ is an order one wavenumber along-the-slope. Substituting eq. II. B-11 in the interior equation we find that the vertical structure of the solution is of the bottom-intensified form.

(II. B-12) $\qquad f_n(z) = A_n \cosh r\lambda_1 \sqrt{n^2 + \gamma^2 \ell^2} \; z$

The above solution automatically satisfies the boundary conditions at the top. For the above expansion to work, we need a few terms to be larger in magnitude than ϵ , which is the first order term in the first expansion of the pressure field. At this point we expect that we

(II. B-13d)

$$e^{i2x}: \quad A_2 q_2 \sinh r\lambda_1 q_2 = -\frac{(r\lambda_1)\ell\gamma}{2\omega^{(1)}}\left[A_1 \cosh r\lambda_1 q_1 + A_3 \cosh r\lambda_1 q_3\right]$$

and so on. q_n is defined as $\sqrt{n^2 + \gamma^2 \ell^2}$ for $n = 0, \pm 1, \pm 2$. The above set of conditions mixes the scales of the different topographic modes. We note that the matching conditions are symmetrical with respect to the indices.

So far no assumptions have been made about $\gamma = L_1/L$ other than its being larger than $\epsilon = a/H$. If $\gamma > 1$, the topographic scale larger than the along-the-slope scale, the series solution does not converge. If $\gamma \simeq 1$, the series converges very slowly, like $1/n$. The most interesting case is $\gamma \ll 1$. This limit can be used to model the interaction of a long-scale forced wave with small-scale topography.

For $\gamma \ll 1$ and $r\lambda_1 \sim O(1)$ we can make some simplifications in the relations II. B-13. Let

$$\sinh r\lambda_1 q_0 = \sinh r\lambda_1 \gamma \ell \simeq r\lambda_1 \gamma \ell$$

and $\cosh r\lambda \gamma \ell \simeq 1$. Also we replace q_0 by $\gamma \ell$ and q_n by n . Substituting in II. B-13 we solve for the coefficients A_1/A_0 and A_{-1}/A_0 as continued fractions. From the first relation in II. B-13, we obtain another relation for A_1/A_0 and A_{-1}/A_0 . Eliminating

the coefficients we obtain the following equation for
the frequency

(II. B-14) $(\omega^{(1)})^2 = \dfrac{\Gamma\lambda_1}{2} \dfrac{1}{\tanh\Gamma\lambda_1} \dfrac{1}{1 - (\Gamma\lambda_1)^2 (\gamma\ell)^2 \dfrac{1}{4(\omega^{(1)})^2} \dfrac{1}{2\tanh\Gamma\lambda_1 \tanh\Gamma\lambda_2} + \cdots}$

where γ is the small parameter L_1/L . We iterate
(II. B-15)

$$(\omega^{(1)})_0 = \pm\left(\dfrac{\Gamma\lambda_1}{2}\dfrac{1}{\tanh\Gamma\lambda_1}\right)^{1/2}$$

and

$$(\omega^{(1)})_1 = \pm\left(\dfrac{\Gamma\lambda_1}{2}\dfrac{1}{\tanh\Gamma\lambda_1}\right)^{\frac{1}{2}}\left(1 + \dfrac{1}{4}\dfrac{\gamma^2\ell^2 \Gamma\lambda_1}{2\tanh\Gamma\lambda_1} + \cdots\right)$$

We see that the first correction is small.

Using the dispersion relation we can calculate
the coefficients A_1/A_0, A_{-1}/A_0 to the first two orders
in γ . We find

(II. B-16)

$$\dfrac{A_1}{A_0} = \dfrac{A_{-1}}{A_0} = \mp\dfrac{1}{\sqrt{2}}\left(\dfrac{\Gamma\lambda_1}{\tanh\Gamma\lambda_1}\right)^{\frac{1}{2}}\dfrac{\gamma\ell}{\cosh\Gamma\lambda_1}\left(1 + \dfrac{1}{8}\dfrac{\gamma^2\ell^2 \Gamma\lambda_1}{\tanh2\Gamma\lambda_1} + \cdots\right)$$

where $(-)$ is associated with $\omega^{(1)} > 0$ and $(+)$ term with
$\omega^{(1)} < 0$. We note that the first term is of order γ .
In order to show that the magnitude of the terms in the
expansion decreases in orders of γ we calculate the
next term

(II. B-17) $\quad \dfrac{A_2}{A_o} = \dfrac{A_{-2}}{A_o} = \dfrac{1}{4} \dfrac{\gamma^2 \ell^2 \, \Gamma\lambda_1}{\tanh 2\Gamma\lambda_1} \dfrac{1}{\cosh 2\Gamma\lambda_1} \left(1 + O(\gamma^2\ell^2)\right)$ [61]

We combine these results into the original expression
II. B-11 for the expansion of $p^{(0)}$ (the pressure
field). We find

(II. B-18)

$$p^{(0)} = A_o \, e^{i\ell y} \Big\{ \dfrac{\cosh \Gamma\lambda_1 \gamma\ell z}{\cosh \Gamma\lambda_1 \gamma\ell} \cos \epsilon \Omega t - \sqrt{2}\,i \left(\dfrac{\Gamma\lambda_1}{\tanh \Gamma\lambda_1}\right)^{1/2} \gamma\ell \left(1 + O(\gamma^2\ell^2)\right)$$

$$\times \dfrac{\cosh \Gamma\lambda_1 z}{\cosh \Gamma\lambda_1} \cos x \, \sin \epsilon \Omega t \quad + \quad \dfrac{\gamma^2 \ell^2}{2} \dfrac{\Gamma\lambda_1}{\tanh 2\Gamma\lambda_1} \dfrac{\cosh 2\Gamma\lambda_1 z}{\cosh 2\Gamma\lambda_1}$$

$$\times \cos 2x \cos \epsilon \Omega t \quad + \quad O(\gamma^3) \Big\}$$

where Ω is the frequency given in eq II. B-15.
Since $p^{(0)}$ is the zeroth order expansion in ϵ we
can only consistently keep terms larger than ϵ .

2. Discussion of Results

In order to discuss the structure of the solution,

it is convenient to replace the non-dimensional para-
meters that appear in eq. II. B-18 by the natural dimen-
sional scales of the problem. Let $\gamma \ell \rightarrow \ell/\mu \ll \ell$ where
ℓ is now the actual along-the-slope wavenumber
and μ the actual topographic wavenumber $\mu \equiv 1/L_1$.
Replacing the symbols in eq. II. B-18 by their definitions,
eqs. II. B-3a to II. B-3c, we obtain

(II. B-19)

$$p^{(o)} = A_0 e^{i\ell y} \left\{ \frac{\cosh \frac{N\ell z}{f}}{\cosh \frac{N\ell H}{f}} \cos \sigma t - \sqrt{2} i \left(\frac{NH\mu}{f \tanh \frac{NH\mu}{f}} \right)^{\frac{1}{2}} \frac{\ell}{\mu} \right.$$

$$\left. \times \frac{\cosh \frac{N\mu z}{f}}{\cosh \frac{N\mu H}{f}} \cos \mu x \, \sin \sigma t \quad + \quad O\left(\frac{\ell}{\mu}\right)^2 + \cdots \right\}$$

where H is the mean depth. The frequency is σ
given by

(II. B-20)
$$\sigma = \frac{af}{\sqrt{2} H} \left(\frac{N\mu H}{f} \frac{1}{\tanh \frac{N\mu H}{f}} \right)^{\frac{1}{2}} \left(1 + O\left(\frac{\ell}{\mu}\right)^2 \right)$$

where $a/\sqrt{2}$ is the R.M.S. topographic amplitude.

The expression for the pressure field is particularly
transparent. The topographic mode consists of an

essentially barotropic term ($\frac{N}{f} \ell H << 1$) and a

series of baroclinic modes with smaller amplitudes. The

most important baroclinic term is the first one. It has

a horizontal structure $\cos \mu x$ directly induced by

the topographic corrugation. It is bottom-intensified

and decays into the interior with a scale $h = \left(N\mu/f \right)^{-1}$.

Its amplitude is roughly given by the ratio of topographic

scale to the along-the-slope scale.

We note that the solution's time-dependence is of

the "standing" type, with the first baroclinic mode

$90°$ out of phase with the barotropic term. The

oscillations are of the standing type because over a

complete topographic wavelength there is no preferred

direction for the propagation of the waves, unlike

the case for the constant slope discussed in section A.

This does not imply that these modes cannot be matched

with traveling disturbances over the topography.

Consider the frequency in eq. II. B-20. When

the scale of the topographic corrugations is larger

than the horizontal scale cut-off for bottom-intensified

motion $L_c = N H/f$ i.e. $L_c \mu \leq .4$,

the frequency becomes independent of stratification and

the corrugation scale. It is simply given by

$$\sigma = \frac{a\,f}{\sqrt{2}\ H}\quad,$$

the R.M.S. topographic height scaled by the mean depth.
This result agrees with the homogeneous limit ($N^2 = 0$)
calculations made by Rhines (11). This result is
understandable by realizing that for depth-independent
topographic oscillations, the frequency is determined by
the fractional change of depth of the topography over
the length scale of the wave, i.e. in this case the

R.m.s. amplitude of the corrugation over the mean
depth.

When $\frac{N}{f}\mu H \geqslant 1$, the frequency increases. The
terms in the equation can be rewritten to bring out the
explicit dependence of the topographic slope.
(II. B-21)

$$\sigma = \frac{a\mu}{\sqrt{2}}\ N \left(\frac{f}{N\mu H}\right)^{1/2} \frac{1}{\left(\tanh \frac{N\mu H}{f}\right)^{1/2}}$$

where $\frac{a\mu}{\sqrt{2}}$ is the R.m.s. topographic slope. The frequency
relation is analogous to the dispersion relation for

bottom-intensified waves over a constant slope with the slope replaced by the actual slope of the corrugations.

The parameter $\left(S/N\mu H\right)^{1/2}$ is the ratio of the penetration scale of the wave to the mean depth H .

If we let $H \to \infty$, the frequency does not go to zero. In this limit the assumption that the along-the-slope scale ℓ^{-1} was larger than $N/S H$ does not remain valid. The first term in eq. II. B-19 becomes bottom-intensified and the frequency relation is given by

$$\sigma = \frac{a\mu}{\sqrt{2}} N \left(\ell/\mu\right)^{1/2}$$

independent of the depth.

The frequency relation from which all the limits discussed above can be obtained is given by

$$\sigma = \frac{a\mu}{\sqrt{2}} N \frac{\ell}{\sqrt{\ell \tanh\frac{N\ell H}{S} \mu \tanh\frac{N\mu H}{S}}}$$

This relation is obtained from eq. II. B-13 by not requiring that the along-the-slope scale be larger than NH/S . We see that the frequency appears to be the geometric mean of two frequencies based on the slope of the corrugations

$$\sigma = \sqrt{\sigma_1 \, \sigma_2}$$

$$\sigma_1 = \frac{a\mu}{\sqrt{2}} N \frac{\ell}{\ell \tanh \frac{NH\ell}{f}} \qquad , \qquad \sigma_2 = \frac{a\mu}{\sqrt{2}} N \frac{\ell}{\mu \tanh \frac{N\mu H}{f}}$$

Each of the frequencies is similar to the dispersion relation for topographic waves over a constant slope (see section A, eq.II. $A-2a$).

Let us take some values to compute the parameters that describe the motion for the case where the along-the-slope scale is larger than NH/f . This limit is the most interesting one. For example, topographic amplitude $a = 100 \, m$; mean depth $H = 5000 m$; along-the-slope wavelength $2\pi L = 2\pi \cdot 250 Km$ and topographic scale $\mu^{-1} = 25 Km$. With these values we compute the period of the oscillations $T = 2\pi/\sigma$ to be 50 days. The amplitude of the bottom-trapped baroclinic wave is 20% of the amplitude of the barotropic wave. The penetration scale of the first mode is 2500m from the bottom. The along-the-slope velocity associated with the bottom-intensified oscillation is of the same order as the barotropic velocity of the long-scale wave. The up-slope velocities of the bottom-intensified mode

are an order of magnitude smaller.

In this simple model the strength of the along-the-slope velocity depends on its position over the corrugated bottom. It is a maximum at the trough and crests of the corrugations. This implies that the particle motions associated with the trapped wave are deflected by the ridges never going over the tops. This condition preserves the wave character of the motion.

It is possible to extend the results of the calculation for the pressure field (eq. II. B-20) to the case where the large-scale barotropic wave contains a long wave scale dependence in the direction of the corrugations. This extension of the solution permits us to match the topographic modes with a disturbance oriented in an arbitrary direction with respect to the topographic corrugations. It works out that to lowest order in the ratio of the long-scale wave to the topographic scale we simply replace ℓ , the along-the-slope wavenumber, by $K = \sqrt{k^2 + \ell^2}$, the total wavenumber of the long wave. The major effect on the solution is the lowering of the frequency of the normal modes by the angle the long-scale wave makes with the direction of the corrugations. Eq. II. B-22 becomes

$$(\text{II. B-23}) \qquad \sigma = \frac{a\mu}{\sqrt{2}} \frac{\ell}{K} N \left(\frac{f}{N\mu H}\right)^{\frac{1}{2}} \frac{1}{\left(\tanh \frac{N\mu H}{S}\right)^{1/2}}$$

This result was expected because increasing the angle that the velocity vector of the long wave makes with the direction of maximum depth change reduces the restoring force on the waves.

3. Corrugations on a Sloping Bottom

In many areas of the ocean the small-scale topography is found superimposed on more gradual variations of depth. In this section we will briefly comment on the competition between the constant-slope and the small-scale topographic corrugations in establishing the spatial and temporal structure of the waves.

Consider a bottom configuration given by $Z = -H - dx - a\sin\mu x$
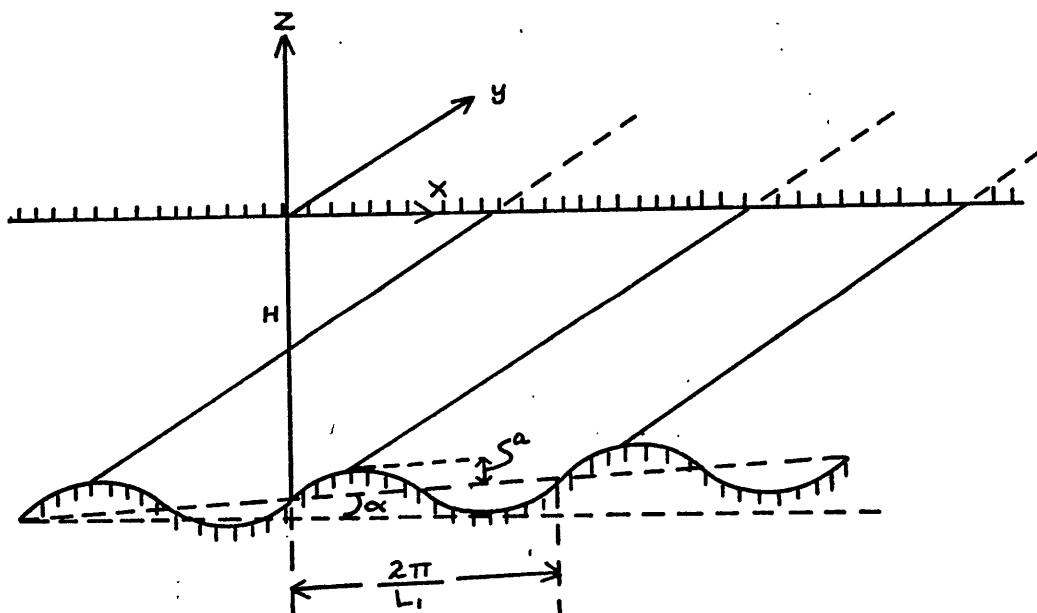
Fig. 2-10. Diagram describing corrugations on a sloping bottom.

where H is the mean depth, α is the constant slope. The term $a \sin \mu x$ represents the topographic corrugations superimposed on the gently sloping bottom. We consider the fractional change of depth over horizontal scales much larger than the scale of the corrugation to be small compared to the mean depth H.

As in the case of no-mean slope ($\alpha = 0$), normal modes can be found when the along-the-slope scale is much larger than the topographic scale μ^{-1}.

There are three distinct cases that can be considered:

1. The net fractional change of depth over a horizontal length of the order the corrugation scale is comparable to the amplitude of the corrugation. In this case the vortex stretching effect of the long wave over the constant sloping bottom dominates the dynamics. To order $\left(\ell/\mu\right)$, where ℓ is the small-scale along-the-slope wavenumber, the modes do not show the scale of the corrugation. The contribution due to the topographic corrugations appears in order $\left(\ell/\mu\right)^2$ which is very small. The solution is simply a barotropic wave propagating to the left when looking up-slope with frequency $\sigma = -\frac{\alpha f}{H} \frac{1}{|\ell|}$.

2. The net fractional change of depth over a horizontal scale of order the large along-the-slope wavelength is comparable to the r.m.s. amplitude of the

corrugation. In this case the effects of the corrugation and the constant slope are comparable. The frequency is given by

$$\sigma = -\frac{\alpha f}{2H|\ell|} \pm \frac{1}{2} \sqrt{\frac{2(a\mu)^2 N^2}{\frac{NH\mu}{f} \tanh \frac{NH\mu}{f}} + \frac{\alpha^2 f^2}{H^2 \ell^2}}$$

where ℓ is the along-the-slope wavenumber, $a\mu$ is the corrugation slope and α is the constant slope. The presence of a mean slope requires that the solution have a phase velocity to the left when an observer looks up the mean slope. Formally as $\alpha \to 0$ we recover our previous solution eq. II. B-22. The mean slope and the corrugations increase the frequency of the standing oscillations. To order (ℓ/μ) the structure of the topographic modes will exhibit the scale of the topographic corrugations.

In the Bermuda rise where the mean slope is of order 10^{-3}, Swallow reported small-scale topographic undulations with amplitudes of order 50m to 100m and horizontal scales of order tens of kilometers. Assuming that the small-scale topography is as simple as the model's, we compute that a forced barotropic wave with horizontal scales of order 100km makes the two effects comparable, i.e. $\frac{a}{H} \simeq 10^{-2}$ and $\frac{\alpha L}{H} \simeq 10^{-2}$.

The reported horizontal scales of the topographic undulations could introduce baroclinicities in the currents with roughly the same horizontal and vertical scales as found in the Aries observations.

3. The constant slope is so small that the net fractional depth change over a horizontal length scale of the order of the along-the-slope scale is much smaller than the amplitude of corrugation. In this limit we essentially obtain the $\alpha \approx 0$ (slope) case to order (ℓ/μ), i.e.

(II. B-20)

$$\sigma = \frac{a\xi}{\sqrt{2}\,H}\left(\frac{N\mu H}{\xi}\,\frac{1}{\tanh\frac{N\mu H}{\xi}}\right)^{\frac{1}{2}}$$

4. Summary

We have seen that a small amplitude, one-dimensional corrugated bottom can support quasigeostrophic, topographic oscillations when the along-the-slope scale is much larger than the corrugation scale. The modes consist of a long-scale, barotropic term and a smaller amplitude term with its horizontal structure given directly by the horizontal scale of the topography. When the topographic scale is smaller than the baroclinic

scale for bottom-intensified waves, $N H_{DEPTH}/\varsigma$ the topographic wave is trapped to the bottom. The vertical corrugation's penetration scale is given by $\varsigma/N\mu$. The frequency of oscillation of the mode is given by the component of N along the r.m.s. topographic slope of the corrugation. If the corrugation scale is larger than $N H_{DEPTH}/\varsigma$, the topographic wave is essentially depth-independent and its frequency is given by the vortex stretching effect associated with the fractional change of depth over the corrugation scale (the r.m.s. amplitude of the topography divided by the mean depth). These topographic modes will be excited to adjust a long-scale, directly-forced barotrophic disturbance to the topography.

A one-dimensional model of topographic roughness has many limitations. The small-scale topography in the ocean is mostly two-dimensional. We expect that if the ridges are as long in length as the depth-independent current's wavelength, the solutions discussed would describe the initial development of baroclinicities due to small-scale topography.

Two-dimensional topography is much harder to treat analytically. Perhaps some features of the problem of one-dimensional topography still remain true.

Numerical computations of depth-independent topographic

oscillations over two-dimensional topography have been

done by Rhines (9). His results indicate that

after a relatively short time the horizontal structure

of the motion resembles that of the small-scale

topography. One can imagine that if the small-scale

topography has baroclinic scales $i.e.$ $L \leq N/_f H_{DEPTH}$,

the resulting motion over two-dimensional topography

will also intensify at the bottom. The other limitation

in our one-dimensional model of small-scale topography

is the neglect of nonlinearities. The largest non-

linear terms in the problem are of order $V_0 \mu/_f$.

For the observed velocities in the Bermuda rise and

for a topographic scale $\mu \sim 1/_{50} Km$, these terms

are of the same order as the local frequency of the

oscillation (scaled by f). Our solutions strictly

apply to smaller amplitude waves. For larger velocities

the solutions describe the initial development of the

currents before the along-the-slope velocities achieve

their maximum value.

Chapter III   Excitation of Topographic Waves by Rossby Waves

In the previous chapter we discussed some of the properties of quasigeostrophic wave motion over local topography. In this chapter we will consider how these motions are coupled with quasigeostrophic motions existing over an adjacent, but different, topographic environment. Rhines (13) has studied this problem for a homogeneous model of the ocean. Here we will be concerned with understanding the coupling between the topographic regions when the effects of stratification are included. In particular, we wish to determine the efficiency of the generation of low-frequency, bottom-intensified, topographic modes by sources located in a different topographic environment. We will discuss this problem in some detail for the simplest possible situation: the matching of Rossby waves with topographic waves.

Consider a one-dimensional, gradually sloping shelf interesecting a constant-depth, featureless ocean (Fig. 3-1). In this simplified geometry, we wish to find the structure of the modes that can be supported over the sloping bottom in response to quasigeostrophic wave motion in the exterior region $X > 0$. The slope is taken to be small in the sense used in the previous chapter, i.e. the change of depth over the length of the shelf is much less
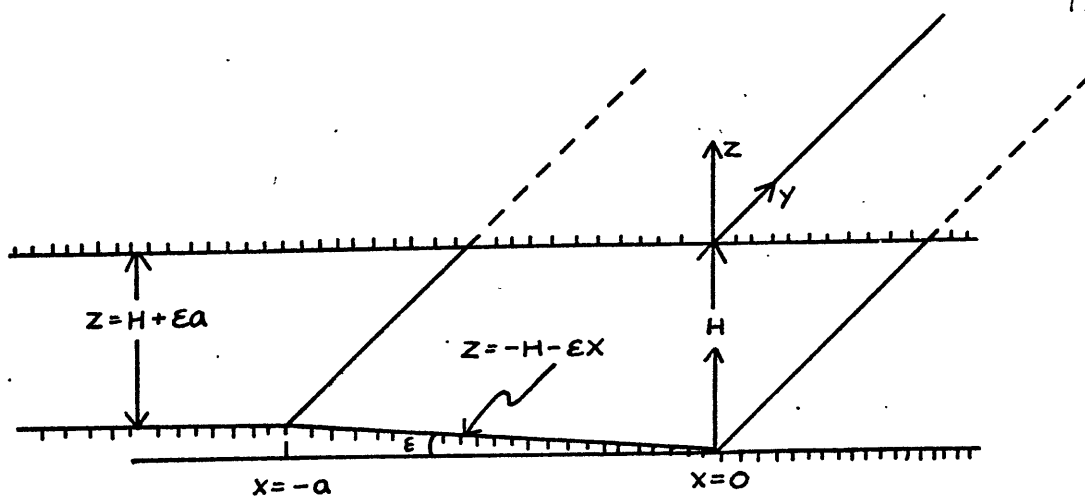
Fig. 3-1. Diagram describing the geometry of a gently sloping shelf.

than one. Under this condition the topographic waves will be quasigeostrophic. To describe the topographic oscillations, we can use the potential vorticity equation II-18 and the boundary conditions at top and bottom, eq. II-19a,b, representing no flow through the boundaries. To be specific, the use of the boundary conditions above, including the planetary β-effect, imply that the shelf in Fig. 3-1 is oriented north-south. The positive y axis points northward, and the positive x axis eastwards.

The matching of the solutions to the above equations
with wave motion in the region $X > 0$ fixes the along-the-
slope wavenumber and frequency of the solutions. Therefore,
we conserve the phase of the wave along the slope dis-
continuity. The resulting vertical structure and the
up-slope wavenumber is determined solely in terms of the
along-the-slope phase velocity and the physical parameters
that describe the region for quasigeostrophic motions
(slope, stratification, coriolis parameter, and the mean
depth of the region of interest). The amplitudes of the
topographic motions will be determined by matching the
quasigeostrophic velocities at the edge of the region.

In order to see this and explicitly calculate the
modes over the topography, let $p^{(0)}$, the lowest-order,
quasigeostrophic, pressure field solution to the potential
vorticity eq. II-18 and boundary conditions II-19a,b be
represented by

(III-1)
$$p^{(0)} = \mathcal{L}(x,z) e^{i(\ell y - \omega t)}$$

In this representation we have extracted the along-the-
slope phase of the waves conserved at the slope discon-
tinuity. Substituting the above form of the solution
into the dimensional form of the vorticity equation II-18,

we obtain

(III-1a) $\quad P_{xx} + \frac{1}{\Gamma^2} P_{zz} + \frac{i\beta}{f_0\omega} P_x - \lambda^2 P = 0$

where β/f_0 of magnitude $\approx 10^{-4} \, Km^{-1}$ is the length scale associated with the variation of f with latitude.

ω is the frequency of the oscillations non-dimensionalized by f . Γ is the ratio of the buoyancy frequency to the inertial frequency N/f . For simplicity we transform the above equation into normal form by extracting the β -effect westward drift. We let P be represented by

(III-2) $\quad P(x,z) = \mathcal{B}(x,z) e^{-\frac{i\beta}{2f_0\omega} x}$

Substituting (III-1a) we obtain

(III-3) $\quad \mathcal{B}_{xx} + \frac{1}{\Gamma^2} \mathcal{B}_{zz} + \left(\frac{\beta^2}{4f_0^2\omega^2} - \lambda^2 \right) \mathcal{B} = 0$

subject to the boundary conditions

(III-4a) $\quad \mathcal{B}_z = 0$ at $z = 0$.

(The vertical velocity is set equal to zero at the top boundary.)

(III-4b) $\quad \mathcal{P}_{\mathbf{z}} = \Gamma^2 \frac{\epsilon}{\omega} \lambda \mathcal{P} \quad$ at $\quad \mathbf{z} = -H$.

(No normal flow into the sloping boundary.)

We again use separation of variables $\mathcal{P}(x, \mathbf{z}) = Q(x) G(\mathbf{z})$ to obtain two more equations. Separation of variables at this point can be done because we have linearized our boundary condition on the sloping bottom. (See page , eq. II-13)

(III-5) $\qquad Q_{xx} + \left(\frac{\beta^2}{4 f_o^2 \omega^2} - \ell^2 - \frac{\gamma}{\Gamma^2} \right) Q = 0$

represents the dependence of the pressure field in the up-slope direction, and

(III-6) $\qquad G_{\mathbf{z}\mathbf{z}} + \gamma G = 0$

represents the dependence of the quasigeostrophic pressure on the vertical coordinate. γ is the separation constant. Substituting $\mathcal{P}(x,\mathbf{z})$ in the boundary conditions III-4a,b, we find that $G(\mathbf{z})$ is subject to the boundary conditions

(III-7a) $\qquad G_{\mathbf{z}} = 0 \quad , \quad \mathbf{z} = 0$

and

$$(III-7b) \qquad G_z = \frac{r^2 \epsilon \ell}{\omega} G \qquad , \quad z = -H$$

1. Vertical Modes

Equations III-6, 7a, and 7b are a statement of a Sturm-Liouville (   ) problem. If $\gamma < 0$, the solution for G is

$$(III-8) \qquad G = \cosh m z$$

where $m^2 = -\gamma$. The boundary condition at $z = -H$ yields

$$(III-9) \qquad m H \tanh m H = - r^2 \epsilon H \ell / \omega$$

There will be a solution only if $\ell < 0$ (we have chosen the frequency $\omega > 0$ by convention). This solution represents the bottom-intensified mode, i.e. stronger motion near the bottom and propagation of the along-the-slope phase veloc-ity to the left when looking up-slope. The transcendental equation III-9 allows the calculation of the vertical structure in terms of the phase velocity along the slope and the physical parameters describing the topographic region. We see that there is only one root (Fig. 3-2).

In the limit of the slope approaching zero ($\epsilon \to 0$) and/or the phase velocity along the slope becoming large ($|\ell| / \omega \to 0$), $\tanh m H \simeq m H \ll 1$ indicating that the vertical scale $h = m^{-1}$ becomes larger than the depth of
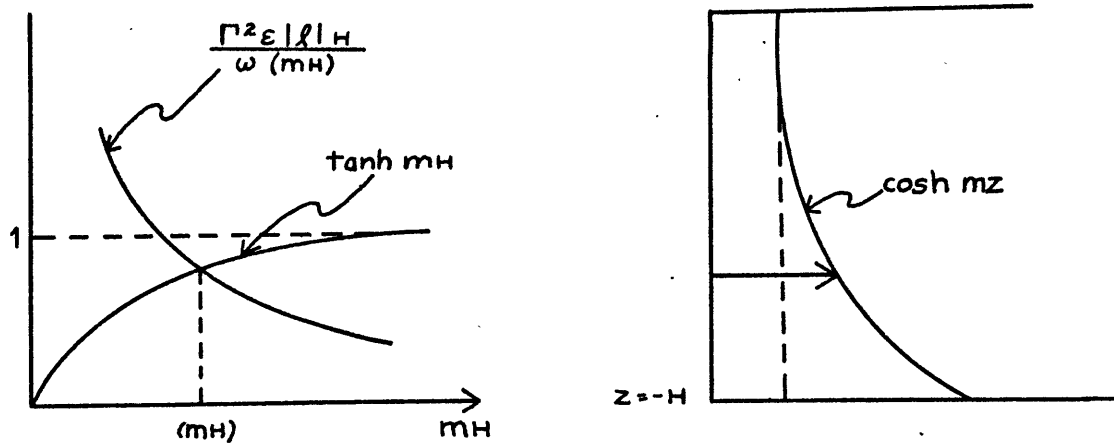
Fig. 3-2. Graphical solution of the transcendental
equation III-9 and a sketch of the vertical structure
of the bottom-intensified mode.

the ocean. The motion becomes essentially barotropic,

$cosh\, mz \to 1$. This is the limit of the depth-independent

topographic waves. In the opposite extreme (for larger

slopes and small along-the-slope phase velocity), the

bottom-intensified mode becomes strongly trapped to the

bottom, decaying exponentially into the interior of the

fluid. In this limit, the penetration scale h is given

by $\omega\, \Gamma^2 \epsilon/|\ell|$ and the vertical structure $cosh\, m z$ reduces

to $exp\, \Gamma^2 \epsilon|\ell|z/\omega$ for $z<0$.

We can use $mH \sim 1$ (the e-folding penetration depth

equal to the depth of the ocean) as the rough dividing

scale between the essentially barotropic motion ($mH<1$)

and bottom-trapped motion ($mH > 1$). With this value

of mH , we can estimate an along-the-slope phase speed

c_s^1 in terms of the physical parameters of the region.

The along-the-slope phase velocity of a disturbance im-

pinging on the edge of a shelf greater than c_s^1 would

excite an essentially barotropic response over the sloping

region, while for smaller values the response would be

bottom-intensified. We set $mH = 1$ in eq. III-9 and

solve for the along-the-slope phase velocity

(III-10) $$c_s^1 = \left(\frac{L}{T_\sigma} \right) = \frac{\epsilon f}{H} (\Gamma H)^2 \frac{1}{1 \tanh 1}$$

For a slope $\epsilon = 10^{-2}$, $N/f = 15$, $f = 10^{-4}$ and $H = 4 km$ we

obtain $c_s^1 \sim 75 km/day$. For smaller slopes

$\epsilon \approx 10^{-3}$ and the same average stratification, c_s^1 is

$7.5 km/day$. The along-the-slope phase velocity

of a barotropic Rossby wave with periods smaller than $30 days$

is larger than $10^3 km/day$. These values are much too

high for the waves at this period range to match with

a strongly trapped mode over the topography. At Site D,

bottom-trapped motion ($mH > 1$) could be excited by

oscillations of the Gulf Stream at the edge of the shelf.

Available records at Sites J and D indeed show Gulf Stream

meanderings with periods of one to two weeks and scales

of approximately 200 km having phase speeds low enough
to excite bottom-intensified motions over the topography.

Returning to eq. III-6, we see that if the separation
constant γ is greater than zero the solution to this
equation is

(III-11) $\qquad G = \cos \gamma z$

where $\qquad \gamma = r^2$

The boundary conditions at $z = -H$ yield

(III-12) $\qquad \gamma H \tan \gamma H = \dfrac{r^2 \epsilon \ell H}{\omega}$

A solution will exist for both $\ell > o$ and $\ell < o$ (both
possible orientations of the along-the-slope phase velocity)
unlike the bottom-intensified mode $\cosh m z$. The $\cos \gamma z$
solutions have the same vertical structure as the Modified
Baroclinic Rossby Waves (MBRW) we found in the previous
chapter, (eq. II-A-3b). We can calculate the roots by
solving the transcendental equation III-12. Fig. 3-3 shows
a schematic graphical solution.
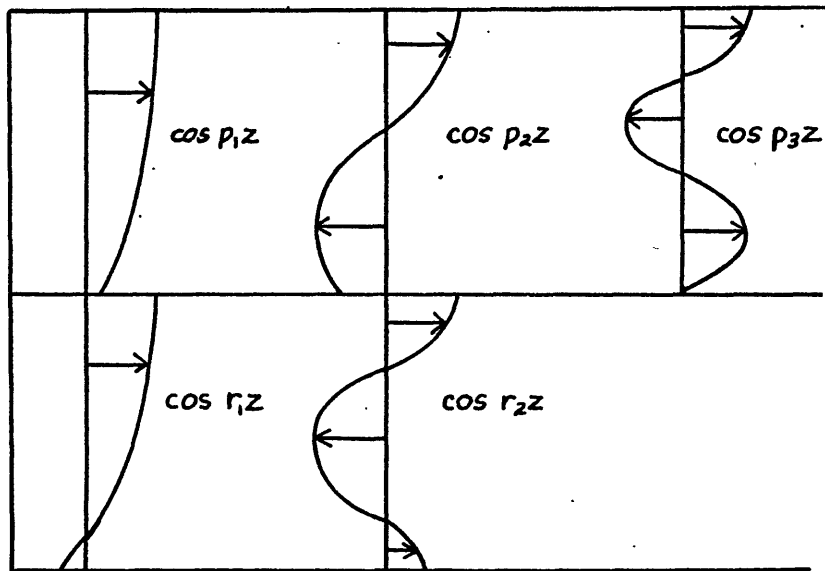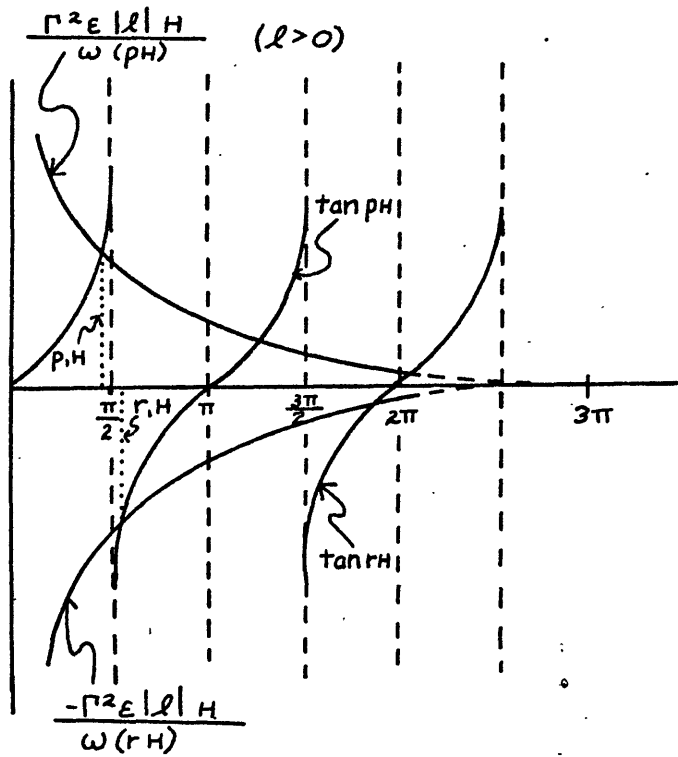
Fig. 3-3. Graphical solution of equation III-12 and a sketch of the vertical structure of the first few MBRW modes.

Again we note that the roots are completely determined
in terms of the along-the-slope phase velocity and the
parameters that describe the topographic region. There
is an infinite sequence of roots to the equation. We
denote the roots for the $\ell < o$ case by γ_j , i.e. $G_j = \cos \gamma_j z$
and for the $\ell > o$ case by p_j , i.e. $G_j = \cos p_j z$
For $\ell < o$, G_j has j nodes in the interval $z = [o, -H]$
(from the surface to the sloping bottom) and $j - 1$ nodes
for $\ell > o$. From Fig. 3-3 we see that as the slope ap-
proaches zero or as the phase velocity $\omega / |\ell|$ becomes very
large along the slope (the barotropic limit for the
bottom-intensified mode), the roots of the $\cos \gamma_j z$ sequence
approach the $j \pi / H$, the usual baroclinic Rossby wave
roots over a constant-depth ocean ($\cos \gamma_j z \to \cos j \pi z / H$).
In this limit, for $\ell < o$, the vertical modal structure
over the topography would consist of a single barotropic
mode and an infinite sequence of baroclinic modes $\cos j \pi z / H$
(just like the set of modes for Rossby waves over a constant-
depth ocean). For $\ell > o$, the $\cos p_j z$ modes have the
same limit. The first root $p_1 H$ approaches zero, and
$\cos p_1 H z / H$ becomes barotropic. All the other roots approach
the usual baroclinic Rossby wave roots $j \pi / H$ as we can
easily see in Fig. 3-3. In the opposite limit, i.e. larger
slope, and/or low phase velocities along the slope (the

strongly trapped limit for the bottom-intensified mode),
the first few roots of the sequences $\{\cos r_j z\}$ and $\{\cos p_j z\}$
approach the half integer values of π/H , i.e. $r_1 \rightarrow \pi/2H$
$p_1 \rightarrow \pi/2H$ and so on. However, if for any given value of
$T' = N/f$, slope, and along-the-slope phase velocity, the
roots of the $\cos p_j z$ and $\cos r_j z$ start with nodes on the
topography as $j \rightarrow \infty$, the roots always approach the
usual baroclinic Rossby wave roots $j \, \pi/H$ (Fig. 3-3).
Thus, there is no sharp difference in kind between the
modes over the topography and the modes over a flat
bottom -- only a difference in degree.

Summarizing then, for $\ell < 0$ (the along-the-slope
phase velocity to the left when looking up-slope), the
topographic slope can support a bottom-intensified mode
and a set of vertically oscillatory modes (MBRW):

(III-13)
$$G = \left\{ \begin{array}{c} \cosh m z \\ \cos r_j z \end{array} \right\} \quad j = 1, 2, \cdots$$

For $\ell > 0$, the only vertical modes possible are

(III-14)
$$G = \left\{ \cos p_j z \right\} \quad j = 1, 2, \cdots$$

Thus we see that the vertical structure of the solution
to the potential vorticity equation over the sloping bottom

exhibits a distinct asymmetry depending on the sense of the phase velocity along the slope.

It might be helpful at this point to sketch the vertical structure of the bottom-intensified mode and the first root of the MBRW, $\cos r_1 z$ and $\cos p_1 z$, for some selected values of the along-the-slope phase velocity (Fig. 3-4). In the Table 3-1 we relate the sketches of the vertical structure of the modes to the actual roots· used to calculate the modes. For a given slope and value of $\Gamma = N/f$, we can associate these·roots with a particular along-the-slope phase velocity by equations III-9, 12. To be specific, we calculated these speeds for a slope $\epsilon = 10^{-2}$ and $\Gamma = 20$. $\Gamma = 20$ implies an average Brunt-Vaisala period of about $72\,min.$. The penetration depth of the bottom-intensified mode in kilometers was calculated on the basis of an average depth of 4 km.

We notice that as the motion associated with the $\cosh mz$ mode concentrates at the bottom, the $\cos r_1 z$ mode develops a node on the topography. Also, we see that the first mode, $\cos p_1 z$ present for the along-the-slope phase velocity to the right when looking up-slope, develops a node on the topography as the phase velocity decreases. In a sense, we see that for low-phase speeds, all of the motion that comes in contact with the topography is taken
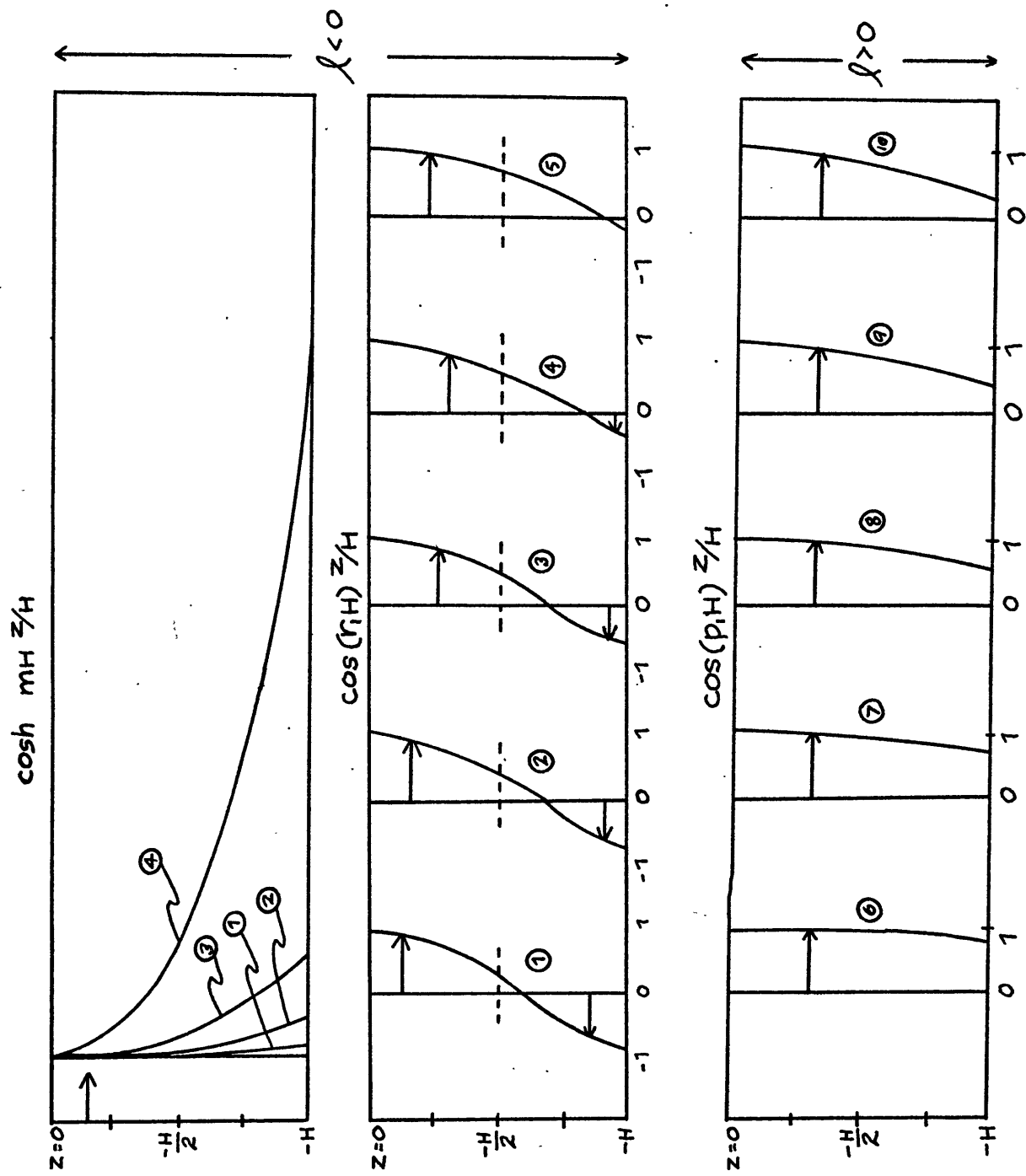
Fig. 3-4. Sketch of the vertical structure of the bottom-intensified mode and the first root of the MBRW, $\cos r_i z$ and $\cos p_i z$ for some selected values of the along-the-slope phase velocity.

	$c_s^{(-)}(\ell<0)$	mH	$m^{-1}, H=4km$	$r \cdot H$		$c_s^{(+)}(\ell>0)$	$(p \cdot H)$
1	300 km/day	.6	6.7 km	2.6	6	300 km/day	.54
2	132 km/day	1.0	4 km	2.36	7	132 km/day	.78
3	70 km/day	1.57	2.55 km	2.17	8	70 km/day	.97
4	32 km/day	3.14	1.27 km	1.94	9	32 km/day	1.20
5	16 km/day	6.28	.63 km	1.79	10	16 km/day	1.35

Table 3-1. Table relating the vertical structure of the modes to their along-the-slope phase velocity.

up by the bottom-intensified mode.

In Fig. 3-5 we show a plot of the resulting vertical scale of the bottom-intensified mode (mH) when its along-the-slope phase speed is determined by the barotropic Rossby wave dispersion relation. These scales would result in matching topographic modes with an incident barotropic Rossby wave at the slope discontinuity (Fig. 3-8).
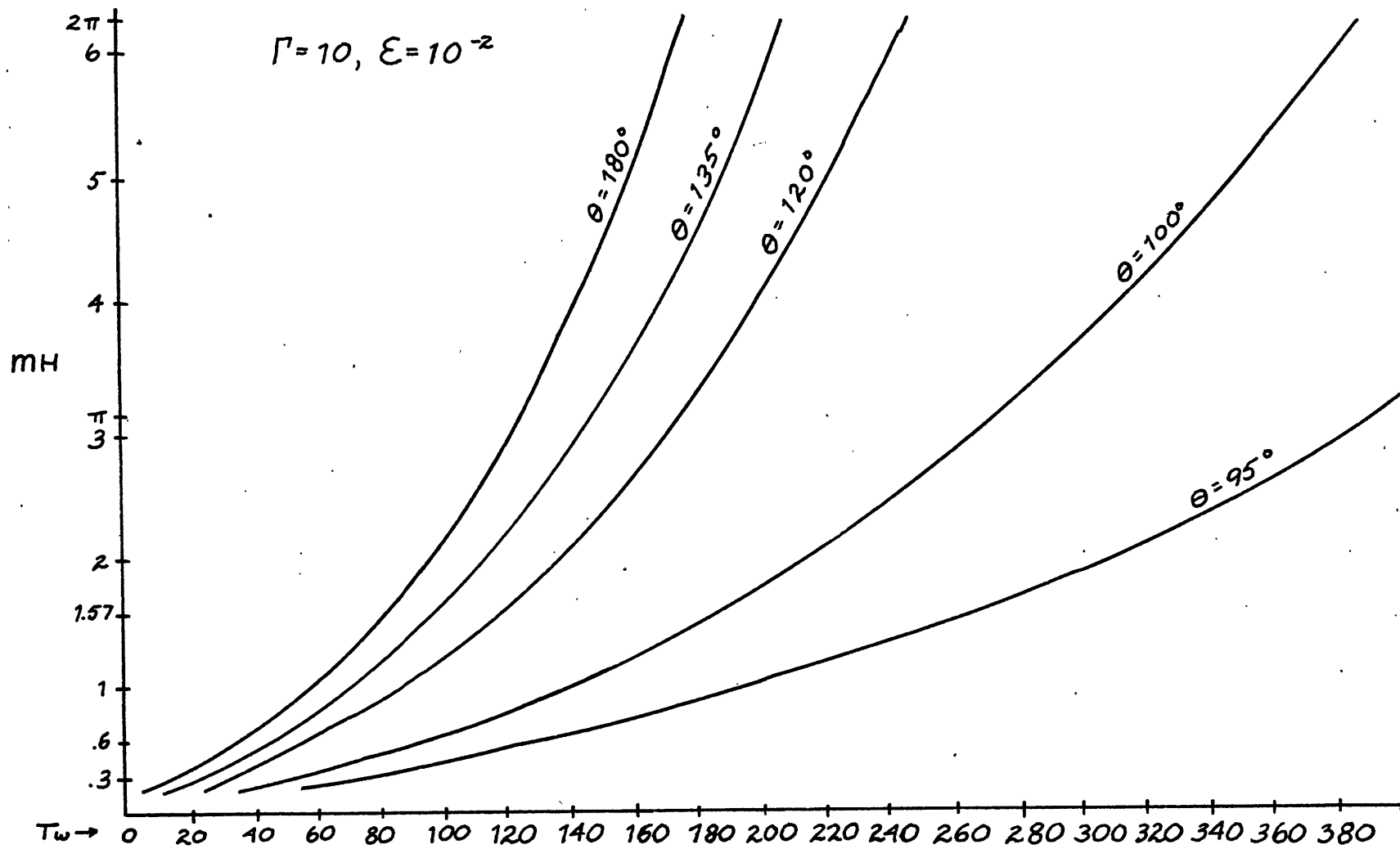
Fig. 3-5. Plot of resulting vertical scale of the bottom-intensified mode when its along-the-slope phase velocity is determined by the barotropic Rossby wave dispersion relation.

The plot of mH is plotted versus the non-dimensional

period of the Rossby wave. To obtain the real period,

we multiply the number by the inertial period in fractions

of days. The numbers denote the period in days at

latitude $30°$. To calculate these curves we used

eq. III-9 with the along-the-slope wavenumber given

by the barotropic dispersion relation . $l = \frac{\beta \cos\theta}{2f_o\omega}$. Eq. III-9

becomes, $mH + \tanh mH = -\Gamma^2 \epsilon H \beta \cos\theta / 2\omega^2 f_o$. If we add

π to the angle θ , it will denote the angle

made by the group velocity vector of the incoming Rossby

wave with respect to north. $(FIG\ 3\text{-}8)$.

The curves in Fig. 3-5 were calculated for a slope

$\epsilon = 10^{-2}$ and $\Gamma = N/f = 10$. If we increase the slope and/or

Γ , the curves are displaced towards the lower periods.

The penetration scale $m^{-1} = h$ becomes smaller, and vice

versa for lower values of ϵ and/or Γ . These

results are physically reasonable since increasing stratifi-

cation "softens" the vertical rigidity of the Taylor

column constraint. For a given stratification, a larger

slope requires that the fluid experience a larger change

in the basic density gradient. Therefore, a unit displace-

ment along the topographic slope will cause stronger trapping.

In Fig. 3-5 we see that for the lower periods from

a week to a month or two, the resulting penetration scale

of the bottom-intensified mode is actually larger than
the depth of the ocean ($h = 1/m > H_{DEPTH}$). The mode
becomes in essence a barotropic wave. The phase velocities
of Rossby waves at these low quasigeostrophic periods
are too large for bottom trapping (see Table 3-1). In
general, the matching of free, high-frequency Rossby
waves with topographic modes over slopes smaller than $\epsilon = 10^{-2}$
leads to essentially barotropic motions over the topography.

We recall that the set of vertical modes $\cosh m z$ and
$\{\cos r_j z\}$ are solutions to a Sturm-Liouville differential
equation when $\ell < 0$ (the phase velocity along the slope
to the left when looking up-slope). The $\{\cos p_j z\}$ modes are
solutions for the case $\ell > 0$. Thus, these solutions
form a complete set, and can be used to expand the vertical
structure of an exterior quasigeostrophic disturbance
impinging on the slope discontinuity $x = 0$ (Fig. 3-1).
We can easily show that these modes are orthogonal. For
$\ell < 0$, we have the set

$$\left\{ \begin{array}{l} \cosh m z \\ \cos r_j z \ , \ j = 1, 2, \ldots \end{array} \right\}$$

Consider the coupling between the bottom-intensified mode
and the MBRW:

$$\int_{-H}^{0} \cosh mz \cos r_j z \, dz = \frac{\cos r_j H \cosh mH}{(mH)^2 + (r_j H)^2} \left[mH \tanh mH + r_j H \tan r_j H \right] = 0$$

because the bottom boundary condition III-9, 12 states that

$$mH \tanh mH = -r_j H \tan r_j H = \frac{r^2 \epsilon H |\ell|}{\omega}$$

Thus the bottom-intensified mode is orthogonal to the MBRW modes. The MBRW modes $\cos r_j z$ are orthogonal to each other

$$\int_{-H}^{0} \cos r_j z \cos r_R z \, dz = \frac{2}{(r_j H)^2 - (r_R H)^2} \cos r_R H \cos r_j H \left[r_j H \tan r_j H - r_R H \tan r_R H \right]$$

$$= 0$$

For $\ell > 0$, we just have the set $\{ \cos p_j z \}$ and clearly,

$$\int_{-H}^{0} \cos p_j z \cos p_R z \, dz = 0$$

We can compute the normalization coefficients,

(III-15a) $\qquad \int_{-H}^{0} \cos^2 r_j z \, dz = \frac{H}{2} \left[1 + \frac{\sin r_j H \cos r_j H}{r_j H} \right]$

(III-15b) $\qquad \int_{-H}^{0} \cosh^2 mz \, dz = \frac{H}{2} \left[1 + \frac{\sinh mH \cosh mH}{mH} \right]$

and

(III-15c)
$$\int_{-H}^{0} \cos^2 p_J z \, dz = \frac{H}{2} \left[1 + \frac{\sin p_J H \cos p_J H}{p_J H} \right]$$

2. Horizontal Structure of the Topographic Modes

In order to fully determine the horizontal propagation properties of the topographic modes, we have to consider the equations describing the dependence of $f(x,z)$ in the up-slope coordinates. For the case $l < 0$, eq. III-5 becomes, for the bottom-intensified mode,

(III-16)
$$Q_{xx}^{(m)} + \left(\frac{\beta^2}{4 f_0^2 \omega^2} - l^2 + \frac{m^2}{n^2} \right) Q^{(m)} = 0$$

The solution is simply

(III-17a)
$$Q^{(m)} = A_m e^{i \lambda_m x} + B_m e^{-i \lambda_m x}$$

where the wave number λ_m is

(III-17b)
$$\lambda_m^2 = \frac{\beta^2}{4 f_0^2 \omega^2} - l^2 + \frac{m^2}{n^2}$$

where ω is the frequency, l the along-the-slope wavenumber, and m the vertical scale of the bottom-intensified mode.

If the bottom-intensified mode is excited by an
impinging Rossby wave at the slope discontinuity
(Fig. 3-8), this wave will propagate in the up-slope
direction since a traveling Rossby wave in the constant-
depth region has

$$\gamma_0^2 \equiv \frac{\beta^2}{4f_0^2\omega^2} - \ell^2 > 0$$

γ_0 is the wavenumber of a barotropic, propaga-
tion Rossby wave in the direction towards the slope
discontinuity (X direction in Fig. 3-1).

In Fig. 3-6 we see a plot of the constant frequency
curves for the same period range and topographic para-
meters as in Fig. 3-5 ($\Gamma = 10$ and the slope $\epsilon = 10^{-2}$).
The along-the-slope wavenumber is calculated using the
barotropic Rossby wave dispersion relation $\ell = \frac{\beta}{2f_0\omega} \cos\theta$.
We note that the orientation of the wavenumbers with
respect to topography indicates that the velocity vector
of the resulting bottom-intensified mode is oriented very
closely along the slope. In fact, it is within $10^\circ \sim 15^\circ$
of the contours. From the above plot we can also deduce
the direction of the energy flow since the group velocity
is perpendicular to the constant-frequency curves and

$\Gamma = 10, \; \mathcal{E} = 10^{-2}$ $|\lambda m| \rightarrow$ $\times 10^{-2} \; Km^{-1}$

.5   1.0   1.5   2.0

$Tw = 120$
$Tw = 100$
$Tw = 80$
$Tw = 30$
$Tw = 40$
$Tw = 60$

.1

$|\ell|$
$\downarrow$

.5
$10^{-2} \times Km^{-1}$
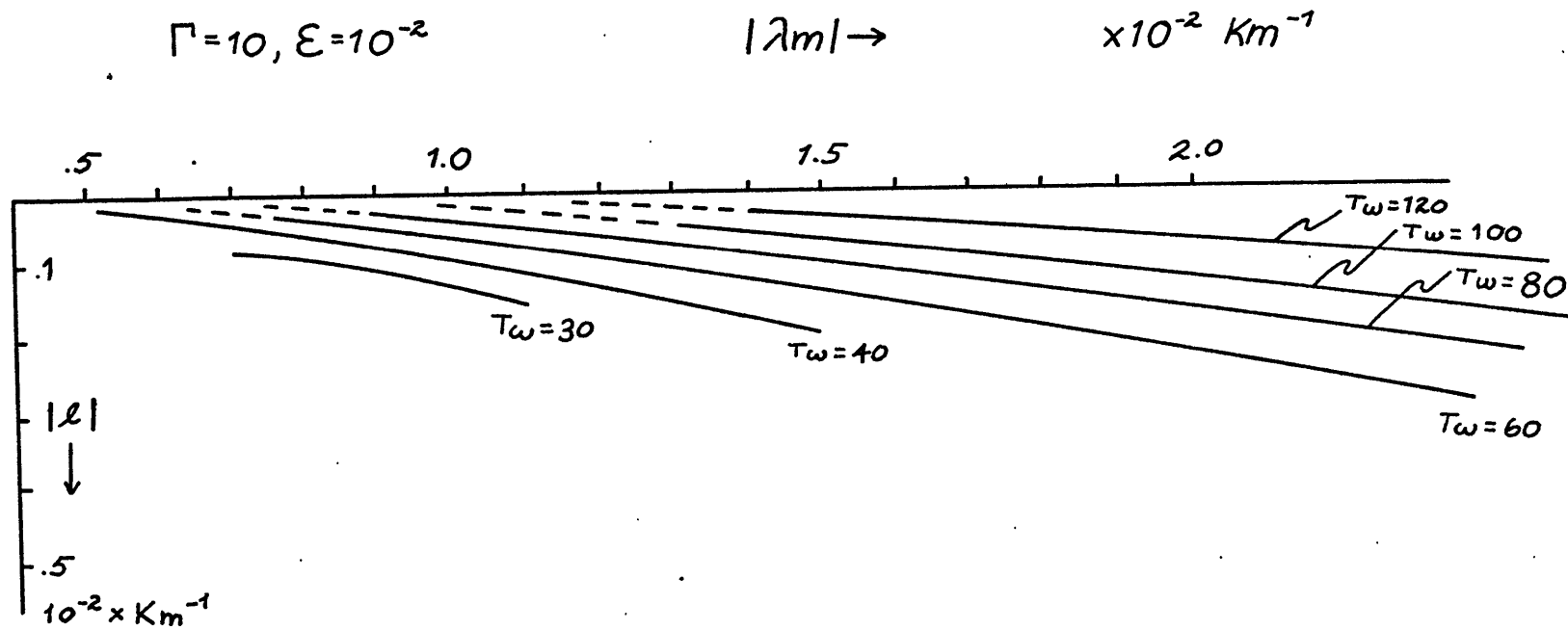
Fig. 3-6. Plot of the constant frequency curves for the bottom-intensified mode for the same period range and topographic parameters as in Fig. 3-5. $|\ell|$ denotes the along-the-slope wavenumber.

points in the direction of decreasing period. The energy

flows with a component to the left when looking up-slope.

The solution $exp\, i\lambda_m x$ corresponds to energy propagating

in the up-slope direction, while $exp -i\lambda_m x$ to energy

propagating in the down-slope direction. We wish to

emphasize that the calculation presented in Fig. 3-6 is

a particular one, done in order to completely describe

the structure of the bottom-intensified modes excited by

Rossby waves. A more general analysis of the dispersion

curves for this mode was presented in Chapter II, page .

For the MBRW, equation III-5 becomes

(III-18) $$Q_{xx}^{(n)} + \left(\frac{\beta^2}{4f_0^2\omega^2} - \ell^2 - r_j^2/r^2 \right) Q^{(j)} = 0$$

The solution is simply

(III-19a) $$Q^{(n)} = A_j\, e^{i\lambda_{r_j} x} + B_j\, e^{-i\lambda_{r_j} x}$$

where λ_{r_j} is

(III-19b) $$\lambda_{r_j}^2 = \frac{\beta^2}{4f_0^2\omega^2} - \ell^2 - r_j^2/r^2$$

For quasigeostrophic periods less than a year, the MBRW
are trapped to the slope discontinuity, and decay in the
direction of decreasing depth, i.e. $\eta_{rj}^2 < 0$ and $\eta_{rj} = -i\phi_{rj}$
where $\phi_{rj} = \sqrt{\eta^2/r^2 - \left(\frac{\beta^2}{4f_0^2\omega^2} - \ell^2\right)}$ for $x < 0$ in
Fig. 3-1. These modes are present to allow the vertical
structure of the bottom-intensified mode to adjust to the
wave impinging upon the sloping region. We can estimate
the decay scale of the MBRW modes. The along-the-slope
wavenumber ℓ is of order $\frac{\beta}{2 f_0 \omega}$ for matching with
Rossby waves in the constant-depth region. For frequencies
greater than $2\pi/1\text{year}$ the scale of the MBRW ϕ_{rj} is
approximately given by η_j/r because $\frac{\beta^2}{4f_0^2\omega^2}$ is so small.
The largest decay scale is clearly given by the first root,
$\phi_{rj}^{-1} = r/\eta_1$, which is of order $\frac{N}{f}H$ where H
is the average depth of the region. For example, if
$N/f = 10$, $H = 4Km$ then $\phi_{rj}^{-1} \simeq 40Km$. Higher
roots have smaller scales. Thus we can say that the
motion associated with the $\cos\eta_j z$ modes is confined
to a distance of the order $N/f H$ from the edge of the
shelf.

Combining the solutions of the up-slope dependence
with their associated vertical modes, we can construct
a representation for the pressure field. This representa-
tion contains all the quasigeostropic, topographic modes

that can be supported over a simple sloping bottom in
response to wave motion specified at the edge of the
slope region.

(III-20)
$$p^{(0)} = e^{-i\left(\mu l y + \omega t + \frac{\beta}{2f_0 \omega} x\right)} \left\{ (A_m e^{i\lambda_m x} + B_m e^{-i\lambda_m x}) \cosh m z + \sum_{j=1}^{\infty} A_{r_j} e^{\phi_{r_j} x} \cos r_j z \right\}$$

where the first term represents the propagating, bottom-
intensified mode. The terms under the summation sign
represent the horizontally confined MBRW modes trapped
to the edge of the slope. It might be helpful at this
point to sketch the instantaneous streamline pattern
of the bottom-intensified mode and the first MBRW mode
over the sloping bottom (Fig. 3-7). The sketch in Fig. 3-7
represents the topographic motions excited over the slope
by a quasigeostrophic disturbance impinging on the slope
discontinuity, having its along-the-slope phase velocity
traveling in the negative y direction. The amplitudes
are not specified.

The whole pattern in Fig. 3-7 is propagating to the
left when looking up-slope. In order that the group
velocity of the bottom-intensified mode have a component
away from the slope discontinuity, the phase of the wave
must propagate towards it. The direction of propagation
of the wave is given by $\lambda_m / |\mu l| \sim \frac{1}{\omega} \sqrt{(\epsilon r)^2 - \omega^2}$. The streamline
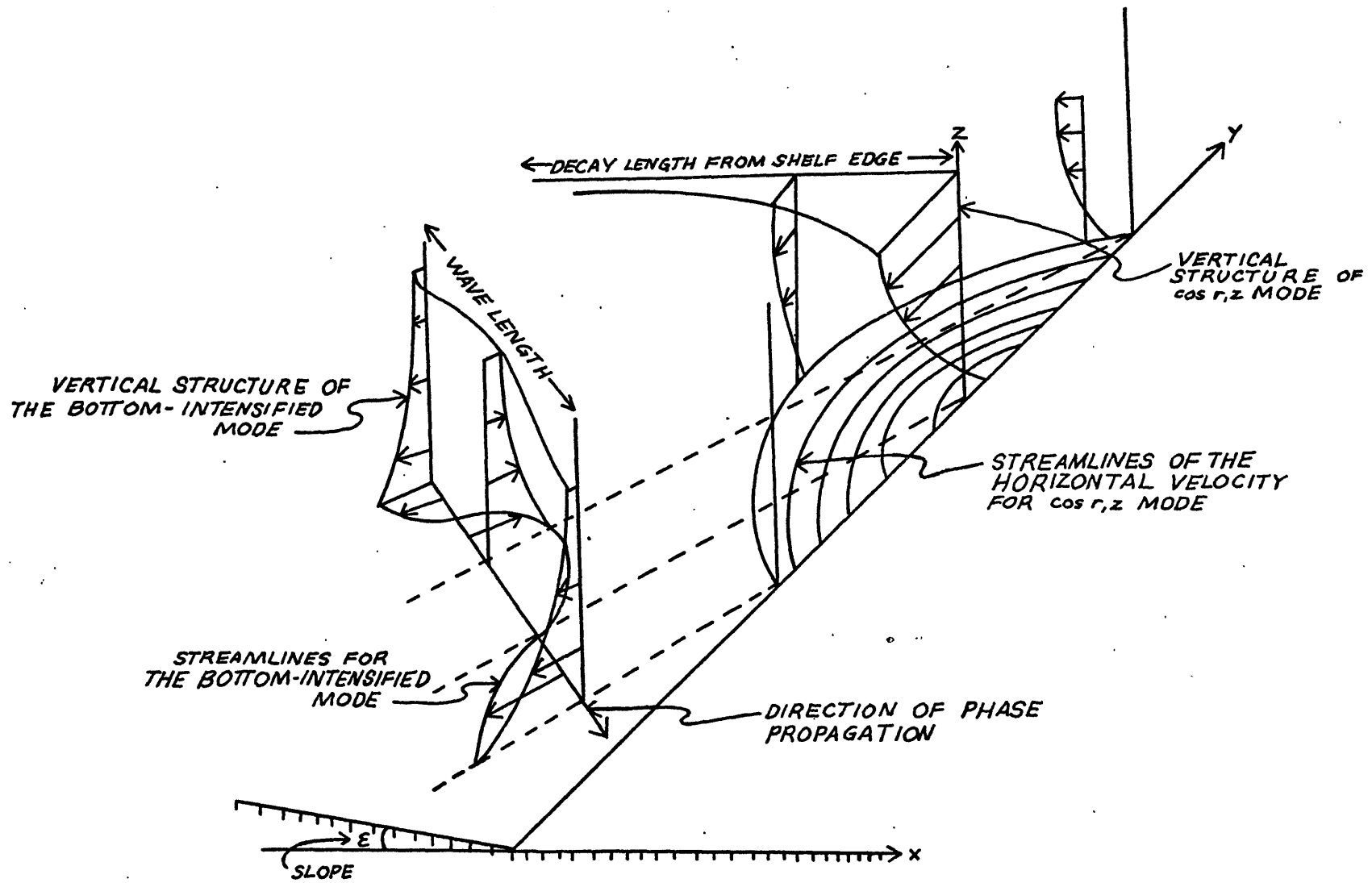
Fig. 3-7. Sketch of the instantaneous streamline pattern of the bottom-intensified mode and the first MBRW mode over the sloping bottom.

pattern of the MBRW is very similar to the pattern of traveling surface waves (in the horizontal direction). The correlation coefficient of the horizontal velocities is zero.

In the case where the disturbance at the slope discontinuity is propagating to the right when looking up-slope ($\ell > 0$), the only possible modes are the $\cos p_j z$, and their up-slope dependence is given by

(III-21)
$$Q^{(p_j)} = A_j \, e^{\phi_{p_j} x}$$

for $x < 0$ where

(III-22)
$$\phi_{p_j} = \sqrt{p_j^2/h^2 - \left(\beta^2/4f_0^2\omega^2 - \ell^2\right)}$$

Again, for quasigeostrophic *periods* less than a year or so, these modes are non-propagating in the up-slope direction. These modes form a complete set and can be used to calculate the penetration of a quasigeostrophic disturbance, specified at the slope discontinuity, into the sloping region.

(III-23)
$$p^{(\omega)} = e^{-i\left(\frac{\beta}{2f_0\omega} x + \omega t\right)} e^{i\ell\ell y} \sum_{j=1}^{\infty} A_j \, e^{\phi_{p_j} x} \cos p_j z$$

In the limit of small slope or large along-the-slope
phase velocity, the largest penetration scale of these
modes, $(\phi_{p_2})^{-1}$, is larger than the penetration scale
for the modes with phase velocity in the opposite direction,
$(\phi_{r_1})^{-1}$, and depends explicitly on the frequency. From
Fig. 3-3 we see that in this limit, the root p_1 is
approximately given by $p_1^2 = \epsilon \Gamma^2 |\ell| / \omega H$ so that $(\phi_{p_1})^{-1} \doteq \sqrt{\dfrac{H}{\epsilon} \dfrac{\omega}{|\ell|}} \sim$
$\sqrt{\dfrac{H}{\epsilon} \dfrac{2f_0}{\beta}} \, \omega$. For $H = 4 Km$ and $\epsilon = 10^{-2}$ and
$\omega \sim 1/30$, $|\ell| \sim \beta/2 f_0 \omega$, $\phi_{p_1}^{-1} \doteq 80 Km$, whereas $\phi_{r_1}^{-1} \sim 40 Km$.
On the other hand, for small phase velocity along-the-slope,
the penetration scale $(\phi_{p_1})^{-1}$ becomes the same as for
the $\cos \gamma_2 z$ MBRW mode $(\phi_{r_1})^{-1}$.

3. Reflection from a Step

We have discussed in general terms the modes of
oscillations that can be supported over a simple sloping
bottom. These modes are excited in response to quasi-
geostrophic motion specified at the intersection of the
sloping region and an adjacent region. We now wish to
apply these results to calculate a specific situation:
the excitation of topographic oscillations by a monochromatic
field of barotropic Rossby waves impinging on the sloping
bottom. We are interested in calculating the amplitudes
of the topographic motions and the coefficient of reflection
relative to the incident wave amplitude. These calculations

will enable us to determine the efficiency of the generation
of the bottom-intensified mode by sources located in an
adjacent topographic region.

Let us consider a topographic region like the one
described in Fig. 3-1. In order to simplify the problem,
we will consider matching the motions only at one boundary,
$x = 0$. The essential features of the problem can be
adequately described without considering matching the
solution at the other boundary, $x = -a$. We will choose
our solutions over the slope as if there were no back
reflection at $x = -a$.

Consider the following situation. We have a baro-
tropic Rossby wave with a specified frequency, wavelength
and amplitude incident upon a gradually sloping bottom
oriented north-south (Fig. 3-8).

We represent the incident barotropic wave by

$$(\text{III-24}) \qquad p_i^{(o)} = e^{i\ell y}\, e^{-i\left(\frac{\beta}{2f_0\omega} x + \omega t\right)}\, B_i\, e^{i\gamma_0 x}$$

where ℓ is the along-the-slope wavenumber, ω is
the non-dimensional frequency scaled by f . γ_0 is
given by the vorticity eq. III-3 with $p_{zz} = 0$, $\gamma_0^2 = \frac{\beta^2}{4f_0^2\omega^2} - \ell^2$ or
$\gamma_0 = \frac{\beta}{2f_0\omega} \sin\theta$, where the angle is measured as in
Fig. 3-8. In Fig. 3-8 we have the Rossby wave incident

$$\vec{K_i} = \left(-\frac{\beta}{2f_o\omega} + \gamma_o, -|\ell|\right)$$

$$\vec{K_r} = \left(-\frac{\beta}{2f_o\omega} \div \gamma_o, -|\ell|\right)$$

TOP VIEW

SIDE VIEW
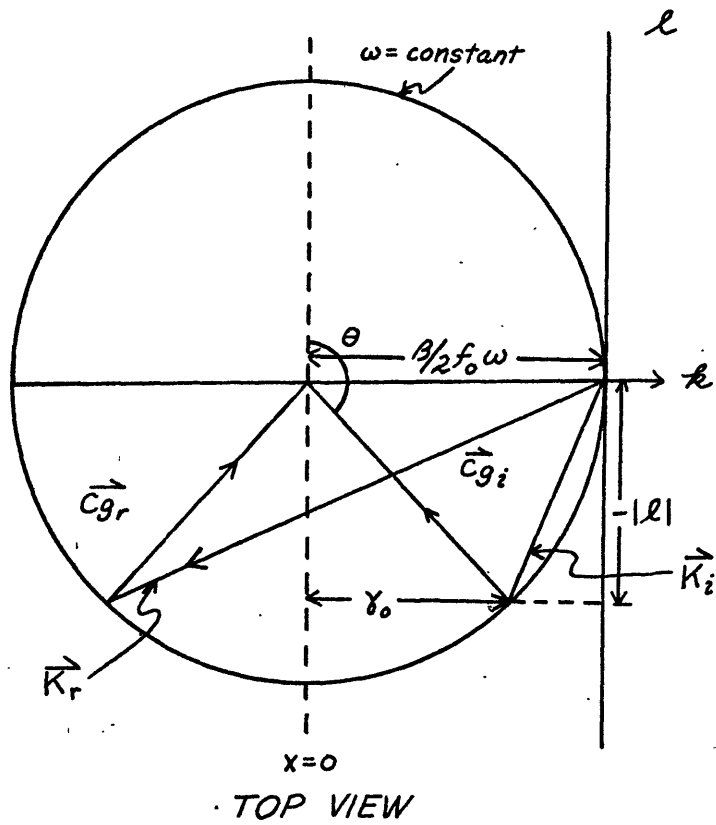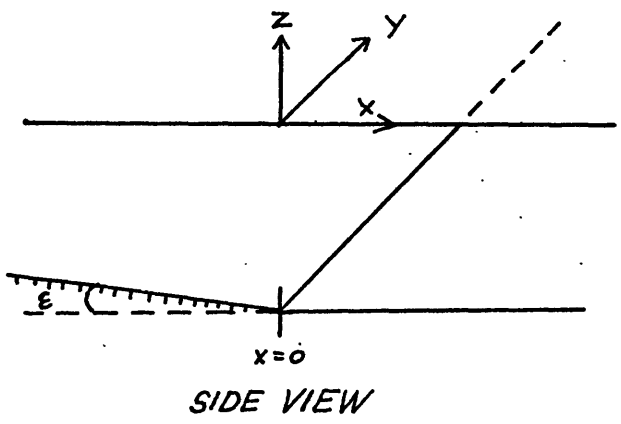
Fig. 3-8. Dispersion diagram for the Rossby wave impinging on the sloping shelf.

from the SE quadrant, so that the along-the-slope phase
velocity will be to the left when looking up-slope. This
is the case in which the topography will be able to
support the bottom-intensified mode.

Away from the slope discontinuity, there will be
a reflected barotropic wave for $x \to \infty$, since no free
baroclinic Rossby waves are possible in the frequency
range we are considering. The reflected wave is represented
by

$$(\text{III-25}) \qquad p_R^{(o)} = e^{i\ell y} \; e^{-i\left(\frac{\beta}{2f_0\omega}x + \omega t\right)} \; B_R \, e^{-i\gamma_0 x}$$

The signs of the oscillatory function in x are chosen
so that the incident wave has its group velocity vector
with a component towards $x=0$ and the reflected wave
field has a component away from $x=0$ (Fig. 3-8).
Over the topography and far away from $x=0$, we have
a transmitted wave of the bottom-intensified form. This
wave is the only propagating solution in the up-slope
direction. We represent it by

$$(\text{III-26}) \qquad p_T^{(\omega)} = e^{-i|\ell|y} \; e^{-i\left(\frac{\beta}{2f_0\omega}x + \omega t\right)} \; A_m \, e^{i\lambda_m x} \cosh mz$$

Close to the slope discontinuity, the adjustment between the sloping region and the constant-depth region is accomplished with the aid of horizontally decaying solutions. These solutions combined with the propagating solutions complete the set of vertical modes possible over the region. In the sloping region these modes are, as we have already seen, the MBRW $\{ e^{\phi_s x} \cos \delta z \}$. In the constant-depth region, these modes are non-propagating, baroclinic Rossby modes $\{ e^{-\phi_n x} \cos n\pi z / H \}$ where

$$\phi_n^2 = \left(n\pi / \Gamma H \right)^2 - \frac{\beta^2}{4 f_0^2 \omega^2} \sin^2 \theta$$

. For periods lower than about one year, the e-folding penetration length of these modes from the slope discontinuity at $x = 0$ towards the interior of the constant-depth region is approximately

$$\phi_n \simeq n\pi / \Gamma H$$

. The lowest mode $\phi_1 = \pi / \Gamma H$ determines the envelope of these scales which is of order $\sim \Gamma H / \pi$. Hence, the non-propagating, baroclinic modes present on both sides of the slope-change define the region of adjustment for the interaction of quasigeostrophic motions. The size of this region is of order ΓH . We can think of this length scale as the region where the abrupt change in the slope is smoothed out.

Close to the slope-change, we can represent the topographic modes by

(III-27)
$$p^{(o)} = e^{-i(\frac{\beta}{2f_o\omega}x + \omega t)} e^{-il\ell y} \left\{ A_m e^{\lambda_m x} \cosh m z + \sum_{j=1}^{\infty} A_j e^{\phi_{r_j} x} \cos r_j z \right\}$$

where A_m is the coefficient of the transmitted bottom-intensified mode. λ_m is the up-slope wavenumber defined in eq. III-17b and ϕ_{r_j} is the decaying scale of the MBRW defined in eq. III-19b. In the constant-depth region, the motion is represented by

(III-28)
$$p^{(o)} = e^{-i(\frac{\beta}{2f_o\omega}x + \omega t)} e^{-il\ell y} \left\{ B_i e^{i\gamma_o x} + B_R e^{-i\gamma_o x} + \sum_{n=1}^{\infty} B_n e^{-\phi_n x} \cos\frac{n\pi z}{H} \right\}$$

At the discontinuity $x = 0$, the horizontal, geostrophic velocities are continuous. Matching $u = -\partial/\partial y\, p^{(o)}$, the velocity perpendicular to the depth contours, we obtain

(III-29)
$$A_m \cosh m z + \sum_{j=1}^{\infty} A_j \cos r_j z = B_i + B_R + \sum_{n=1}^{\infty} B_n \cos\frac{n\pi z}{H}$$

Matching $v = \partial/\partial x\, p^{(o)}$, the velocity along the depth contours, we obtain

(III-30)
$$i\lambda_m A_m \cosh m z + \sum_{j=1}^{\infty} \phi_{r_j} A_j \cos r_j z = i\gamma_o (B_i - B_R) - \sum_{n=1}^{\infty} \phi_n B_n \cos\frac{n\pi z}{H}$$

The problem consists of determining the magnitudes and
phases of the coefficients A_m , A_j's , B_n and
B_n' in terms of the incident wave amplitude B_i .

We have already seen that, given the set of parameters
that determine the topographic region (slope $\in$, $\Gamma = N/f$ and
the depth H), the resulting vertical structure and
horizontal scales of the modes over the sloping bottom
are determined in terms of the along-the-slope phase
velocity of the incident Rossby wave. We have already
pointed out that the roots γ_j of the MBRW $\cos \gamma_j z$ always
converge on the roots of the baroclinic Rossby waves over
the constant-depth region as the index j increases, i.e.
$\gamma_j \rightarrow j\pi/H$ (Fig. 3-3). The bottom-intensified mode
$\cosh mz$ and the MBRW modes $\cos \gamma_j z$ form an orthogonal
set. This implies that the coupling of these modes with
the baroclinic modes over the constant-depth region
continually decreases as the mode number increases. Hence,
for any particular set of parameters defining the match-
ing problem (slope $\in$, Γ , H and along-the-
slope phase velocity), only a finite number of modes
($\cos \gamma_j z$ and $\cos j\pi z/H$) will suffice to accurately describe
the interaction at the slope discontinuity.

In the barotropic limit $mH \ll 1$, for example, we
need only the depth-independent topographic mode and a

reflected barotropic wave. As the transmitted topographic mode intensifies near the bottom, we need the first modes to account for that part of the motion which is not near the bottom. In Fig. 3-4 we saw how the structure of the $\cos r_j z$ mode compliments the bottom-intensified mode. Since the reflected barotropic wave cannot by itself account for the topographic modes' vertical structure at the slope discontinuity, baroclinic modes in the constant-depth region are needed.

The simplest way to perform the matching at the intersection of the two regions is to expand the modes of one region in terms of the modes of the other. Let us expand the bottom-intensified mode and the $\cos r_j z$ modes in terms of a cosine series

(III-31)

$$\cosh m z = \frac{\sinh m H}{m H} \left(1 + 2 \sum_{n=1}^{\infty} \frac{(-)^n}{1 + \left(\frac{n\pi}{mH}\right)^2} \cos \frac{n\pi z}{H} \right)$$

and

(III-32)

$$\cos r_j z = \frac{\sin r_j H}{r_j H} \left(1 + 2 \sum_{n=1}^{\infty} \frac{(-)^n}{1 - \left(\frac{n\pi}{r_j H}\right)^2} \cos \frac{n\pi z}{H} \right)$$

Substituting these expansions in III-29, 30, we match the

terms with the same cosine dependence $1, \cos \frac{n\pi z}{H}$. For convenience we define the symbols

(III-33a)

$$\epsilon_o^m \equiv \frac{\sinh mH}{mH}$$

and

(III-33b)

$$\epsilon_n^m \equiv 2 \frac{\sinh mH}{mH} \frac{(-)^n}{1 + \left(\frac{n\pi}{mH}\right)^2}$$

Similarly,

(III-33c)

$$\delta_o^j \equiv \frac{\sin \zeta H}{\zeta H}$$

and

(III-33d)

$$\delta_n^j = 2 \frac{\sin \zeta H}{\zeta H} \frac{(-)^n}{1 - \left(\frac{n\pi}{\zeta H}\right)^2}$$

Matching term by term, we find for the barotropic term

(III-34a)

$$A_m \epsilon_o^m + A_1 \delta_o^1 + A_2 \delta_o^2 + \cdots = B_i + B_n$$

and

(III-34b)

$$i \lambda_m A_m \epsilon_o^m + \phi_{r_1} A_1 \delta_o^1 + \phi_{r_2} A_2 \delta_o^2 + \cdots = i \gamma_o (B_i - B_n)$$

for the first baroclinic mode,

(III-34c)

$$A_m \epsilon_1^m + A_1 \delta_1^1 + A_2 \delta_1^2 + \cdots = B_1$$

and

(III-34d)

$$i \lambda_m A_m \epsilon_1^m + \phi_{r_2} A_1 \delta_1^1 + A_2 \phi_{r_2} \delta_1^2 + \cdots = -\phi_1 B_1$$

and so on. Since we have two equations for each mode,
we can eliminate the coefficient of the reflected baro-
tropic wave B_n and the coefficients of all the baro-
clinic modes in the constant-depth region B_n . Finally,
we can combine all of these relations in a matrix relating
the amplitudes of the topographic modes to the incident
wave amplitude.

(III-35)

$$
\begin{pmatrix}
\epsilon_0^m(\lambda m + \gamma_0) & -i(\phi_{r_1}+i\gamma_0)\delta_0^1 & -i(\phi_{r_2}+i\gamma_0)\delta_0^2 \cdots \\[2mm]
\epsilon_1^m(\phi_1+i\lambda_m) & (\phi_{r_1}+\phi_1)\delta_1^1 & (\phi_{r_2}+\phi_1)\delta_1^2 \cdots \\[2mm]
\epsilon_2^m(\phi_2+i\lambda_m) & (\phi_2+\phi_{r_1})\delta_2^1 & (\phi_2+\phi_{r_2})\delta_2^2 \cdots \\
\vdots & \vdots &
\end{pmatrix}
\begin{pmatrix} A_m \\[2mm] A_1 \\[2mm] A_2 \\ \vdots \end{pmatrix}
= 2\gamma_0
\begin{pmatrix} B_i \\[2mm] 0 \\[2mm] 0 \\ \vdots \end{pmatrix}
$$

For any particular set of parameters defining the matching problem in terms of an incident Rossby wave at the sloping region (slope ϵ, $\Gamma = N/f$, H_{DEPTH} and along-the-slope phase velocity), the matrix tends to be diagonal, after a number of columns, indicating that only a limited number of modes are required to perform the matching. We solved the matrix equation as a system of finite linear equations. For the range of bottom-trapping scales (mH) considered, enough terms were kept so that the coefficient of the reflected wave did not deviate much more than about 1%. We kept successively 2, 3, 4 terms and equations for bottom-trapped scales greater than the average depth of the region $mH < 1$ (the barotropic range). The variation found in the coefficient of reflection was about 1%. For the bottom-trapped scales smaller than the depth of the region $mH > 1$, we calculated up to $mH = 2\pi$ (or the e-folding distance of the bottom-intensified mode about 1/6 of the depth). For this case we kept successively

3, 4, 5 and 6 terms and equations. The variation in the
coefficient of reflection was between 1% and 2%. The
phases converged more slowly. For the upper limit of the
calculation $mH = 2\pi$, the variation was about 10%.

In Fig. 3-9 we show the results of the calculation
for the reflected coefficient using the same topographic
parameters used to calculate Fig. 3-5, (slope $\epsilon = 10^{-2}$,
$\Gamma = N/f = 10$ and an average depth 4km). The reflection
coefficient is defined as the ratio of the reflected
energy flux in the $\hat{x}$ direction over the incident
energy flux in the same direction.

(III-36)

$$R = \left| \frac{B_R}{B_i} \right|^2$$

where B_R is the coefficient of the reflected wave, and
B_i the amplitude of the incident wave. The coefficient
B_R/B_i was obtained by substituting the calculated
values of the coefficients A_m/B_i , A_1/B_i ,... etc. in
eq. III-34a. The period T_ω in Fig. 3-9 is non-
dimensionalized by the inertial period T_f . The lines
of constant mH indicate the penetration scale of the
bottom-intensified mode into the interior of the fluid.
They are drawn to aid in relating the reflection coefficient
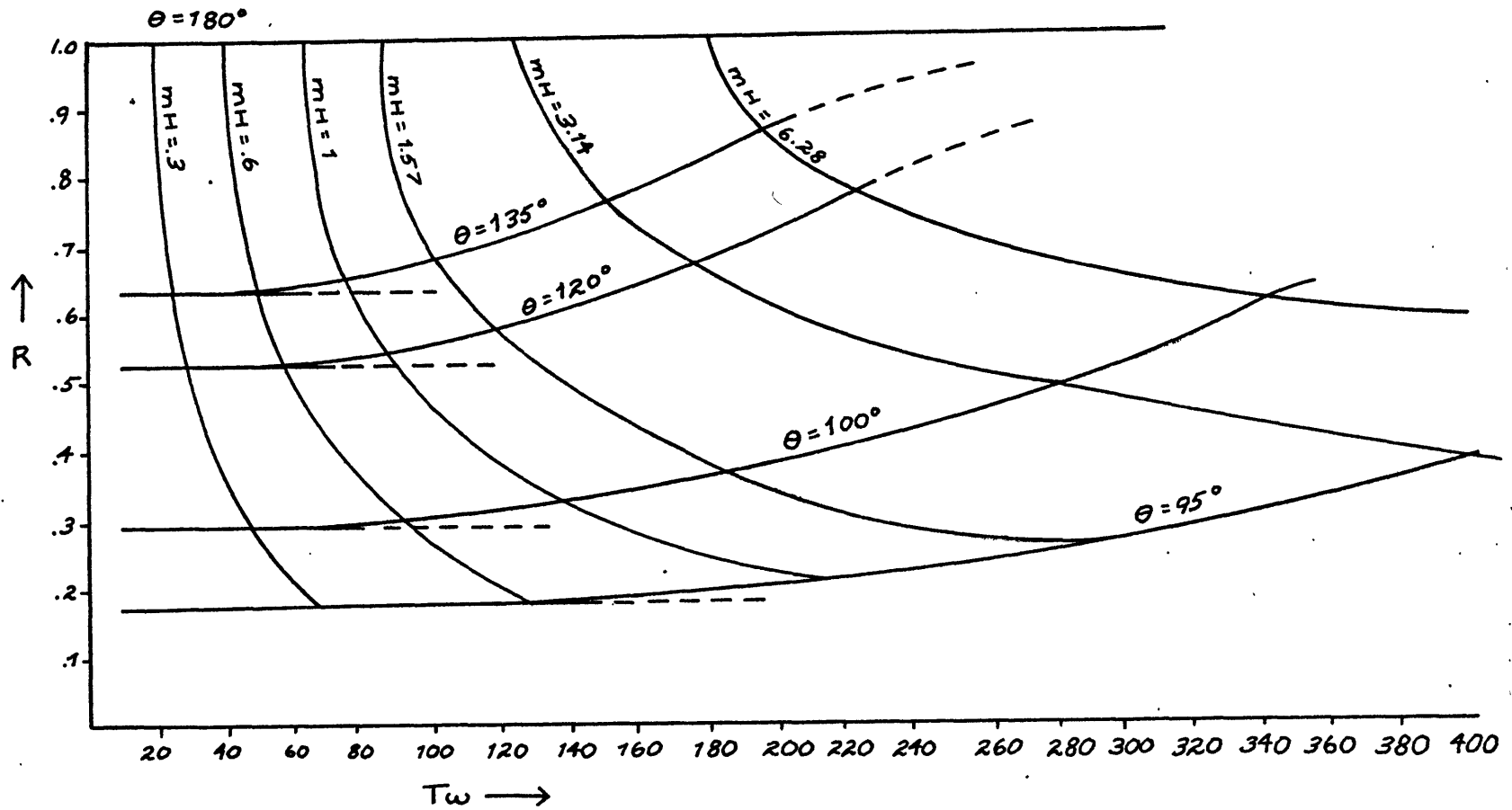
Fig. 3-9. Reflection coefficient describing the interaction of Rossby waves with topographic waves. The lines of constant m_H indicate the penetration scale of the excited bottom-intensified mode. T_ω is the period of the wave in days.

to the particular bottom-intensified mode excited in response to the impinging Rossby wave at the slope discontinuity $x = 0$ (Fig. 3-8). The plot clearly shows that for a given angle of incidence, the reflection coefficient R increases as the penetration scale of the bottom-intensified mode decreases beyond $mH \sim 1$, or $h^{-1} = m^{-1} \sim H_{DEPTH}$. This increase in R indicates that the bottom-intensified mode is not effectively generated by the impinging Rossby wave.

The greatest transmission of energy for any given angle of incidence occurs at the low periods, in the nearly barotropic limit $mH < 1$. In the homogeneous approximation for topographic waves $N^2 = 0$, the reflection coefficient for any given angle of incidence is independent of frequency (as long as we do not consider the matching of the topographic waves at the other end of the shelf, $x = -a$, as in Fig. 3-1). The results for the homogeneous limit are shown by the dashed lines in Fig. 3-9. We note that in agreement with the homogeneous model $N^2 = 0$, the reflection coefficient does not vary much with period until we reach the $mH \sim 1$ curve.

Physically, the increase in the reflection coefficient beyond the curve $mH = 1$ is due to two effects. As the resulting penetration scale of the bottom-intensified

mode decreases, the up-slope wavenumber λ_m increases

much faster than the exterior Rossby wave wavenumber in

the same direction, γ_o . (In the barotropic limit,

$m H < 1$ or in a homogeneous model, $N^2 \approx o$, the ratio of

γ_o / λ_m is independent of frequency.) This large change

in the wavenumbers decreases the transmission amplitude

over the slope. Furthermore, as the resulting penetration

scale decreases, the amplitudes of the horizontally de-

caying baroclinic modes must increase so that the modes

over the topography can adjust to the barotropic vertical

structure of the incoming wave. Hence, part of the amplitude

of the incident wave is redistributed among the topographic

modes decaying away from the edge of the shelf. This

redistribution occurs at the expense of the amplitude

of the bottom-intensified mode. Since the horizontally

decaying modes carry no energy, the reflection coefficient

increases. In Fig. 3-10 we show the change in the amplitudes

of the bottom-intensified mode, $\cos h m z$ and the first two

modes $\cos r_1 z$ and $\cos r_2 z$ as a function of the penetration

scale $m H$ for a constant angle of incidence. We refer

to Fig. 3-4 for a sketch of the vertical structure of

these modes.

It is clear that while the amplitude of the bottom-

intensified mode decreases, the MBRW modes gain in strength.

From this it would seem that when the scales of the
incident Rossby wave match with a strongly trapped bottom-
intensified mode, the edge of the shelf behaves like an
elastic membrane. It yields under the influence of the
impinging wave and springs back with little energy lost.
The penetration of the wave into the sloping region is
given by the longest decay length scale of the $\cos r_j z$ modes,

$$\frac{2}{\pi}\frac{N}{f}H \ .$$
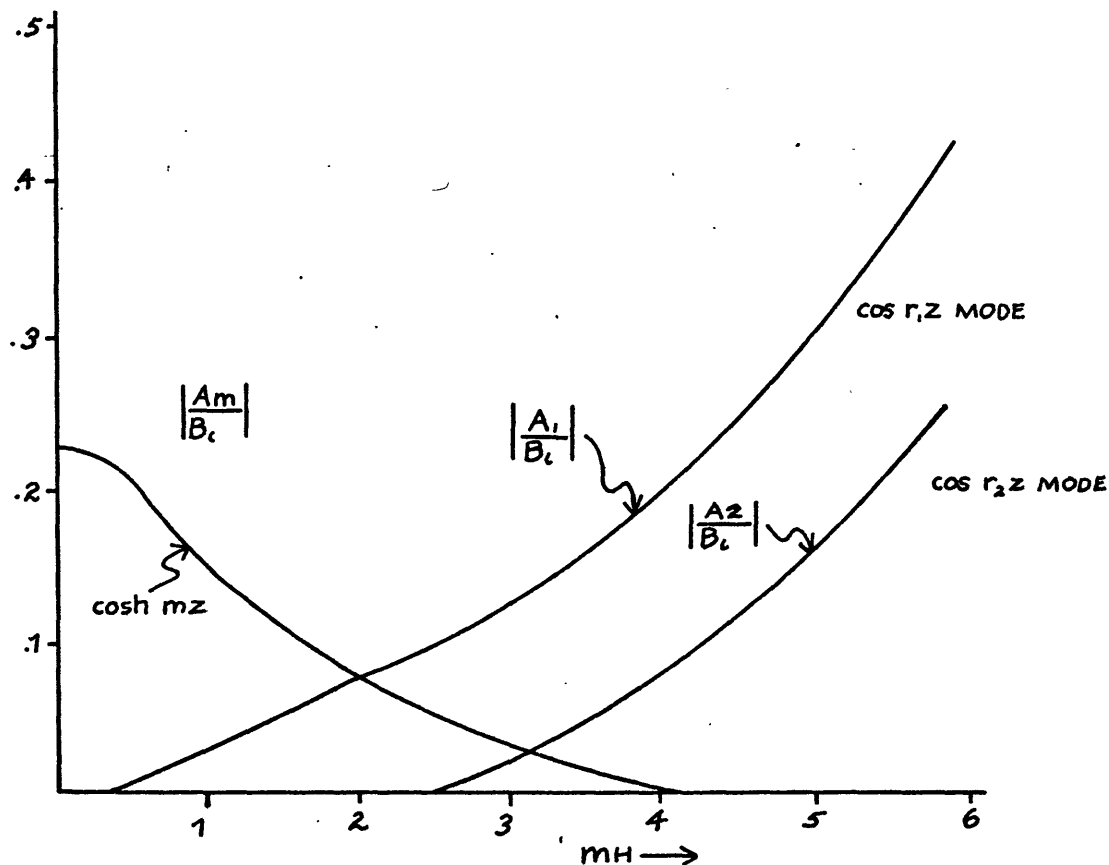
Fig. 3-10. Amplitudes of the bottom-intensified mode and
the first two modes $\cos r_1 z$ and $\cos r_2 z$ as a function of the
penetration scale mH for a constant angle of incidence.

In Fig. 3-11 we show a plot of the calculated amplitude
of the bottom-intensified mode as a function of frequency.
We clearly see that as the penetration scale decreases,
the amplitude of the mode decreases. Along a line of
constant penetration scale, the amplitude increases as
the angle of incidence of the Rossby wave group velocity
turns in the direction perpendicular to the slope (Fig.
3-8). . This increase in the amplitude corresponds to the
decrease in the reflection coefficient in Fig. 3-9 (along
the lines of constant mH). The amplitude of the
bottom-intensified mode increases because as $\theta \to 90^{\circ}$, the
velocity of this mode over the sloping bottom is turning
in the along-the-slope direction and is experiencing a
smaller effective slope. In fact, this effect is responsible
for the concavity of the $mH = constant$ lines (see
Figs. 3-9, 3-11). The dashed lines in Fig. 3-11 denote
the amplitude of topographic motion if the effect of
stratification were neglected. We note that the calculations
presented above were made for a bottom slope of order one
in one-hundred. Smaller slopes essentially displace the
calculated curves in Figs. 3-9, 3-11 towards the longer
periods. The nearly barotropic limit $mH < 1$ is extended
for a larger period range.
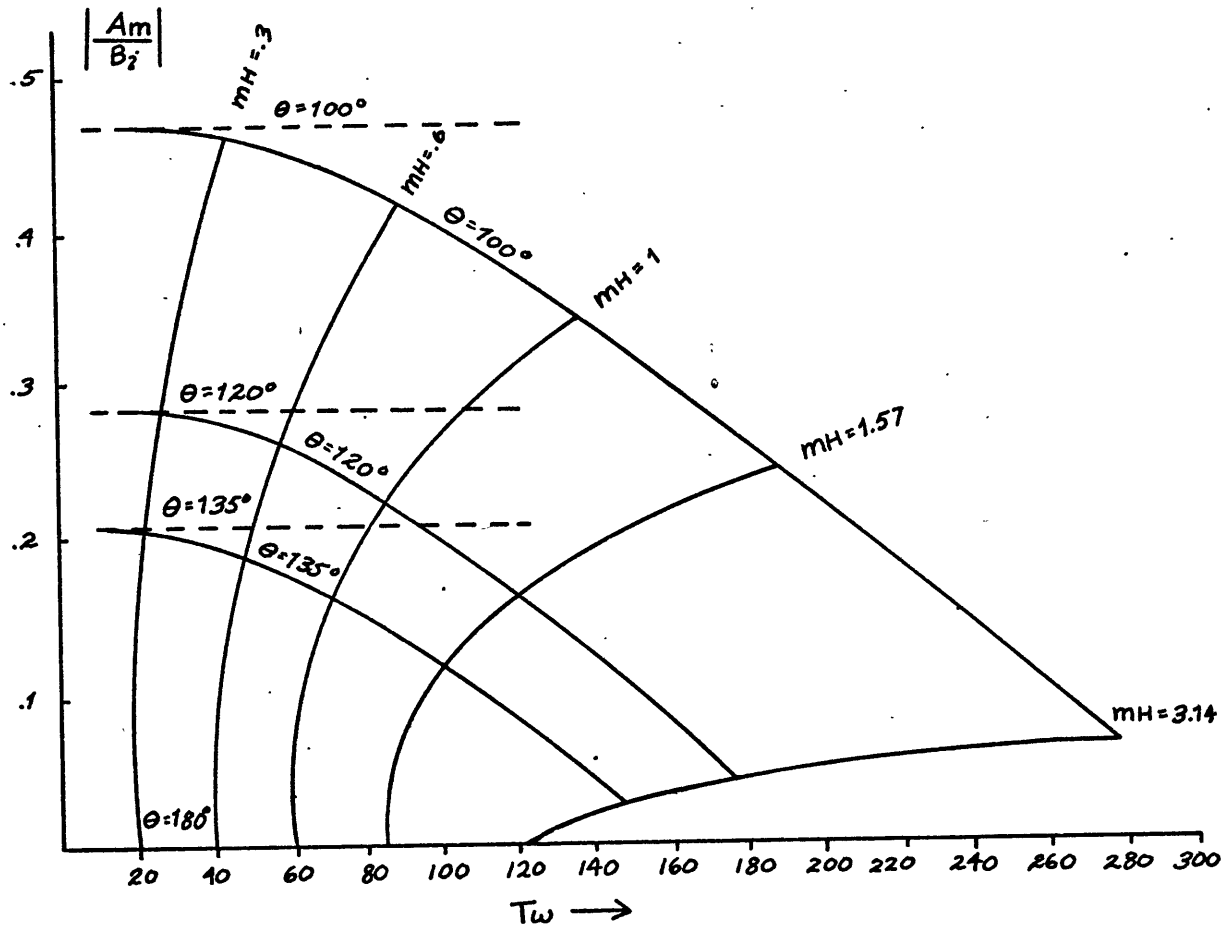
Fig. 3-11.   Plot of the calculated amplitude of the bottom-intensified mode as a function of period.

Up to the present, we have considered the matching of Rossby waves only at one boundary. In principle there is no difficulty in treating more complicated topography such as a full sloping step, a small amplitude ridge and a series of sloping bottoms back-to-back to simulate the variation of the slope. In the case of a ridge, for example, we would have to use vertical modes $\cos p_j z$ in eq. III-23, in order to match the bottom-intensified mode across the ridge top. The details of the computation become increasingly more involved as the number of boundaries to be considered increases. The physical conclusions appear to be essentially the same as those we found in the simpler problem: Rossby waves transmit energy most effectively over topography in the long-scale, high-frequency range. For quasigeostrophic slopes, the resulting topographic motions under these conditions are essentially barotropic. Bottom-intensified modes appear for low along-the-slope phase velocities, but their amplitudes, except for occasional resonances, are small.

The results of the calculation of the reflection coefficient (Fig. 3-9) indicate the following: 1. Rossby waves cannot excite bottom-intensified waves with any significant amplitude. 2. In the low quasigeostrophic periods ($T \leq 30 \, days$), Rossby waves produce essentially

barotropic topographic oscillations. 3. For low frequencies Rossby waves excite waves trapped to the edge of slope (Fig. 3-7) which have larger velocities close to the surface and a node on the topography. These waves have larger amplitudes than the bottom-intensified wave. These conclusions indicate that bottom-intensified waves over topography must have a local origin.

4. Wave Trapping

It is possible for topographic features in the ocean to support wave motions which cannot be coupled (or are weakly coupled) to propagating waves outside the topographic region. This trapping of wave energy occurs because the wave motion over the topography experiences internal reflections at the edge of the region. Internal reflections occur, in turn, because the along-the-slope phase velocity of the topographic oscillations is too slow to match with freely propagating waves outside the region.

Rhines (13) has studied wave trapping over simple one-dimensional and cylindrically symmetric topography within the homogeneous approximation. When the effects of stratification are included, the vertical structure of the normal modes of oscillation will intensify at the bottom, $mH > 1$, whenever the horizontal scales

of the modes are less than $N/_f H$ where H is the average depth. Also, the adjustment of the vertical structure of the bottom-intensified oscillations at the edge of the sloping region will excite horizontally trapped, baroclinic waves. These baroclinic waves decay away in both directions from the edge of the sloping region.

When compared to the homogeneous problem, the major effect of these horizontally trapped, baroclinic oscillations is to further weaken the coupling of the normal modes over the topographic feature with the exterior. This reduces the possibility of coupling with other nearby features which could support similar modes of oscillation.

To illustrate the weakening of the coupling, let us consider the calculation of the normal modes over a shelf with a wall at one end and a constant-depth region at the other.
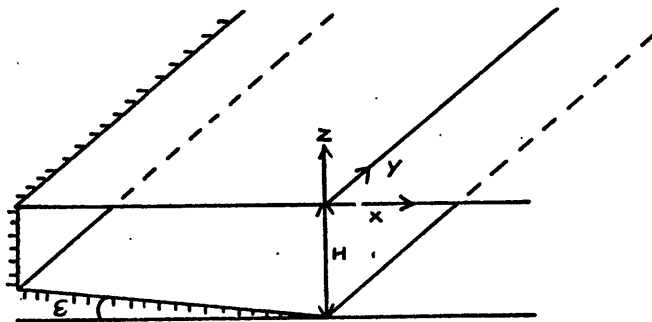
Fig. 3-12. Diagram describing the shelf for the calculation of topographic normal modes.

We would like to point out that the simplest way to demonstrate the weakening of the coupling with increasing bottom-intensification is to calculate the reflection of an incident bottom-intensified mode on a slope dis- continuity such as we described in Fig. 3-8. We would find that for a given topographic region, as we decrease the penetration scale of the wave into the interior of the fluid mH , the phase of the reflected wave would be larger than the phase obtained for the homogeneous case, tending towards π , that is, perfect reflection. Similarly, when one considers discrete modes, a measure of the coupling with the exterior region is given by the way the eigenvalues approach the solutions for a rigid wall at $x=0$. We will show that the eigenvalues of the normal modes are increased over the homogeneous values when the baroclinic, horizontally trapped motions are included to adjust the vertical structure of the bottom- intensified motion. The eigenvalues tend toward the solu- tions one would obtain for a rigid wall at $x=0$ instead of an open region.

The shelf in Fig. 3-12 is considered infinite along the y-direction. This topographic region might represent an idealized continental shelf. For small slopes, i.e.

$\epsilon \alpha/H \ll 1$, the topographic motion will be

quasigeostrophic, and we can apply the vertical normal mode decomposition of the previous section. For simplicity we set $\beta = 0$, which implies we are dealing with along-the-slope scales $\ell^{-1} \ll 2 f_0 \omega / \beta$.

Over the slope, the only possible oscillatory solution in the up-slope direction has the form of the bottom-intensified mode

$$(\text{III-37}) \qquad p = e^{-i(\ell|y + \omega t)} \cosh mz \, \sin \lambda_m (x+a)$$

where λ_m, the wavenumber in the up-slope direction, is given by

$$(\text{III-38}) \qquad \lambda_m^2 = \frac{m^2}{\Gamma^2} - \ell^2$$

where ℓ is the along-the-slope wavenumber and the m inverse of the penetration scale of the bottom-intensified mode. As we have already seen, this mode only exists for $\ell < 0$, that is when the along-the-slope phase propagates to the left when looking up-slope. We note that the solution above already satisfies the condition of no flow into the boundary at $z = -a$. In the case of a rigid

wall, the condition of no flow $\sin \lambda_n a = 0$ at $x=0$ yields
the eigenvalues for m_H and its associated frequency
for each possible value of the along-the-slope wavenumber
ℓ , i.e. $m_n^2 = \Gamma^2 \left(\left(\frac{n\pi}{a} \right)^2 + \ell^2 \right)$

and

$$\frac{\omega_n}{\Gamma \epsilon} = \frac{|\ell| a}{\sqrt{(n\pi)^2 + (\ell a)^2}} \tanh \frac{\Gamma H}{a} \sqrt{(n\pi)^2 + (\ell a)^2}$$

In the case of an open region, the motion extends
its influence beyond the edge. Since the vertical depend-
ence of the bottom-intensified mode has to be adjusted
at the edge, we need the set of solutions $\cos r_j z \exp \phi_{r_j} z$
which decays in the up-slope direction (see page **96**).
Over the sloping bottom, we represent the lowest order
quasigeostrophic pressure field as

(III-39)

$$p^{(0)} = e^{-i(\ell |\ell| y + \omega t)} \left[A_m \sin \lambda_m (x+a) \cosh m z + \sum_{j=1}^{\sim} A_j \sinh \phi_{r_j} (x+a) \cos r_j z \right]$$

where the terms under the summation sign represent the
MBRW we found in the previous section. ϕ_{r_j} , the
decay scale of these modes, is given by $\phi_{r_j}^2 = (r_j^2/\Gamma^2 + \ell^2)$.
The roots r_j are determined in terms of particular
values of the bottom-intensified scale by the relation

$$mH \tanh mH = - r_j H \tanh r_j H$$

We note that the pressure field $p^{(o)}$ satisfies the no-flow condition at $x = -a$.

In the open region $x > o$, we use the vorticity equation II-18 with $\beta = o$ to find the complete set of solutions in the vertical. They satisfy the top and bottom boundary conditions of no-flow. These solutions do not exist by themselves. They are used to represent the influence of the topographic motion beyond $x = o$. For the region beyond the shelf, we represent the solution by (III-40)

$$p^{(o)} = e^{-i(|\ell|y + \omega t)} \left[B_o e^{-\phi_o x} + \sum_{n=1}^{\infty} B_n e^{-\phi_n x} \cos\frac{n\pi z}{H} \right]$$

where $\phi_o = |\ell|$, $|\ell|$ is the along-the-slope wavelength and $\phi_n = \sqrt{\left(\frac{n\pi}{\rho H}\right)^2 + \ell^2}$. The barotropic solution decays with scale ϕ_o^{-1} given by the along-the-slope wavelength of the topographic oscillation. The penetration depth defines the maximum region of influence of the topographic oscillations. The baroclinic solutions decay much faster.

At $x = o$ we match the horizontal quasigeostrophic

velocities u, v . For $u = -\frac{\partial p^{(o)}}{\partial y}$ we have

(III-41)

$$A_m \sin \lambda_m a \cosh mz + \sum_{j=1}^{\infty} A_j \sinh \phi_{r_j} a \cos r_j z = B_o + \sum_{n=1}^{\infty} B_n \cos \frac{n\pi z}{H}$$

and for $v = \partial p^{(o)}/\partial x$

(III-42)

$$A_m \lambda_m \cos \lambda_m a \cosh mz + \sum_{j=1}^{\infty} A_j \phi_{r_j} \cosh \phi_{r_j} a \cos r_j z = -\phi_o B_o - \sum_{n=1}^{\infty} \phi_n B_n \cos \frac{n\pi z}{H}$$

For any given along-the-slope wavenumber, the above
equations are satisfied by a discrete set of bottom-
intensified scales and their associated frequencies. As
in the reflection problem in the previous section, we
expand the $\cosh mz$ and each $\cos r_j z$ mode in
terms of the complete set of functions $1, \cos \frac{n\pi z}{H}$.

(III-43)

$$\cosh mz = \epsilon_o^m + \sum_{n=1}^{\infty} \epsilon_n^m \cos \frac{n\pi z}{H}$$

and

(III-44) $\quad \cos r_j z = \delta_o^j + \sum_{n=1}^{\infty} \delta_n^j \cos \frac{n\pi z}{H}$

where the symbols $\epsilon_o{}^m, \epsilon_n{}^m, \delta_o{}^j$ and $\delta_n{}^j$ have

been defined in eq. III-33 (page   ). We substitute

the above expansions in the eqs. III-41, 42 and match

term by term

$$A_m \sin \lambda_m a \, \epsilon_o{}^m + A_1 \sinh \phi_{r_1} a \, \delta_o{}^1 + A_2 \sinh \phi_{r_2} a \, \delta_o{}^2 + \cdots = B_o$$

$$\lambda_m A_m \cos \lambda_m a \, \epsilon_o{}^m + A_1 \phi_{r_1} \sinh \phi_{r_1} a \, \delta_o{}^1 + A_2 \phi_{r_2} \sinh \phi_{r_2} a \, \delta_o{}^2 + \cdots = -\phi_o B_o$$

We eliminate the coefficients in the right-hand side by

combining u and v equations term by term. We

obtain an infinite set of homogeneous equations.

(III-45)

$$\begin{pmatrix} \epsilon_o{}^m(\phi_o \sin \lambda_m a + \lambda_m \cos \lambda_m a) & \delta_o{}^1(\phi_o \sinh \phi_{r_1} a + \phi_{r_1} \cosh \phi_{r_1} a) & \cdots \\ \epsilon_1{}^m(\phi_1 \sin \lambda_m a + \lambda_m \cos \lambda_m a) & \delta_1{}^1(\phi_1 \sinh \phi_{r_1} a + \phi_{r_1} \cosh \phi_{r_1} a) & \cdots \\ \epsilon_2{}^m(\phi_2 \sin \lambda_m a + \lambda_m \cos \lambda_m a) & \cdots \\ \vdots \end{pmatrix} \begin{pmatrix} A_m \\ A_1 \\ A_2 \\ \vdots \end{pmatrix} = 0$$

Setting the determinant of the matrix equal to zero allows

us to calculate the eigenvalues of the problem.

The eigenvalues were calculated as follows. Particu-

lar values of the vertical scale of the bottom-intensified

mode mH were chosen, then a number of roots of the
MBRW modes were calculated by using the relation

$$r_j H \tan r_j H = - mH \tanh mH$$

We calculated all the other parameters that appear in the
matrix $\lambda_m, \phi_{r_j}, \epsilon_n^m, \delta_n^j$ for a number of rows and columns.
The value of partial determinants were obtained by
evaluating the first element and the second, third and
fourth rows and columns. We denoted these values by
D_1, D_2, D_3, D_4. We repeated the calculations for other
values of mH, and the results were plotted versus
mH. We noted that the results of D_2, D_3, D_4
passed practically through the same point on the axis,
indicating that the roots of D_2, D_3, D_4 converged rapidly
to a fixed value, which is the root of the determinant.

The range of values mH can be estimated for each
eigenvalue as follows. In the case of a rigid wall at
$x = 0$, the first eigenvalue is given by $\sin \lambda_m a$
or $\lambda_m = \pi/a$ where a is the width of the shelf. We
know that the case of $n.0$-wall at $x = 0$, the root has
to be smaller (Fig. 3-13). So $mH < \Gamma H \sqrt{(\frac{\pi}{a})^2 + \ell^2}$.
The minimum value can be obtained by setting $\lambda_m a = 0$.
Then $mH > \Gamma H \ell$. The range of possible roots
mH is within $\Gamma H \ell < mH < \Gamma H \sqrt{(\frac{\pi}{a})^2 + \ell^2}$ for
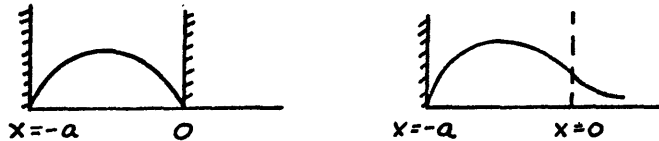
Fig. 3-13. Sketch of the first eigenvalue for a rigid wall at $x = o$ and an open region at $x = o$. the first eigenvalue. The second mode of oscillation can be calculated by choosing mH between the first calculated eigenvalue and the second eigenvalue for the rigid wall case, and so on for higher roots. For example, imagine a shelf 100 km. wide and 4 km. deep. Set the along-the-slope wavenumber $\ell = \frac{1}{100} km$ and $\Gamma = N/_f$

10 . The value of mH for the first eigenvalue is within the range $.4 < mH < 1.32$, that is, within a vertical scale 2.5 times larger than the depth and about .75 of the depth. The second eigenvalue is within $(mH)_2$ and 2.54. For the above case $\ell a = 1$ and

$\Gamma H/_a = .4$, we show in Table 3-2 the actual numerical values of the determinants used in obtaining the vertical structure of the lowest eigenvalue. For this particular case, D_4 is beyond the accuracy of our calculations because we are dealing with the difference of very large

mH	D_1	D_2	D_3
.6	$+1.47 \cdot 10^{-2}$	$+.643$	
.8	$+.786 \cdot 10^{-2}$	$+.299$	
.9	$+.021 \cdot 10^{-2}$	$+.089$	$+594.46 \cdot 10^{2}$
.92		$+.042$	$+102.15 \cdot 10^{2}$
.93	$-.231 \cdot 10^{-2}$	$-.0015$	$-32.01 \cdot 10^{+2}$
1.0	$-.927 \cdot 10^{-2}$	$-.163$	$-793.02 \cdot 10^{2}$
1.2	$-3.0 \cdot 10^{-2}$	$-.506$	

Table 3-2. Table showing the numerical values of the
determinants used in obtaining the vertical structure
of the lowest eigenvalue.

numbers close to the root. However, it is clear that the
roots are converging between .92 and .93. Graphically,
the intersection of mH on the axis is about .927
(Fig. 3-14). The horizontal eigenvalue $(\lambda_m a)$
corresponding to the vertical scale $mH = .927$ is $\lambda_m a = 2.1$.
In the homogeneous case, that is, neglecting the baroclinic
modes trapped at the edge of the slope, we obtain $\lambda_m a = 2.03$.
For larger stratification or a narrower shelf, for example
$\frac{\Gamma H}{a} = 1$ and $a\ell = 1$, we obtain $mH = 2.36$ and
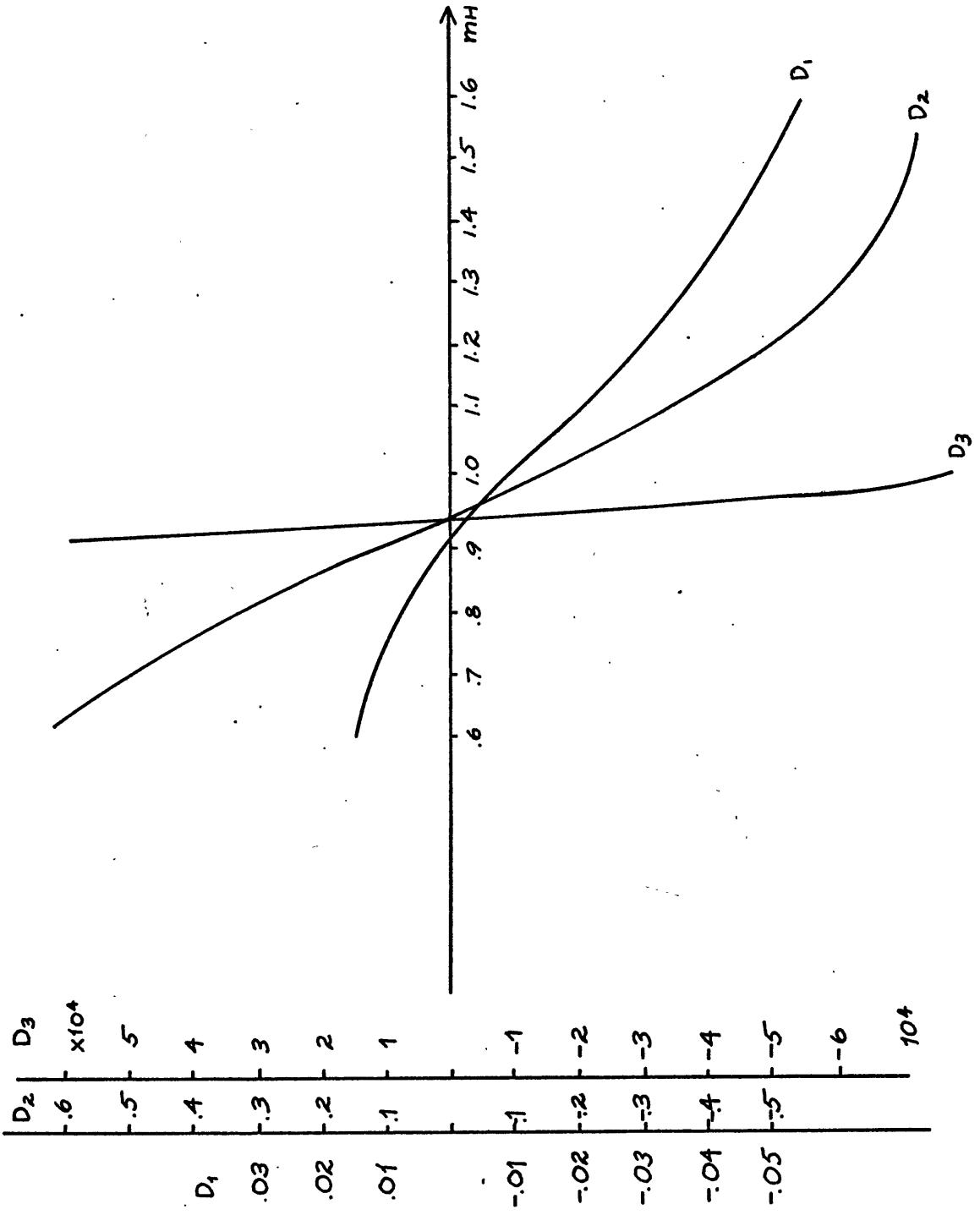
Fig. 3-14. Graphical solution to eq. III-43 in terms of
partial determinants.

$\lambda_m a \simeq 2.14$ compared to $\lambda_m a \simeq 2.03$ for the homogeneous case. It is clear that the presence of the baroclinic modes at the edge of the shelf is pulling the horizontal eigenvalues closer to the rigid wall limit $\lambda_m a \simeq 3.14$.

In Fig. 3-15 we show a plot of the calculated values of the vertical intensification scale mH as a function of the along-the-slope wavenumber for different values of the parameter $\Gamma H/a$. For all mH the corresponding eigenvalues $\lambda_m a$ are larger than the homogeneous case and approach the rigid wall values as ℓa increases.

The dashed line (Fig. 3-15) meeting the $\Gamma H/a = 1$ curve denotes the vertical eigenvalues of the rigid wall at $x = 0$ case. We notice that for small values of $\Gamma H/a$, mH is smaller than 1 until $a\ell \sim 1/(\Gamma H/a)$, or when $\Gamma H/\ell| \sim 1$. For the case $\Gamma H/a = 1$, the vertical intensification scale mH is always greater than 1, indicating that all the modes show vertical intensification.

In Fig. 3-16 we show a plot of the frequency scaled by $\in N/S$ (the topographic buoyancy frequency), as a function of the along-the-slope wavenumber (ℓa) , scaled by the shelf width.
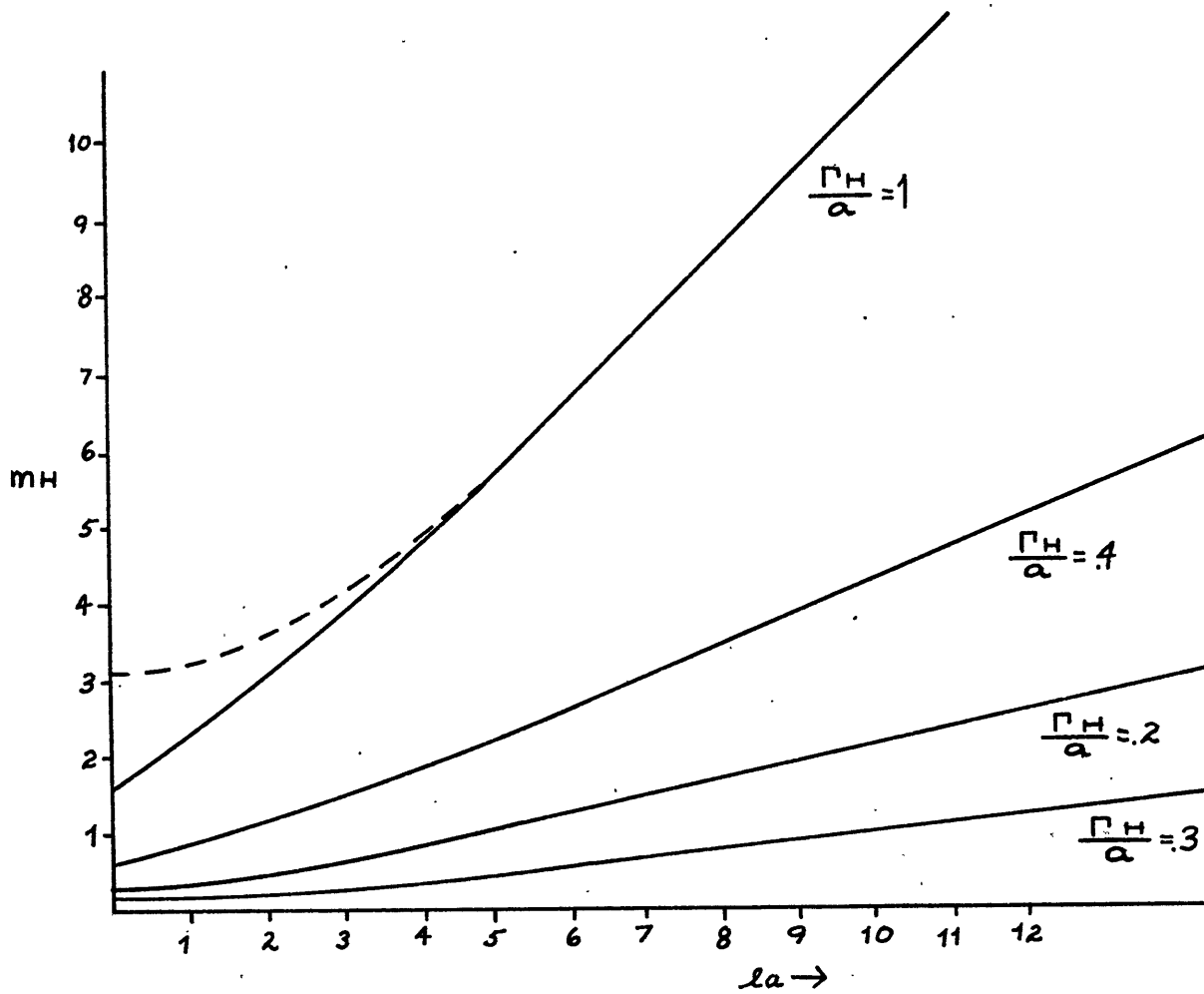
Fig. 3-15. Plot of the calculated values of the vertical intensification scale as a function of the along-the-slope wavenumber.

We plotted the curves for different values of $\Gamma H/\alpha$.

$\Gamma H/\alpha$ roughly compares the topographic scale α to the cut-off scale for bottom-intensification ΓH . For
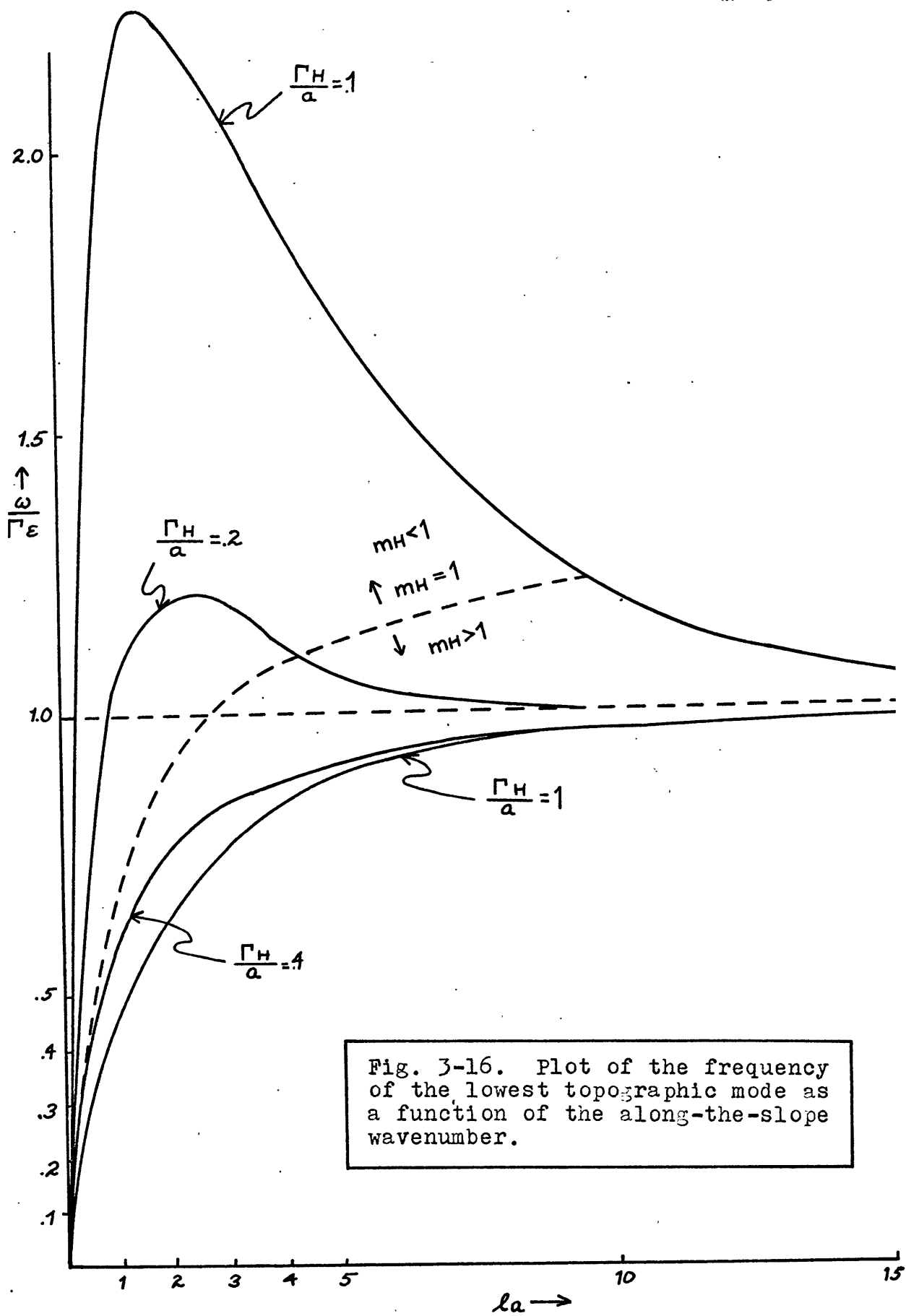
Fig. 3-16. Plot of the frequency of the lowest topographic mode as a function of the along-the-slope wavenumber.

a constant ΓH , we can think of $\Gamma H/a$ as defining

the dispersion relations for shelfs of different widths.

For example, if $\Gamma = 10$ and $H = 4 km$, $\Gamma H/a = .1$

implies a width $a = 400 km$; for $\Gamma H/a = 1, a = 40 km.$

The line of constant penetration depth mH has been

drawn to help identify the regions of vertical intensifica-

tion. There is a problem in visualizing the lines of

constant mH in a plot for ω vs (la) because their pro-

jections on this plane appear to converge on the origin.

In Fig. 3-17 we will show a sketch of the three-dimensional

surface.

We notice that for small values of la the curves

are nondispersive and in agreement with the homogeneous

calculations. This is due to the fact that the velocities

of the waves lie very closely along the depth contours.

For the curve $\Gamma H/a = .1$, for example, as la increases,

the frequency rises rapidly beyond the buoyancy limit

$\Gamma \epsilon = \omega$. The topographic waves do not feel the

effects of stratification at such long wavelengths. The

frequency reaches a maximum at approximately the point

where the along-the-slope wavelength becomes about the

same order as the up-slope wavenumber $\lambda_m a \sim 2$

(fixed by the mode number). It is in this range of

wavelengths that the motion can feel the full impact

of vortex stretching. As la increases, the frequency decreases because the wavelength becomes small. However, unlike the homogeneous limit, the frequency cannot decrease indefinitely. As soon as the length scales become less than $N/_{S} H \text{DEPTH}$, the buoyancy regime begins to dominate. The frequency does not decrease below $(\Gamma \epsilon)$ because, as la increases, the velocity field is turning all the time in the direction of maximum depth change (the up-slope direction).

For $\Gamma H/_{a} = 1$ and $\Gamma H/_{a} = .4°$, the vertical structure of the oscillations is vertically intensified for all the values of al. Therefore, the buoyancy effect dominates and the frequency never rises above $\Gamma \epsilon$. For large al, the frequency approaches $\epsilon \Gamma$ because the velocity vector turns in the up-slope direction feeling the full restoring force of the buoyancy effect $\epsilon \Gamma$.

We recall that the above calculations were made for the lowest mode of oscillation. Higher modes displace the curves towards the lower frequencies for any given along-the slope wavenumber. It is possible to find the normal modes for more complicated topography, such as a full sloping step, a ridge and a cylindrically symmetric seamount or island. The same general conclusions apply.
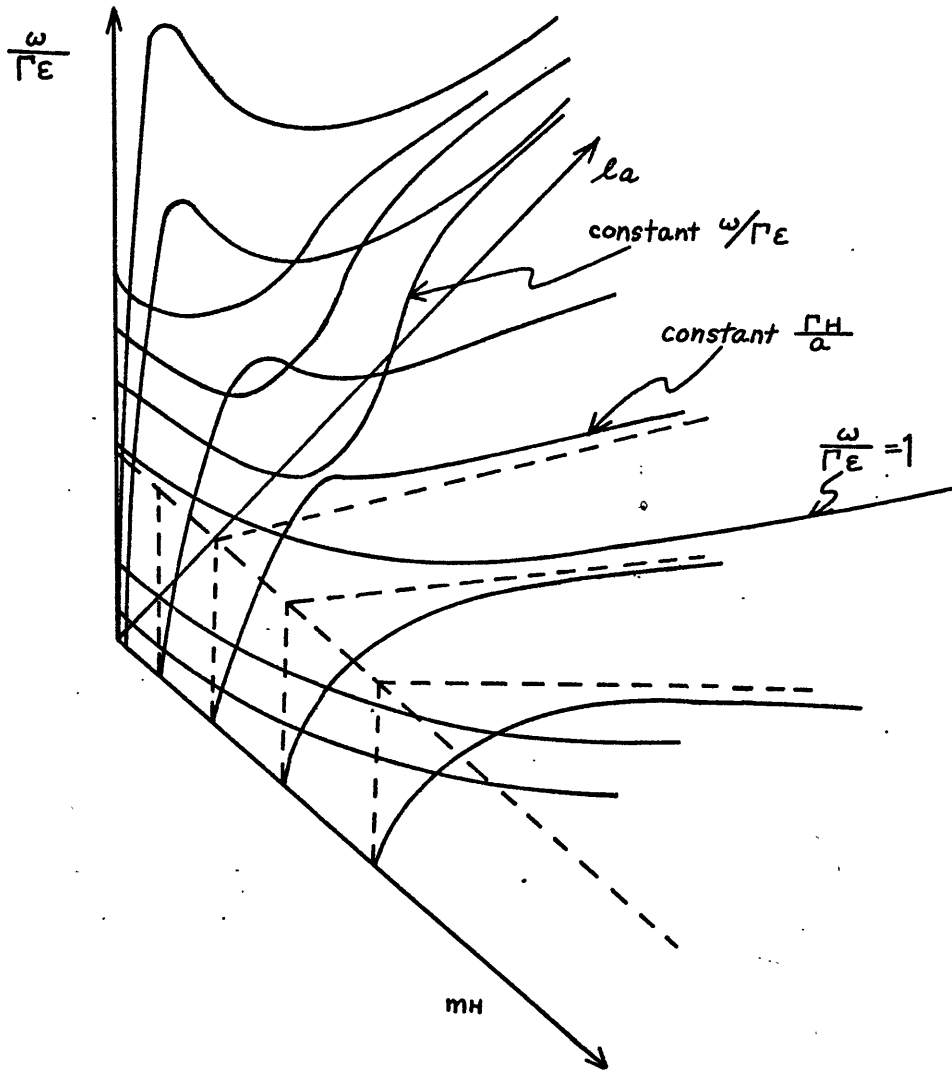
Fig. 3-17. A sketch of the three-dimensional surface
defined by the frequency, along-the-slope wavenumber and
the vertical intensification scale.

When the horizontal scale of the actual modes is less

than $\frac{N}{S}H_{DEPTH}$, their vertical structure shows

bottom-intensification. The eigenvalues of the modes are larger than those found in the homogeneous limit, indicating that the inclusion of stratification confines the motion more strongly to the topography.

Chapter IV. Some Aspects of the Local Generation of Bottom-intensified Topographic Oscillations

In the previous chapter we determined that bottom-intensified oscillations were not effectively generated by sources located in an adjacent topographic environment. The matching conditions at the intersection of the topographic regions yielded very small amplitudes for the waves with bottom-intensified scales $mH > 1$. Furthermore, in the high quasigeostrophic frequencies, Rossby waves could only excite depth-independent topographic oscillations. Our discussion on wave trapping also showed that bottom-intensified normal modes tended to remain confined within the immediate vicinity of the topography. From all this, it would seem that the presence of bottom-intensified oscillations at a given location in the ocean topography must be ascribed to local sources.

Sources of local energy for bottom-intensified motions can be divided roughly into two kinds. 1. Direct forcing of the topographic oscillations by some initially prescribed flow which has to be adjusted at a sloping boundary. We note that in order for the topographic oscillations resulting from such an adjustment to be bottom-intensified, the initially imposed flow must have

horizontal scales smaller than NH_{DEPTH}/ζ. 2. Indirect
forcing of the oscillations by the interaction of long-
scale, directly forced waves with bottom topography
possessing baroclinic scales, that is, $fL_T/N < H_{DEPTH}$
where L_T is a characteristic length scale for the
bottom topography, and H_{DEPTH} is the average depth of the
ocean in the general location. We discussed the free
solutions to such a situation in Chapter II, section
B, for a one-dimensional corrugated bottom.

In this chapter we will concentrate on the first
kind of source for bottom-intensified motions. In
section A we will discuss the response of a stratified
fluid over a sloping bottom to an initially imposed
geostrophic flow. In section B we will comment on the
wind generation of bottom-intensified oscillations.
In section C we will discuss the local interaction of
a steady shear current with topographic waves.

In the following pages we will deal with the
excitation of topographic oscillations over regions
which are horizontally unbounded. This kind of model
is clearly unrealistic, especially for the very long
scales. However, it is useful because the simplicity
obtained in the results leads to a clear understanding
of the character of the motion. In principle we are not

restricted to this over-simplification. The normal
modes that we found in the previous chapter could be
used to match the forced response over the topography
with regions exterior to it.

Section A. Response of the Fluid over a Sloping Bottom
to an Initially Imposed Geostrophic Flow

This problem is interesting because it illustrates
simply how the field of motion adjusts to the topographic
slope. Consider a simple sloping bottom described in
Fig. 4-1.
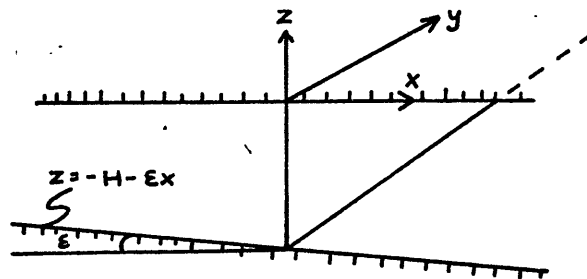
Fig. 4-1. Diagram describing the topographic region.

At a given time, over a sloping bottom, we prescribe
a geostrophic flow satisfying the thermal wind equations.
This state of motion may not be consistent with the
physical requirement of zero normal velocity over the
sloping bottom. This implies that the initial geostrophic
motion cannot remain unchanged, unless it was originally

prescribed to flow along constant-depth contours. In
general terms what happens is that the slope wipes out
that part of the initial disturbance that came in
contact with the bottom, and replaces the motion there
with time-dependent topographic oscillations. The
vertical structure of the topographic oscillations
will be bottom-intensified if the scales of the initially
imposed motion are less than $N/f \, H_{DEPTH}$.

Let us consider the problem in detail. When the
horizontal scales of the imposed motion L are small
enough so that the fractional change of depth over L
are small , $\delta \equiv \epsilon L/H \ll 1$, we can use the system of
equations derived in Chapter II,eqs. II-18, II-19a,b.
We recall that their derivation is based on a lineariza-
tion of the boundary condition on the sloping bottom,
and a scaling of the time-dependence by the small
parameter δ . The velocity, the pressure and the
density perturbation fields were expanded in terms of
δ to preserve the requirement that the basic state
of the system be geostrophic. The equations are

(IV. A-1)
$$\frac{\partial}{\partial \tau} \left(\nabla_1^2 p + \frac{1}{(r\lambda)^2} \, p_{zz} \right) = 0$$

the potential vorticity equation, to the lowest order in δ. Γ is the ratio $N/_{\xi}$ and λ measures the ratio of the horizontal scale L to the depth H. For simplicity we have set the planetary β -effect equal to zero. We will later discuss its effects. We recall that the above equation was derived under the assumption that the Rossby number R_o was small compared to the topographic parameter δ. The condition of no normal flow at the bottom slope yields

(IV. A-2)
$$\frac{1}{(\Gamma\lambda)^2} \frac{\partial}{\partial T} p_z = -p_y \qquad z = -1$$

and the condition of zero vertical velocity at the top yields

(IV. A-3)
$$\frac{1}{(\Gamma\lambda)^2} \frac{\partial}{\partial T} p_z = 0 \qquad z = 0$$

In order to calculate the topographic response for an initially imposed geostrophic flow we find it convenient to Laplace transform our equations. Let the Laplace transform of p be represented by $\bar{p}$.

(IV. A-4)
$$\bar{p}(x,y,z,s) = \int_0^\infty p(x,y,z,T) e^{-sT} dT$$

For simplicity we will say that the initial geostrophic flow is depth-independent. We will see, however, that the result can be extended to an initial geostrophic flow with arbitrary depth-dependence. We can think of the situation in two ways. At time $T=0$ a geostrophic flow is set up over the slope, or at $T=0$ the bottom is tilted over a region supporting a geostrophic flow. In both cases, $T=0$ actually denotes a time interval much longer than an inertial period.

We represent the geostrophic flow at $T=0$ simply by

(IV. A-5a) $$\frac{\partial}{\partial x} p(\vec{x},0) = \frac{\partial}{\partial x} P \equiv V(\vec{x},0)$$

(IV. A-5b) $$\frac{\partial}{\partial y} p(\vec{x},0) = \frac{\partial}{\partial y} P \equiv -U(\vec{x},0)$$

We find the eq. IV. A-1 becomes

(IV. A-6) $$\nabla_1^2 \bar{p} + \frac{1}{(\Gamma\lambda)^2} \bar{p}_{zz} = \frac{1}{S} \nabla_1^2 P$$

and the boundary conditions

(IV. A-7a) $$\frac{\partial}{\partial z} \bar{p} = 0 \qquad z=0$$

and

(IV. A-7b)
$$\frac{\partial}{\partial z}\bar{p} = -\frac{(\Gamma\lambda)^2}{s}\bar{p}_Y \qquad at \quad z = -1$$

In order to make the horizontal dependence as general as
possible we Fourier transform the equations in x, y.

(IV. A-9)
$$\bar{p} = \frac{1}{2\pi}\iint\limits_{-\infty}^{\infty} dk\, dl \, e^{-i(kx+ly)} \hat{p}(k,l,z,s)$$

and for the initial disturbance,

(IV. A-10)
$$P(x,y) = \frac{1}{2\pi}\iint\limits_{-\infty}^{\infty} e^{-i(kx+ly)} P(k,l)\, dk\, dl$$

In spectral form the equations become,

(IV. A-11)
$$\frac{d^2}{dz^2}\hat{p} - (\Gamma\lambda K)^2 \hat{p} = -\frac{(\Gamma\lambda K)^2}{s} P(k,l)$$

and

(IV. A-12a)
$$\hat{p}_z = 0 \qquad z = 0$$

(IV. A-12b)
$$\hat{p}_z = \frac{i(\Gamma\lambda)^2 l}{s}\hat{p} \qquad z = -1$$

The advantage of this scheme is that we generalize as
much as possible the form of x-, y-dependence of the
initial condition, while at the same time we single
out the z-dependence for special treatment. Let
be represented by,

(IV. A-13)
$$\hat{\wp} = A(k,\ell,s)\cosh mz + C(k,\ell,s)$$

Substituting in IV. A-11 we obtain, $m^2 = (\Gamma\lambda k)^2$ and
$C = \frac{1}{5}\wp(k,\ell)$. The vertical structure of the bottom-
intensified solution is given directly by the horizontal
scales of the motion times the ratio $N/_f$, as we
have seen before (in dimensional form $m = N/_f K$).
Solution IV. A-13 automatically satisfies the boundary
condition at the top, $z = o$. The boundary condition
at the bottom slope, eq. IV. A-12b, provides the coupling
between the amplitude of the depth-independent geostrophic
flow and the induced bottom-intensified motion. Substitu-
ting eq. IV. A-13 in IV. A-12b, we find

$$A(k,\ell,s) = -\wp(k,\ell)\left[\frac{1}{s} - \frac{1}{s+i(\Gamma\lambda)\frac{\ell}{k}\frac{1}{\tanh\Gamma\lambda k}}\right]\frac{1}{\cosh\Gamma\lambda k}$$

for the amplitude of the bottom-intensified motion.
Let $\dfrac{\Gamma\lambda}{\tanh\Gamma\lambda k} \equiv \Omega(k)$ which in the theory of

bottom-intensified oscillations represents the buoyancy

oscillation frequency, or the maximum allowed frequency

of the waves for a given topographic slope (see Chapter II,

eq. II. A-2). The solution to eq. IV. A-11 can be

written as,

(IV. A-15)

$$\hat{p}(k,\ell,z,s) = \mathcal{P}(k,\ell)\left\{\frac{1}{s}\left(1-\frac{\cosh \eta k z}{\cosh \eta k}\right) + \frac{1}{s+i\frac{\ell}{k}\Omega(k)}\frac{\cosh \eta k z}{\cosh \eta k}\right\}$$

By inspection we see that the Laplace transform inverse

can be readily performed. The solution,

(IV. A-16)

$$p(x,y,z,T) = \iint\limits_{-\infty}^{\infty} \frac{dk\,d\ell}{2\pi}\, \mathcal{P}(k,\ell)\left\{\left(1-\frac{\cosh \eta k z}{\cosh \eta k}\right)e^{-i(kx+\ell y)} + \frac{\cosh \eta k z}{\cosh \eta k}\right.$$

$$\left. \times \exp{-i(kx+\ell(y+\frac{\Omega T}{k}))}\right\}, T>0$$

$$= 0 \quad , \quad T<0$$

The elementary response (the solution inside the

parenthesis) consists of two parts: a steady component

which has zero horizontal velocity at the bottom, and a

wave component which has the general form of the bottom-

intensified mode, and which propagates with a component

of the phase velocity to the left when looking up-slope.

We notice that at $T=0$ the hyperbolic solutions cancel each other and we are left with the initial disturbance. For $T>0$ the slope has cancelled out that part of the initial disturbance that came in contact with the bottom, and replaced the motion there by time-dependent topographic oscillations.

If we substitute eq. IV. A-16 in the original eqs. IV. A-1, IV. A-2 and IV. A-3, we see that after $T=0$ the steady term has no effect on the equations because it is time-independent and is zero at the bottom slope. From this is clear that the initial geostrophic disturbance could have been dependent on the vertical coordinate because the only part of the flow that induces the topographic oscillations is its value at the bottom. We can generalize the solution to be

(IV. A-17)

$$p(x,y,z,T) = \iint_{-\infty}^{\infty} \frac{dk\,dl}{2\pi} P(k,l) f_{\vec{k}}(z=-1) \left\{ \left(\frac{f_{\vec{k}}(z)}{f_{\vec{k}}(z=-1)} - \frac{\cosh \eta \lambda k z}{\cosh \eta \lambda k} \right) e^{-i\vec{k}\cdot\vec{x}} \right.$$

$$\left. + \frac{\cosh \eta \lambda k z}{\cosh \eta \lambda k} e^{-i\left(kx + l\left(y + \frac{\Omega}{k}T\right)\right)} \right\}$$

where $f_{\vec{k}}(z)$ is the z-dependence of the $\vec{k}$ component of the initial pressure disturbance. As one expects if $f_{\vec{k}}(z=-1) = 0$ there is no adjustment required. In Fig. 4-2

we show a sketch of the horizontal velocity field

projected in the up-slope direction.
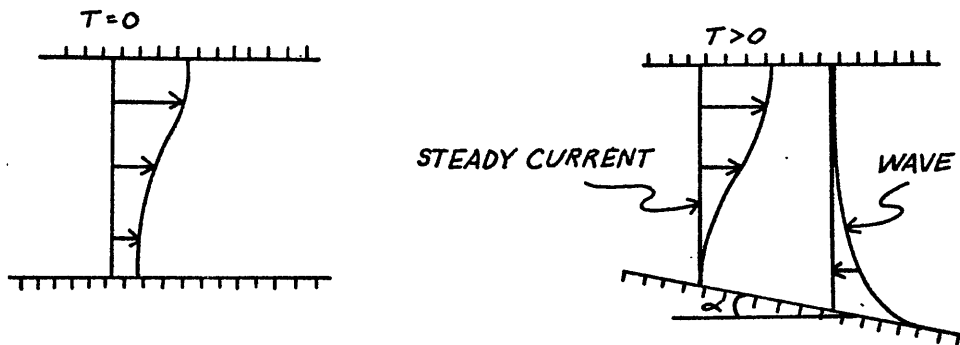
Fig. 4-2. Diagram illustrating the vertical structure
of geostrophic currents.

In order to best discuss the solution we change the

representation of p to dimensional form

(IV. A-18)

$$p(x,y,z,T) = \iint_{-\infty}^{\infty} \frac{dk\,dl}{2\pi}\, P(k,l) \left\{ \left(1 - \frac{\cosh \pi k z}{\cosh \pi k H}\right) e^{-i(kx+ly)} + \frac{\cosh \pi k z}{\cosh \pi k H} e^{-i\left(kx+l\left(y+\frac{\alpha}{k}T\right)\right)} \right\}$$

for the depth-independent initial disturbance. H is

the depth and α in the time dependence is $\epsilon \Gamma / \tanh \pi k H$,

where ϵ is the slope. Let us take a specific form of $P(k,l)$

$$P(k,l) = 2\pi\, \delta(k-k_0)\, \delta(l-l_0)$$

which corresponds to a simple sinosoidal wave oriented

at an angle with $\theta = \tan^{-1}\frac{l_0}{k_0}$ respect to the slope. We

first note that expression IV. A-18 yields the homogeneous
limit for very small ΓK_0 , as one expects. The
topographic motion will be depth-independent when the
horizontal scales of the imposed motion yield a vertical
penetration scale $\frac{1}{\Gamma K_0}$ larger than the depth of the
ocean, $\frac{1}{\Gamma K_0} >> H$. The frequency α in this limit becomes
the well-known topographic β-effect frequency, independent
of stratification, but dependent on the horizontal scale,
$\alpha = \epsilon/k_0 H$. The steady part of the solution essentially
disappears, i.e. $\frac{\cosh \Gamma K_0 z}{\cosh \Gamma K_0 H} \rightarrow 1$ and the whole column of
fluid is rigidly coupled in the vertical to execute the
oscillations

(IV. A-19)
$$p(x,y,z,T) = e^{-i\left(k_0 x + l_0 y + \frac{l_0}{k_0^2}\epsilon T\right)}$$

When the scales of the imposed motion are less than
$(\Gamma k)^{-1} < H$, the elementary solutions become decoupled
in the vertical because stratification weakens the
rigidity of the vertical columns of fluid. There is a
steady part which is not in contact with the topography
(that is why it is steady), and a time-dependent oscilla-
tion which is concentrated at the bottom. We notice
that the steady geostrophic flow can be quite arbitrary
in its horizontal structure. It does not have to flow

along the depth contours to remain steady as in the
homogeneous limit because its motion does come in contact
with the topography. We notice that if $\ell = 0$, that is,
a current flow along the contours, then the initial
motion is not disturbed by the topography and there
are no waves excited.

It might be helpful at this point to sketch the
streamline pattern (instantaneous) for the simple
disturbance in the case of bottom-intensification,
$\Gamma(k_0^2 + \ell_0^2)^{1/2} \ll H$ (Fig. 4-3). We set
$P(k,\ell) = 2\pi\, \delta(k-k_0)\, \delta(\ell+\ell_0)$ in eq. IV. A-18 and take the
real part to obtain

(IV. A-20)

$$Re\, p = \left(1 - \frac{\cosh \Gamma k_0 z}{\cosh \Gamma k_0 H}\right)\cos(k_0 x + \ell_0 y) + \frac{\cosh \Gamma k_0 z}{\cosh \Gamma k_0 H}$$

$$\times \cos\left(k_0 x + \ell_0 \left(y + \frac{\alpha T}{k_0}\right)\right)$$

Another simple calculation can be made if we take
the initial disturbance to be a cylindrically symmetric
δ-function in K-space, i.e. $P(K) = \frac{1}{K}\,\delta(k - k_0)$.
This corresponds to the zeroth order Bessel function
in the space coordinates $P(r) = J_0(k_0 r)$. The above
disturbance is interesting because the dispersion
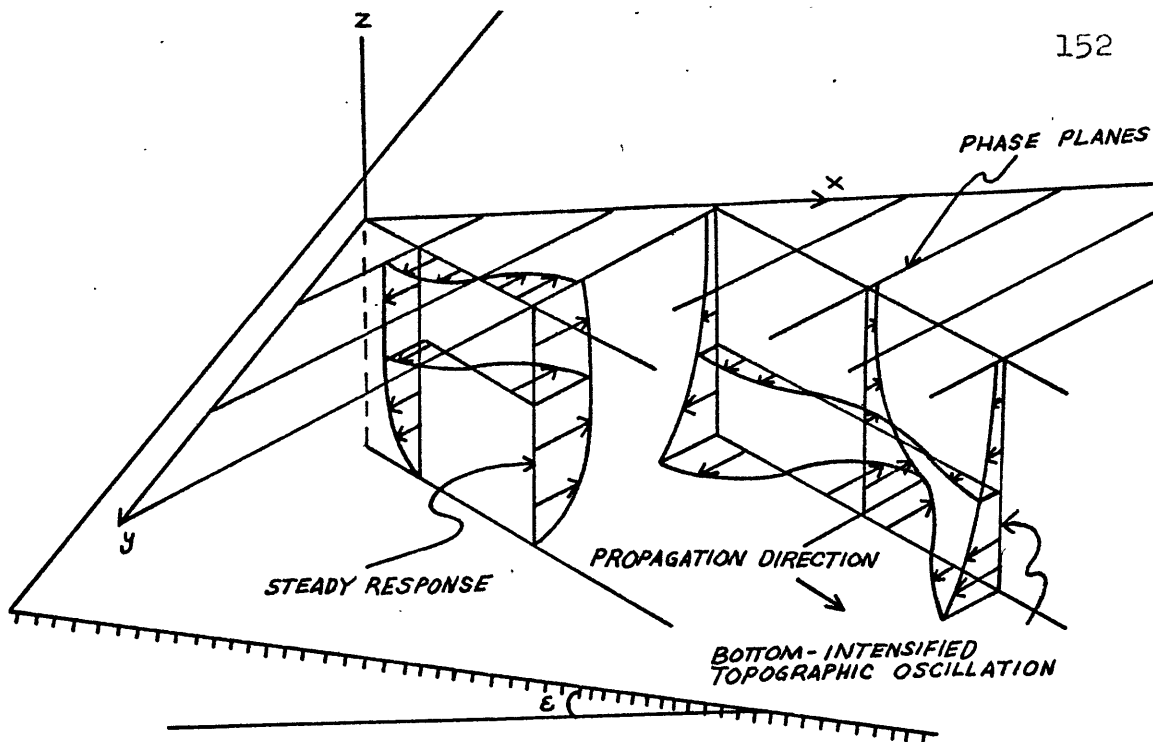
Fig. 4-3. A sketch of the bottom-intensified wave and the steady current resulting from the adjustment of an initial disturbance to the topography.

relation of the topographic oscillations is highly directional, as we already saw in Chapter II, section A, and as we can readily see in the time-dependence of integral IV. A-18, i.e. $\omega = - \ell/\kappa \frac{\Gamma\epsilon}{\tanh \Gamma\kappa H}$. A disturbance of the form $J_0(\kappa_o r)$ is the simplest way one can model the directional properties (in this case we fix the magnitude of the wavenumber but not its direction). Substituting for $P(k)$ in eq. IV. A-18 we find

(IV. A-21)

$$p(x,y,z,\tau) = \left(1 - \frac{\cosh \Pi \kappa_o z}{\cosh \Pi \kappa_o H}\right) J_0(\kappa_o r) + \frac{\cosh \Pi \kappa_o z}{\cosh \Pi \kappa_o H} \int_0^{2\Pi} \frac{d\theta}{2\Pi} e^{-i\left(\kappa_o r \cos(\theta-\beta) + \frac{\epsilon \Gamma \cos\theta \tau}{\tanh \Pi \kappa_o H}\right)}$$

where the angles appearing in the integral are defined

in Fig. 4-4.
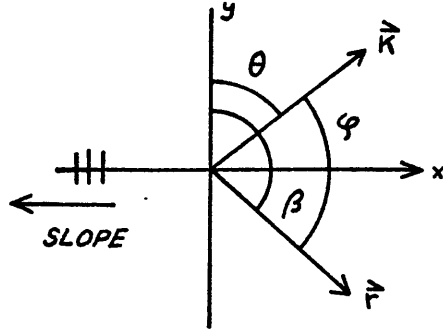
Fig. 4-4. Figure describing the angles appearing in eq. IV. A-21.

The integral is just equal to

(IV. A-22a)

$$\int_0^{2\pi} \frac{d\theta}{2\pi} e^{-i\left(k_0 r \cos(\theta-\beta) + \frac{\epsilon \Gamma \cos\theta}{\tanh \Gamma k_0 H} T\right)} = J_0\left(\sqrt{k_0^2 r^2 + 2k_0 r \epsilon \Gamma T \frac{\cos\beta}{\tanh \Gamma k_0 H} + \frac{\epsilon^2 \Gamma^2 T^2}{\tanh^2 \Gamma k_0 H}}\right)$$

or in terms of x- and y-coordinates

(IV. A-22b)

$$J_0\left(\sqrt{k_0^2 x^2 + \left(k_0 y + \frac{\epsilon \Gamma}{\tanh \Gamma k_0 H}\right)^2}\right)$$

Again the topographic slope has wiped out the initial

disturbance at the bottom. The topographic response,

concentrated at the bottom if $\Gamma k_0 H > 1$, propagates

as a whole along the slope without change of shape (Fig. 4-5).
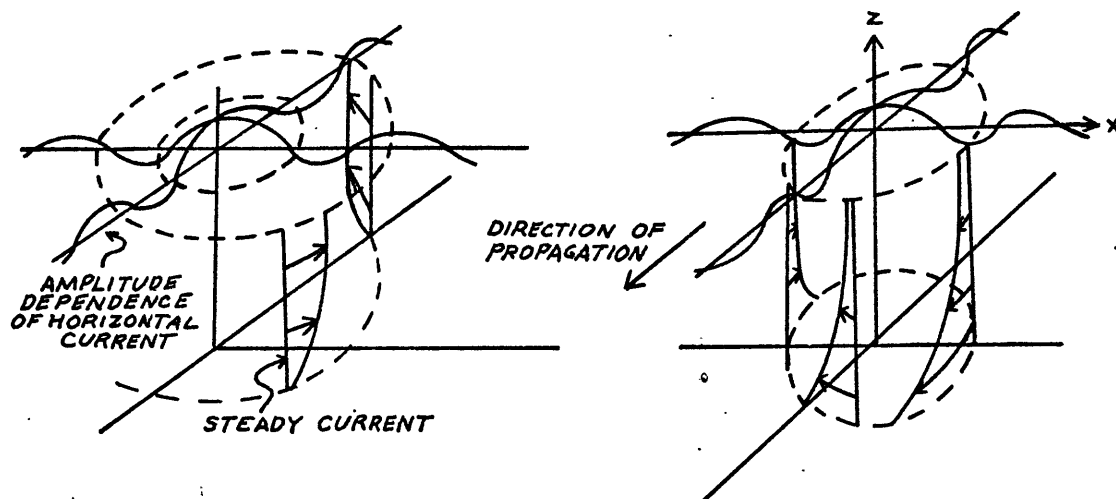
Fig. 4-5. Sketch of the topographic oscillations excited by a cylindrically symmetric disturbance over a sloping shelf.

The propagation without change of shape is understandable in terms of the propagation of the elementary plane waves that appear in the integral IV. A-22a.

If we set $P(k,\ell)=1$ in eq. IV. A-18, the integral represents the Fourier transform of the two-dimensional Green's function that describes the response of the fluid

to a unit impulse. Eq. IV. A-21 is the actual form
of the transform where ρ now means the distance
between the source point and the point of observation.
Eq. IV. A-22b is the form of the horizontal and time-
dependence of the elementary components of the topographic
oscillations.

The effects of viscous dissipation at the sloping
boundary can be introduced by the use of the Ekman
compatibility condition. The modifications to the
normal mode solutions have been discussed in Chapter II,
section A (page 48). Here we wish to make the point
that if the scales of the initially imposed motion lead
to topographic bottom-intensified oscillations, the steady
part of the solution is unaffected by the dissipative
processes at the lower boundary. The topographic
oscillations concentrated at the bottom eventually decay
due to frictional effects, whereas the steady flow
persists for a much longer time. (For horizontal scales
longer than $N H_{DEPTH}/f$ the whole column is affected by
the frictional effects at the bottom.) The implications
of this partition of the motion in the vertical is
that over a sloping bottom one would expect to find
low-frequency horizontal kinetic energy in the baroclinic
scales leading to bottom intensification, $L \leq \dfrac{N}{f} H_{DEPTH}$.

This energy will decrease as we approach the bottom
slope. This simple picture is complicated by the
fact that surface stresses with horizontal baroclinic
scales would produce an equivalent effect.

In the above paragraph we used the phrase "low-
frequency" for two reasons. 1. If we include the
planetary β -effect in the considerations that
lead to the solution of the initial value problem, the
interior flow over the topographic slope will no
longer remain steady. The general solution including
both effects is quite difficult to solve analytically.
In the special case where the topographic restoring
force is much stronger than the planetary β -effect
and the horizontal scales $L \leq \frac{N}{f} H_{DEPTH}$, the modifica-
tion to the interior flow is simply to introduce a phase
propagation with a component to the west. The bottom-
intensified oscillations essentially remain unchanged
because they are in contact with the bottom slope where
the topographic effect dominates. 2. We neglected non-
linear effects in the solution. This is justifiable for
the bottom-intensified oscillations because we assumed
that the topographic restoring force dominated the process.
However, we see that since the interior flow is not in
contact with the topography, the small nonlinearities

will eventually affect the motion. The structure
of the "steady" flow will slowly evolve with time due
to nonlinear advection.

At this point one cannot help but speculate about
the previously mentioned Site D observations. The
frequency spectrum calculated by Thompson showed that
the horizontal kinetic energy decreased with depth for
periods greater than about 30 days. For smaller periods
the frequency spectrum was depth-independent. Thompson
(19) and Rhines (20) suggested that the
high-frequency contributions to the spectrum were
due to depth-independent Rossby topographic oscillations,
implying that the horizontal scales of these motions
had to be larger than $N H_{DEPTH} / f$. Perhaps part
of the energy found at the lower frequencies is due
to drifting eddies originating in the adjustment of
disturbances with the baroclinic scales($L \leq N H_{DEPTH} / f$)
to the sloping bottom. These disturbances will also
generate bottom-intensified oscillations, but they
decay due to frictional effects. Of course, this does
not rule out the possibility that part of the low-frequency
contributions to the energy spectrum could be due to
horizontally trapped waves of the sort we discussed in
the previous chapter. We recall that for low,

along-the-slope phase velocities, these waves had a
node on the topography. They are excited in the
adjustment of a time-dependent disturbance impinging
on a region with a sloping bottom. We also recall,
however, that the $\overline{uv}$ correlation of these waves
was zero, whereas there is no reason why the advecting
eddies produced by the vertical decoupling of the motion
would have such a property.

Section B.   Wind Generated Bottom-intensified Oscillations

In the open ocean one possible source of local energy for bottom-intensified oscillations is wind stress over the surface. We wish to comment on the effectiveness of this source of energy in exciting bottom-intensified topographic waves.

Let us consider a constant sloping bottom. The slope is constant in the sense that it does not vary over distances larger than the imposed horizontal scales on the fluid. We also take the slope to be small in the sense that the fractional change of height over the imposed wave scale is small compared to the mean depth. We will show that over a constant sloping bottom the direct effects of wind stress over the surface will not effectively excite bottom-intensified oscillations with penetration scales smaller than the mean depth of the region.

Consider a sloping bottom represented by Fig. 4-6.
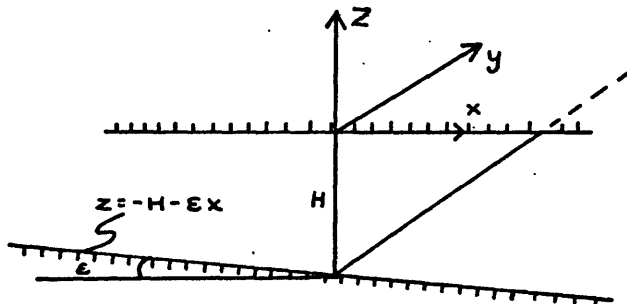
Fig. 4-6.   Diagram describing the topographic region.

We are interested in the excitation of topographic oscillations by an applied wind stress that is gradually turned on and after some time is again gradually turned off. The time scale for the changes in the wind is considered to be long compared to an inertial period. Following Holton (3) we represent the effects of the wind stress by a vertical velocity at the base of the Ekman layer at the surface

$$w_E = \hat{k} \cdot \text{curl } \vec{\tau}/_f$$

where $\vec{\tau}$ is the wind stress and f the coriolis parameter.

For the treatment of this problem we can use eqs. II-11a to II-11e in Chapter II. By assumption we set the Rossby number and the planetary β -effect equal to zero. In this problem the interior vertical velocity is matched to the wind stress vertical velocity at the base of the Ekman layer. The boundary condition on the sloping bottom is given by the condition of no flow into the boundary. Since we are interested in topographic oscillations excited by the wind, we scale our time dependence by the topographic parameter $\delta = \epsilon l/H \ll 1$. We recall that this parameter measures the fractional change of depth of the topographic region over a wave

scale (L). In this case (L) refers to the
imposed scale of the wind. We scale the amplitude of
the horizontal velocities in the interior by $\tau_0/H f \delta$
where τ_0 is the amplitude of the wind stress and
H is the mean depth. This guarantees that our non-
dimensional interior horizontal velocities will be
order one.

Following the procedure described in Chapter II
we obtain a set of non-dimensional scaled equations
for the lowest order quasigeostrophic pressure field.
For the interior motion we have

(IV. B-1)

$$\frac{\partial}{\partial T}\left(\nabla_1^2 p^{(o)} + \frac{1}{(\Gamma\lambda)^2} p_{zz}^{(o)} \right) = 0$$

where $\Gamma\lambda$ is equal to $NH/f L$. L is the imposed
scale of the wind stress and H is the mean depth. At
the surface we have

(IV. B-2)

$$\frac{1}{(\Gamma\lambda)^2} \frac{\partial}{\partial T} p_z^{(o)} = -\tilde{w}$$

where $\tilde{w}$ is the non-dimensional vertical velocity
at the base of the surface Ekman layer induced by the

stress. The above equation describes the matching between the interior motion and the wind. At the sloping bottom we have the condition of no flow into the boundary

(IV. B-3)
$$\frac{1}{(\Gamma\lambda)^2}\frac{\partial}{\partial T}p_z^{(0)} = -p_y^{(0)} \qquad z = -1$$

We recall that the bottom boundary condition was linearized about the mean depth because $\delta \ll 1$.

Let us take a simple spatial and time representation for $\tilde{w}$.

(IV. B-4)
$$\tilde{w} = \tilde{w}_0\, e^{-i(kx+ly)} \begin{cases} 0 & T < 0 \\ 1 & T_0 > T > 0 \\ 0 & T > T_0 \end{cases}$$

Using Laplace transform techniques as in the previous section we arrive at the following solution for $p^{(0)}$. During the forcing period $0 < T < T_0$ we find

(IV. B-5)
$$p^{(0)} = -\frac{\Gamma\lambda}{k}\tilde{w}_0 \left\{ T\frac{\sinh\Gamma\lambda K(1+z)}{\cosh\Gamma\lambda K} + \frac{1}{i\frac{l}{k}\Omega}\frac{(1-\tanh^2\Gamma\lambda K)\cosh\Gamma\lambda Kz}{\tanh\Gamma\lambda K} \right.$$
$$\left. -\frac{1}{i\frac{l}{k}\Omega}e^{-i\frac{l}{k}\Omega T}\frac{(1-\tanh^2\Gamma\lambda K)\cosh\Gamma\lambda Kz}{\tanh\Gamma\lambda K} \right\}e^{-i(kx+ly)}$$

After the forcing stops $T > T_0$ we find

(IV. B-6)

$$p^{(0)} = -\frac{\Gamma\lambda}{k}\tilde{W}_0 \left\{ \frac{T_0 \sinh \Gamma\lambda k(1+z)}{\cosh \Gamma\lambda k} + \frac{1}{\frac{i\ell}{k}} \left(e^{-i\frac{\ell}{k}\Omega(T-T_0)} - e^{-i\frac{\ell}{k}\Omega T} \right) \right.$$
$$\left. \times \frac{(1-\tanh^2\Gamma\lambda k)}{\tanh \Gamma\lambda k} \cosh \Gamma\lambda k z \right\} e^{-i(kx+\ell y)}$$

Solution IV. B-5 satisfies the initial condition of no motion at $T=0$. In the above solutions $\Omega = \Gamma\lambda/\tanh\Gamma\lambda k$. For the vertical penetration scale of the topographic oscillations smaller than the mean depth of the region,

$\Gamma\lambda k > 1$, Ω is the buoyancy frequency of the bottom-intensified oscillations (see Chapter II, page 35). For $\Gamma\lambda k \ll 1$, the vertical penetration scale of the

$\cosh \Gamma\lambda k z$ function larger than the depth of the region, Ω is the maximum frequency due to the vortex stretching of the fluid over the sloping bottom. We see that the actual frequency of the oscillations depends on the angle the wavenumber makes with the along-the-slope direction ℓ/k. We also note that the oscillations propagate with a component of the phase velocity to the left when looking up-slope. The solution for $p^{(0)}$ is not singular at $\ell=0$ as can be easily demonstrated by taking the limit $\ell \to 0$.

Some of the features of the solution are: 1. During

the forcing period there is a directly driven horizontal current with a node on the topography. As in the initial value problem discussed in section A, topographic oscillations are excited to compensate for the adjustment of the directly driven horizontal current on the sloping bottom. However, associated with the directly driven flow, there is a small vertical velocity. To compensate, the fluid responds with a time-independent bottom-intensified wave. This makes the velocity normal to the sloping bottom zero. When the forcing stops,

$T > T_o$, there is no longer a directly driven current. The previously time-independent bottom-intensified response becomes a topographic oscillation.

Our main interest here lies in the factor $(1 - \tanh^2 \Gamma \lambda K)$ multiplying all the terms with the bottom-intensified form $\cosh \Gamma \lambda K \, Z$. We see that when $\Gamma \lambda K$ is numerically larger than 2 , the term becomes negligibly small. This indicates that the amplitude of the bottom-intensified mode becomes very small when the e-folding penetration distance of the surface stress is smaller than about half the mean depth of the region. For $\Gamma \lambda K = 1$, that is, an e-folding penetration distance equal to the mean depth, the term $(1 - \tanh^2 \Gamma \lambda K)$ is equal to .5 indicating that weak

bottom-intensification of topographic waves can be

excited by surface stresses with horizontal scales

L equal to $N H_{DEPTH} / f$. For example, if $N/f = 20$

and $H = 5 Km$, then $L = 100 Km$. The behavior of

the function $1 - \tanh^2 N/f \, K H_{DEPTH}$ versus $\frac{N K}{f} H_{DEPTH}$,

the ratio of the depth to the penetration scale of the

topographic oscillations, indicates that there is a

sharp cut-off in the amplitude of the oscillations

beyond $N/f \, K H_{DEPTH} = 1$. As one expected, the topographic

oscillations most effectively generated by the wind

over a constant slope have essentially a barotropic

structure, $N/f K H_{DEPTH} \ll 1$. This is so because for

horizontal scales $L \doteq K^{-1}$ much larger than $N H_{DEPTH} / f$,

the direct effects of surface stresses can penetrate

to the bottom without attenuation.

We should emphasize that the above calculations

were done for constant Brunt-Vaisala frequency. The

highter values of N found in the thermocline will

tend to further reduce the penetration of the wind

stress for a given horizontal scale. This implies that

the scale of effective surface disturbances would have

to be larger than the simple constant N theory suggests.

As a final point we wish to mention that the

effectiveness of wind stress in generating bottom-

intensified oscillations is considerably enhanced if
the topography has small-scale features. The condition
for the surface stresses to be effective is the same
as before, that is, they must be sufficiently long-
scaled to penetrate to the topography. However, the
response of the fluid will now partially consist of
topographic motions with horizontal scales induced by
the topography. If the typical topographic scale L_T
is baroclinic ($L_T \leq \frac{N}{f} H_{DEPTH}$), a portion of the
energy of the wind should go to support bottom-intensified
motions.

Section C. The Local Interaction of Topographic Waves
with a Steady Shear Current

We wish to consider the interaction of topographic
oscillations with a steady horizontal shear current
over a simple sloping bottom without considering the
source of the topographic waves' energy. In order to
consider the problem in its simplest possible context,
we assume that the current is flowing along depth
contours. We also assume that the current is being
supported by a pressure gradient whose presence is
external to the problem.

The situation described above is interesting for
the following reasons. 1. The main effect of the
shear is to rotate the phase planes in the direction
of the current. The turning of the phase planes shortens
the wavelengths of the topographic oscillations. We
recall that the vertical structure of the topographic
oscillations is simply coupled to the horizontal
wavelengths by the interior potential vorticity equation.
As the wavelengths decrease due to the tilting of the
phase planes by the shear, the vertical structure
intensifies at the bottom. Thus we see that the shear
provides a mechanism for the continuous production of
bottom-intensified oscillations. A depth-independent

wave entering the region of shear could be transformed
into a bottom-intensified oscillation as the wave propagates
into the shear current. 2. The local interaction of
the topographic oscillations with the shear reduces the
frequency of the oscillations and leads to a gradual
transfer of the wave energy to the mean current.

1. Derivation of the Equations

Consider a topographic region described in Fig. 4-7 .
The slope is taken to be small in the usual sense, that
is, the fractional change of depth over a wave scale
is small compared to the mean depth $\epsilon^{L}/\mu \equiv \delta \ll 1$.
Flowing along depth contours we have a barotropic current
with a mean shear in the up-slope direction. We consider
that the variation of the velocity with the up-slope
coordinate over a scale of order the horizontal wavelength
of the topographic waves can be approximated locally
by a linear shear

$$V(x) \simeq V_o + \gamma x$$

From equations II-1 to II-6b in Chapter II we can
obtain a quasilinearized set of equations to describe
the interaction of the topographic oscillations with
the mean steady flow. We assume that the Rossby
number of the self-interaction of the perturbation
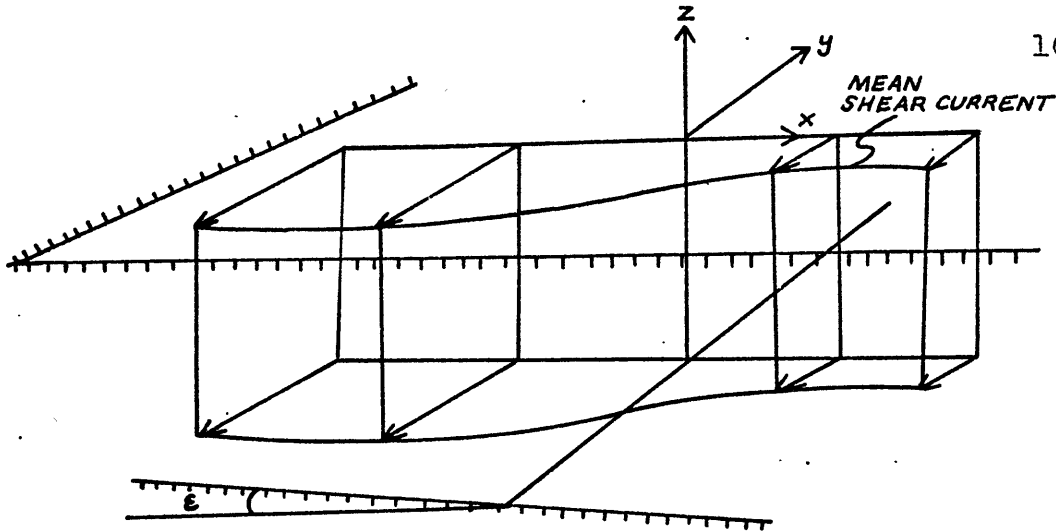
Fig. 4-7. Illustration of a mean shear over a sloping shelf.

fields is much smaller than the Rossby number that describes the interaction of the perturbation fields with the mean flow. This simply means that the amplitudes of velocities associated with the topographic oscillations are taken to be much smaller than the amplitude of the mean flow.

We recall that in the derivation of the equations describing the topographic oscillations in Chapter II, the time dependence was scaled by the small topographic parameter δ . The boundary condition at the bottom slope was linearized about the mean depth using a Taylor expansion in the small parameter δ . The fields were then expanded in terms of δ to obtain the lowest order equations for the quasigeostrophic

pressure field. Here we are interested in the interaction
of the quasigeostrophic topographic oscillations with
the mean shear. We take the Rossby number describing
this interaction to be comparable to the topographic
parameter. In the expansion of the equations we formally
keep the ratio of this Rossby number to the topographic
parameter δ whenever it appears in the equations.
Following the procedure described in Chapter II we
obtain a set of non-dimensional scaled equations for
the lowest order quasigeostrophic pressure field $p^{(0)}$.
For the interior equation we obtain

(IV. C-1)
$$\left(\frac{\partial}{\partial \tau} + \frac{R_o}{\delta} (1+\beta x) \frac{\partial}{\partial y} \right) \left[\nabla_1^2 p^{(0)} + \frac{1}{(\bar{\lambda})^2} p_{zz}^{(0)} \right] = 0$$

where $\bar{\lambda} = NH/fL$, R_o is the Rossby number based
on the amplitude of the mean flow over the topographic
wave scale. β is a non-dimensional shear which we
take to be order one. We do not make the assumption
that the shear is weak compared to the topographic
parameter δ . The potential vorticity equation
has been modified by the introduction of an advective
term due to the mean current.

At the rigid surface at the top we have the condition

of zero vertical velocity

(IV. C-2) $\qquad \left(\dfrac{\partial}{\partial \tau} + \dfrac{R_o}{\delta} \left(1 + \beta x \right) \dfrac{\partial}{\partial y} \right) p_z^{(o)} = 0 \qquad z = 0$

and at the sloping boundary we have the condition of
no normal flow into the boundary

(IV. C-3)
$$\left(\frac{\partial}{\partial \tau} + \frac{R_o}{\delta} \left(1 + \beta x \right) \frac{\partial}{\partial y} \right) p_z^{(o)} = - \left(\Gamma \lambda \right)^2 p_y^{(o)} \qquad z = -1$$

The above equations constitute our model equations to
study the interaction of topographic waves with a mean
shear. These equations bring to mind the equations
Rhines used in his study of two-dimensional turbulence
on a β -plane (12). His equations can be
obtained by vertically integrating the above equations
and replacing the advective term due to the mean shear
by the actual nonlinear advection due to the self-
interaction of the perturbation fields.

2. Solutions and Interpretations

To solve eqs. IV. C-1, 2 and 3 we assume a solution
of the form

(IV. C-4)

$$p^{(0)}(x,y,z,T) = f(T)\cosh\Gamma\lambda|\ell|(1+\alpha^2\beta^2T^2)^{1/2}z \; e^{\pm i|\ell|(y-\alpha(x+\beta x)T)}$$

where ℓ is the along-the-slope wavenumber of the solution. α is a symbol denoting the ratio of the Rossby number to the topographic parameter and β is the non-dimensional shear. The above solution can be interpreted as a quasigeostrophic topographic wave whose velocity at $T=0$ was oriented in the up-slope direction. The vertical structure of the solution at $T=0$ is given by $\cosh\Gamma\lambda|\ell|z$. The term $|\ell|\alpha\beta T$ denotes the up-slope wavenumber which is continually changing due to the turning of the phase planes by the shear. The equation for $p^{(0)}$ satisfies the interior equation IV. C-1 and the top boundary condition identically. The form of the function $f(T)$ and its dependence on time is determined by matching IV. C-4 in the lower boundary condition. We find that $f(T)$ is given by

(IV. C-5)

$$f(T) = \frac{G\,\Gamma\lambda|\ell|}{(1+\alpha^2\beta^2T^2)^{1/2}} \; \frac{1}{\sinh\Gamma\lambda|\ell|(1+\alpha^2\beta^2T^2)^{1/2}} \; \exp\left[\pm i\Gamma\lambda\int_0^T \frac{dT'}{(1+\alpha^2\beta^2T'^2)^{1/2}\tanh\Gamma\lambda|\ell|(1+\alpha^2\beta^2T^2)^{1/2}}\right]$$

where G is an arbitrary constant. Combining the above result with equation IV. C-4 we obtain an exact solution to our model equations for the lowest order quasigeostrophic pressure field.

(IV. C-6)

$$p^{(0)} = \frac{G \Gamma \lambda |\ell|}{(1+\alpha^2\beta^2\tau^2)^{1/2}} \frac{1}{+\tanh \Gamma\lambda|\ell|((1+\alpha^2\beta^2\tau^2)^{1/2}} \frac{\cosh \Gamma\lambda|\ell|(1+\alpha^2\beta^2\tau^2)^{1/2} z}{\cosh \Gamma\lambda|\ell|(1+\alpha^2\beta^2\tau^2)^{1/2}}$$

$$\times \exp \pm i\left(|\ell|(y-\alpha(1+\beta x)\tau + \Gamma\lambda \int_0^\tau \frac{d\tau'}{(1+\alpha^2\beta^2\tau'^2)^{1/2}} \frac{1}{+\tanh\Gamma\lambda|\ell|(1+\alpha^2\beta^2\tau^2)^{1/2}}\right)$$

The solution above represents a quasigeostrophic wave imbedded in the shear current. The wave amplitude, wavenumber, vertical structure and direction of propagation are being continually changed as the phase planes are rotated by the mean shear. The total wavenumber increases as $|\ell|(1+\alpha^2\beta^2\tau^2)^{1/2}$. Since the shear does not affect the along-the-slope wavenumber, the only way the phase planes can turn is by continually increasing the up-slope wavenumber. The associated velocity field continually rotates in the direction of the current, which is also the along-the-slope direction. We note that as the wavenumber increases the vertical structure of the topographic wave intensifies at the bottom slope. In a sense the steady shear current is bottom-intensifying the

topographic oscillations.

Differentiating the phase of the wave with respect to time, we determine that the frequency of the wave decreases as the angle of orientation of the wavenumber with respect to the along-the-slope direction increases

IV. C-7

$$\omega = -|\ell|\alpha(1+\beta x) + \frac{\Gamma\lambda}{(1+\alpha^2\beta^2\Gamma^2)^{1/2}} \frac{1}{\tanh \Gamma\lambda|\ell|(1+\alpha^2\beta^2\Gamma^2)^{1/2}}$$

The first term corresponds to the apparent frequency due to the translation of the waves by the mean current, while the second term corresponds to the actual frequency of the oscillations. The form of the last term is analogous to the frequency relation we found in Chapter II for topographic waves on the slope (eq. II. A-2). To see this, we simply replace $|\ell|(1+\alpha^2\beta^2\Gamma^2)^{1/2}$ by the wavenumber K . In Fig. 4- 8 we show a sketch of the phase planes being turned by the shear current. This figure is similar to the figure shown by Phillips (6) in his calculation of internal waves on a shear current.

In Fig. 4-9 we show a plot of the vertical structure of the wave at different instances in the turning of the phase planes by the shear. In this calculation we have chosen the following values for the
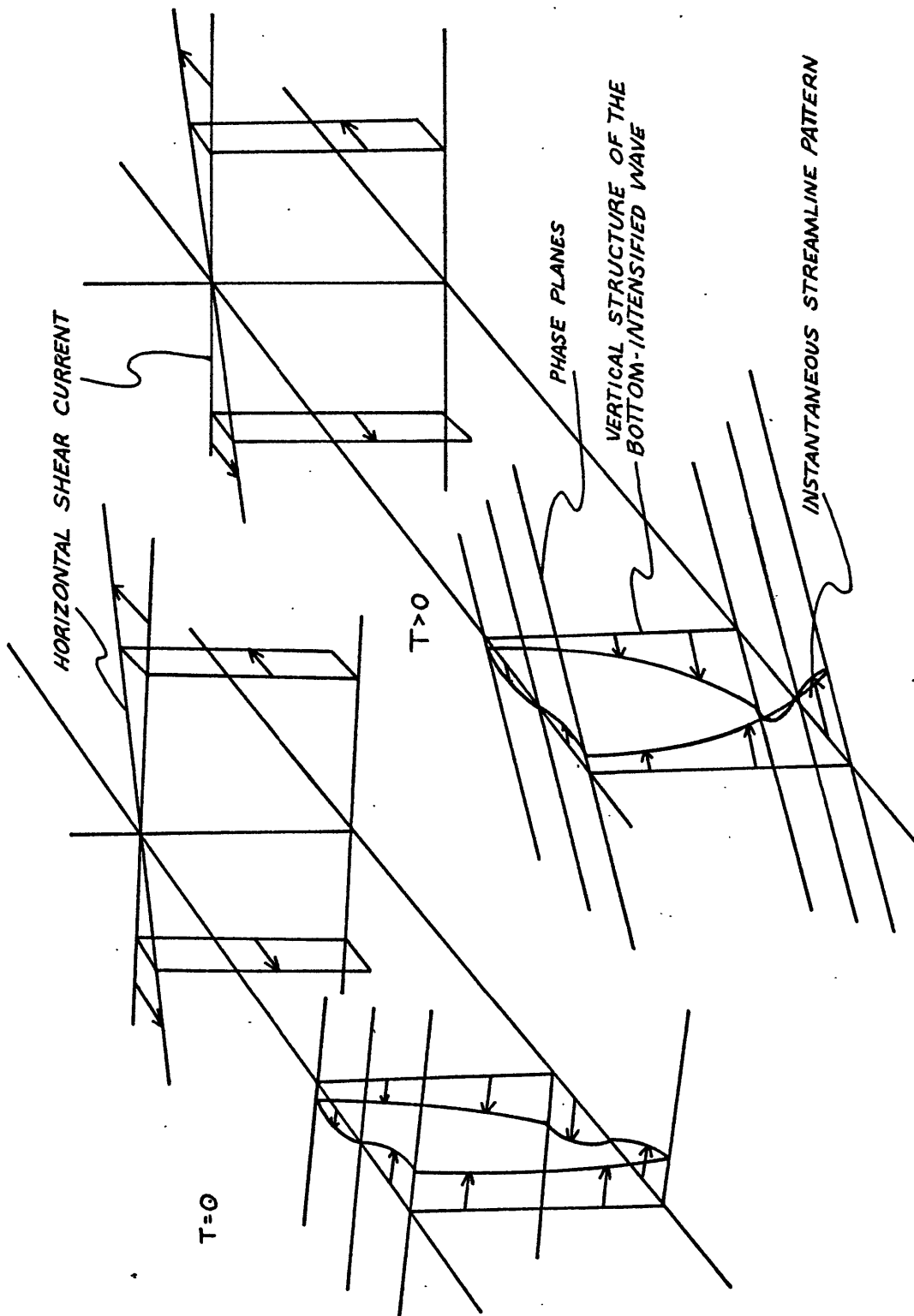
Fig. 4-8. Sketch of the intensification of a topographic wave due to the interaction with a mean shear.
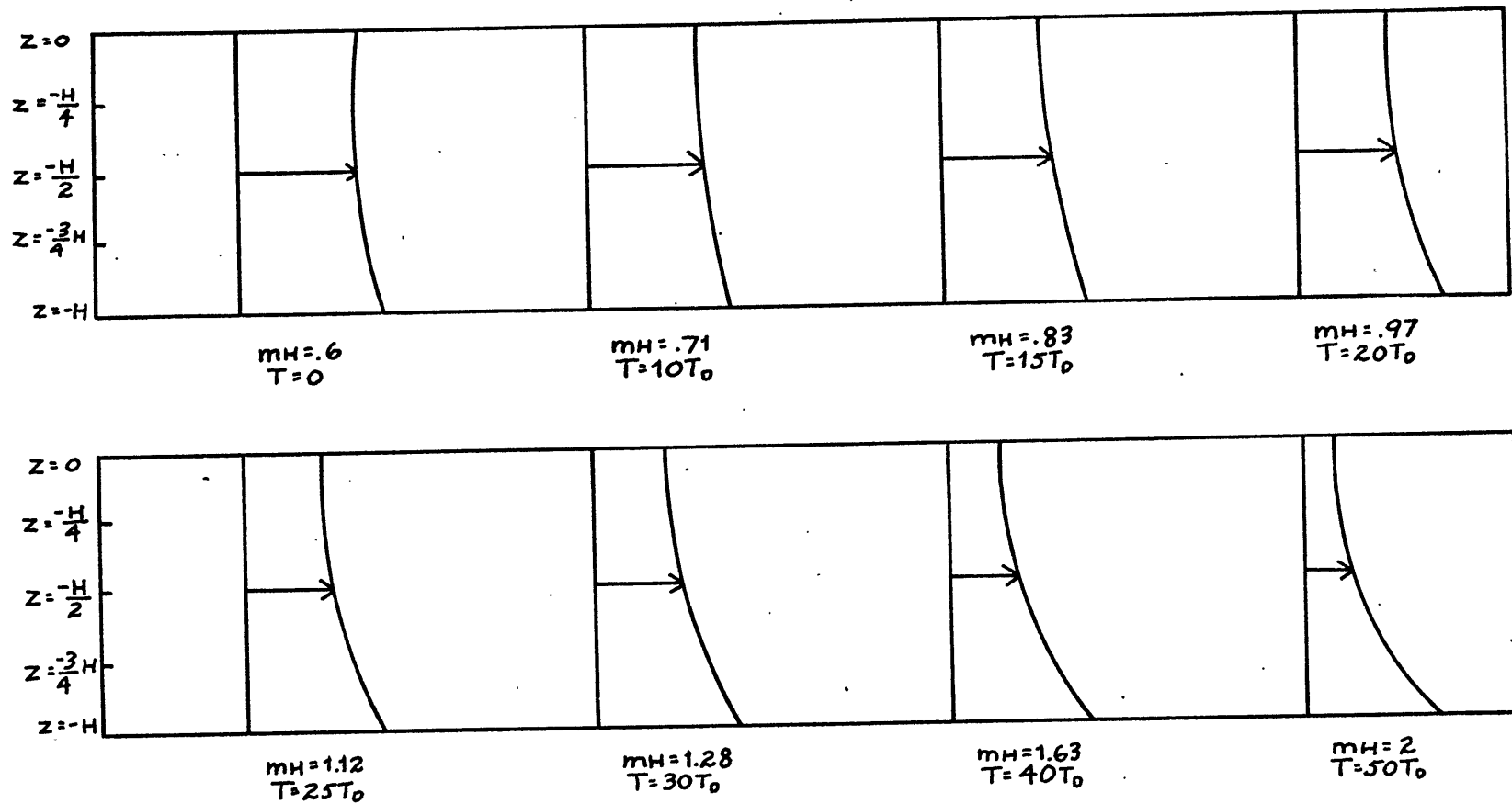
Fig. 4-9. Plot of the vertical structure of the topographic wave at different times during the interaction with the mean shear.

the parameters that determine the vertical structure.

$N/\varsigma \equiv \Gamma = 15$, depth $H = 4Km$ and the along-the-slope wavenumber $|\mathcal{L}| = \frac{1}{100} Km$. For the value of the dimensional shear we have chosen $U_x \simeq 10^{-2} f$, that is, horizontal shear with a strength one one-hundredth of the coriolis parameter. It corresponds to a change in horizontal velocity of $10 cm/sec$ in a distance of one hundred kilometers. The times in the figure are plotted as multiples of the inertial period. We see that the interaction of a topographic wave with a shear has resulted in the production of a bottom-intensified wave.

In order to evaluate the effectiveness of this process in producing bottom-intensified oscillations, we calculate the energy of the waves in the shear current. The total energy of the topographic oscillations is given to order δ^2 by the horizontal kinetic energy and the potential energy associated with the density surface deformation over the basic density field. From the pressure field (eq. IV. C-6) we calculate the horizontal velocities and the density field. The kinetic energy is given by

(IV. C-8) $\quad E_T = \frac{1}{4} |G|^2 (\Gamma \lambda \ell)^2 \ell^2 \dfrac{\cosh^2 \Gamma \lambda |\ell| (1 + \alpha^2 \beta^2 T^2)^{1/2} z}{\sinh^2 \Gamma \lambda |\ell| (1 + \alpha^2 \beta^2 T^2)^{1/2}}$

where G is the arbitrary amplitude of the topographic oscillations. ℓ is the along-the-slope wavenumber. The potential energy is given by

(IV. C-9)

$$\frac{g^2}{2(\Gamma\lambda)^2} = \frac{1}{4} |G|^2 (\Gamma\lambda|\ell|)^2 \ell^2 \frac{\sinh^2 \Gamma\lambda|\ell|(1+\alpha^2\beta^2 T^2)^{1/2} z}{\sinh^2 \Gamma\lambda|\ell|(1+\alpha^2\beta^2 T^2)^{1/2}}$$

Adding the two contributions we find that the total energy is given by

(IV. C-10)

$$E = \frac{1}{4} |G|^2 (\Gamma\lambda|\ell|)^2 \ell^2 \frac{\cosh 2 \Gamma\lambda|\ell|(1+\alpha^2\beta^2 T^2)^{1/2} z}{\sinh^2 \Gamma\lambda|\ell|(1+\alpha^2\beta^2 T^2)^{1/2}}$$

Integrating the above equation along the vertical, one finds that the total energy is given by

(IV. C-11)

$$\int_{-1}^{0} E\,dz = \frac{1}{4} |G|^2 \ell^2 \frac{\Gamma\lambda|\ell|}{(1+\alpha^2\beta^2 T^2)^{1/2} \tanh \Gamma\lambda|\ell|(1+\alpha^2\beta^2 T^2)^{1/2}}$$

By inspection we realize that the terms dependent on time are directly proportional to the frequency of the topographic oscillations measured relative to a frame moving with the mean current (eq. IV. C-7). This implies that as the shear turns the phase planes of the topographic

oscillations, the total energy decreases in direct proportion to the frequency. The energy lost by the wave must be compensated for by an equivalent gain by the mean current. However, our analysis cannot describe this process. In Fig. 4-10 we show a plot of the total energy of the topographic oscillations versus time. For this computation we have chosen the same value for the parameters that was used in the calculation of the vertical structure of the oscillations in Fig. 4-9 . The energy has been normalized by the value of the energy at $T = 0$.
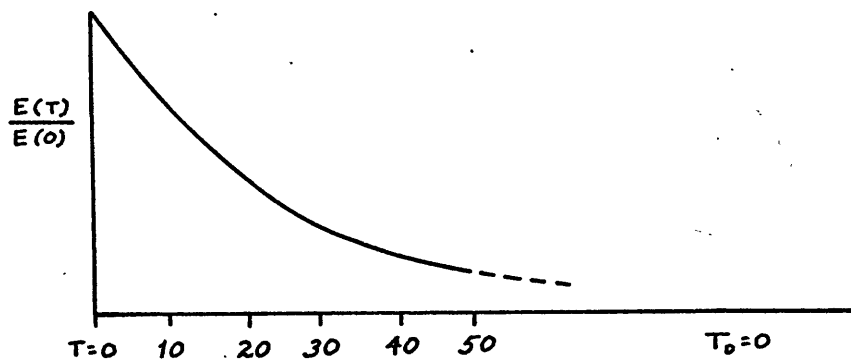
Fig. 4-10. Plot of the total energy decay of the topographic oscillations during the interaction with the mean shear.

In general terms, Fig. 4-10 shows that the wave
energy decreases as the topographic oscillation is turned
by the shear. From the plot in the above figure and from
eq. IV. C-11, we see that there are actually two regimes
of energy decay. For the barotropic limit $\Gamma \lambda |\ell| (1 + \alpha^2 \beta^2 \tau^2)^{1/2}$
the energy of the topographic oscillations decays much
faster, like $(1 + \alpha^2 \beta^2 \tau^2)^{-1}$, while for the bottom-
intensified limit the energy decays like $(1 + \alpha^2 \beta^2 \tau^2)^{1/2}$.
(A homogeneous model of the interaction of topographic
oscillations with a shear misses the second limit.)
These two regimes are related to the different restor-
ing forces on the waves. One can think that the reason
wave energy is lost to the mean current is that the
effect of the shear is to turn the wave in the direction
where the restoring force on the wave is least effective
(the constant-depth contours). In the barotropic limit
the vortex stretching effect requires that the frequency
of the waves diminishes as the scale of wave and as the
projection of the wavenumber along the maximum depth
change decreases. So, as the scale of the wave decreases
due to the turning of the phase planes by the shear, the
current can more effectively extract the energy from the
waves. However, in the more complete three-dimensional
problem when the horizontal scale of the wave becomes

smaller than $N/_\zeta H_{DEPTH}$, where H is the mean depth, the restoring force on the waves is fundamentally different. It is now given only by the projection of the wavenumber in the direction of the component of stratification up the slope. The effectiveness of the restoring force lasts much longer.

In order to further investigate the interaction of the oscillations with the mean flow, we calculate the Reynold stress that the wave exerts on the mean flow. We find that it is given by

(IV. C-12)

$$R = -\overline{u\,v} = -\frac{1}{4}\frac{|G|^2 (\Gamma\lambda\ell)^2 \ell^2 \alpha\beta T \cosh^2 \Gamma\lambda|\ell|(1+\alpha^2\beta^2 T^2)^{1/2} z}{(1+\alpha^2\beta^2 T^2)\tanh^2\Gamma\lambda|\ell|(1+\alpha^2\beta^2 T^2)^{1/2}\cosh^2\Gamma\lambda|\ell|(1+\alpha^2\beta^2 T^2)^{1/2}}$$

For the initial conditions imposed on the waves at time $T=0$, we see that the Reynold stress is negative and decreasing with time. This is interpreted to mean that the wave energy is feeding the mean flow. This conclusion agrees with our previous result that the wave energy decreases with time due to the interaction. Another interesting property is the following. If we plot the total energy of the oscillations as a function of depth at different times during the interaction

(eq. IV. C-10), we find that after the topographic

oscillation crosses over from the depth-independent

regime to the bottom-intensified regime, the energy

of the wave remains constant at the bottom while it

continues to decrease in the interior of the fluid.

This fact coupled with the effect of the Reynold stress

of the wave on the mean flow (eq. IV. C-12) would seem

to indicate that dynamically the oscillation is bottom-

intensifying because the mean current is extracting

wave energy from the interior of the fluid. This in

turn implies that the "steady" current is being built

up baroclinically. A more complete analysis would

show the mean current increasing in strength with

the larger velocities at the top. It is interesting

to speculate whether the steady baroclinic current

observed at Site D might not be sustained by a more

complicated version of this process, particularly in

view that recent analysis of the data seems to show no

permanent tilt of the density surfaces (Schmitz, 15).

Finally we would like to point out that our

solutions for the interaction of the topographic

oscillations with a mean shear can be interpreted from

the point of view of ray theory. The time T appearing

in our equations now refers to the time interval between

the initial position of the wave packet and its present
position, determined by integrating the group velocity
equations with respect to time. The absolute frequency
of the waves (the frequency measured with respect to a
fixed point in the topography) is constant. The relative
frequency of the waves varies just enough in the shear
to compensate for the variation in the apparent frequency
due to the waves being translated by the current. The
statement that wave energy is proportional to the
frequency of the oscillations can now be interpreted as
the conservation of the energy of the wave packet
over the relative frequency in agreement with the
results found by Bretherton (1).

Summarizing, we have seen that the local interaction
of a mean shear with topographic waves can lead to
the bottom-intensification of the oscillations. This
interaction leads to the transfer of the wave energy
to the mean current and as such is not an effective
generator of bottom-intensified waves. The suggestion
that the wave energy goes into the mean flow baroclinically
is interesting in itself and should be studied further.

Chapter V Conclusion

In this thesis we have investigated the propagation and generation of topographic oscillations in simplified models of ocean topography. We have concentrated on those topographic oscillations which show the effects of stratification. The basic element in this study has been the bottom-intensified quasigeostrophic topographic wave. In our investigation we have discovered that the presence of bottom-intensified oscillations invariably implied the presence of other quasigeostrophic motions which have a velocity node on the topography. Perhaps this is representative of the role of bottom-intensified oscillations in the scheme of low-frequency motions in the ocean. Their role is simply to adjust low-frequency disturbances to the constraints imposed by the oceanic topography on the resulting flows.

In Chapter II we reviewed the topographic characteristics of the western North Atlantic and found that except for the continental rise, the topographic slopes were on the average consistent with the quasigeostrophic approximation for topographic waves. After deriving the basic equations for this study, we applied our model in a simple calculation based on the Aries measurements. We found that for the observed vertical structure and

orientation of the velocity field with respect to the
sloping bottom, the theory predicted frequencies and
wavelengths which were in rough agreement with the deduced
values from the data. In section B, Chapter II, we calcu-
lated the quasigeostrophic normal modes of oscillation
over a small-amplitude one-dimensional corrugated bottom.
This was done to model the interaction of large-scale
forced motions in the ocean with small-scale topography.
We found the modes consisted of a long-scale wave and a
smaller-amplitude component with horizontal scales
directly induced by the topographic scale. We found that
if the topographic scale was baroclinic $L_T \leq N/_S H_{DEPTH}$, the
structure of the small-scale term was bottom-intensified.
Since the small-scale topography in the ocean is clearly
not one-dimensional, the value of this calculation was
to illustrate the possibility of energy transfer from
the long-scale directly forced waves to small-scale
topography.

In Chapter III we studied the problem of the excitation
of quasigeostrophic oscillations on a sloping shelf by a
field of Rossby waves impinging at the edge of the shelf.
We found that for the high quasigeostrophic frequencies,
Rossby waves could only excite depth-independent topographic
oscillations. This result agrees with calculations made

by Rhines (13) for a homogeneous model of the ocean.
Physically this result depends on the fact that the
topographic oscillations induced by high frequency Rossby
waves have such long horizontal scales that they are not
affected by stratification. For low quasigeostrophic
frequencies, Rossby waves matched with topographic waves
showing the effects of stratification. The topographic
modes consisted of a bottom-intensified wave and a
collection of topographic baroclinic waves which had a
node on the topography. For the frequency range that
we considered, these baroclinic waves were trapped to
the edge of the shelf decreasing exponentially into the
interior of the shelf. They were excited to adjust
the vertical structure of the Rossby wave to the vertical
structure of the bottom-intensified mode which was the
only propagating solution in the slope region.

The most important result found was that the
amplitude of the bottom-intensified mode was very small
when the scales of the impinging Rossby wave matched the
bottom-intensified mode. Most of the energy was reflected
back. However, the amplitude of the baroclinic modes
trapped to the edge of the shelf was large. The physical
picture that one extracts from this process is that the
edge of the shelf acts like an elastic membrane yielding

under the effect of the impinging Rossby wave but
springing back with little energy lost. It is interesting
to speculate if the very low frequency contributions to
the horizontal kinetic spectrum calculated by Thompson
(19) from the Site D data might not be due to a process
such as this. We recall that the very low frequency energy
of the spectrum decreased with depth -- exactly the
property that the baroclinic wave trapped to the edge of
the shelf would have.

In the last part of Chapter III we discussed the
question of topographic trapping of bottom-intensified
waves. We found that the adjustment of the vertical
structure of the bottom-intensified wave at the edge
of the shelf excited other low-frequency baroclinic
waves. These baroclinic waves were trapped to the
edge of the shelf decaying horizontally in both direc-
tions. We found that their presence was responsible for
enhancing the efficiency of wave trapping by the topog-
raphy. The implication of these results is that bottom-
intensified oscillations do not couple well with near-by
regions which could support similar modes. In this
chapter we concluded that bottom-intensified oscillations
are not effectively generated by sources located exterior
to their topographic environment, and that once excited

over local topography, their energy tends to remain
confined within the topographic region of their generation.
From this it would seem that the presence of the bottom-
intensified oscillations at a given location must be
ascribed to local sources.

In Chapter IV we discussed some aspects of the local
generation of bottom-intensified oscillations. In section
A we studied the generation of topographic oscillations
by an initially imposed geostrophic current. We found
that when the scales of the initial disturbance were
smaller than $L \leq NH/f$ where H is the mean depth
of the region, the topographic response consisted of
a bottom-intensified oscillation and a steady current
with a node on the sloping bottom. When the imposed
scale of the initial disturbance was larger than NH/f ,
the whole column of fluid was set in oscillation. In
general terms, what happens is this: When the imposed
scales are smaller than NH/f , stratification becomes
important and its effect is to weaken the vertical
rigidity of the column of fluid. Since the only part
of the initial motion that needs adjusting is the part
that comes in contact with the slope, the resulting
motion decouples in the vertical. The steady geostrophic
flow which results from the adjustment can be quite

arbitrary. It does not have to flow along the depth
contours as in the homogeneous limit to remain steady.
The bottom-intensified oscillation resulting from the
adjustment of the initial disturbance to the topography
eventually decays due to frictional effects, while the
steady flow persists for a much longer time. This
vertical partition of the motion for initial-value-like
disturbances has interesting implications. It says that
over a sloping bottom one would expect to find very
low-frequency horizontal kinetic energy in the baroclinic
scales leading to the bottom-intensification of the
topographic oscillations. This energy will decrease
with depth as we approach the bottom slope. However,
the interior flow over the topographic slope will not
remain steady if we include the planetary β-effect.
Furthermore, the neglected nonlinearities should also
affect the steady flow because the topographic restoring
force is not restraining its influence. The structure
of the steady flow will slowly evolve with time due to
nonlinear advection.

We can speculate that part of the energy found at
the low frequencies in the horizontal kinetic energy
spectrum calculated by Thompson (19) might be due
to drifting eddies originating in the adjustment of

disturbances with baroclinic scales $L \leq \frac{NH}{f}_D$ to the
sloping bottom around Site D. These disturbances will
also generate bottom-intensified oscillations, but they
decay due to frictional effects. It is interesting to
point out that this general decrease of energy with
depth was obtained by considering the interaction of
Rossby waves with a sloping shelf.

In section B of Chapter IV we discussed the wind
generation of topographic oscillations. We found that
bottom-intensified oscillations were not effectively
generated by the wind because surface stresses with
horizontal scales leading to bottom-intensified response
do not penetrate to the bottom slope. However, long-
scaled wind forces at the surface can generate a forced
barotropic current which in turn can interact with
small-scale topography to produce bottom-intensified
oscillations (see Chapter II, section B).

In section C of Chapter IV we discussed the interaction
of a steady shear current with topographic oscillations.
We found that the turning of the wave crests of the
oscillations by the shear resulted in the production of
bottom-intensified oscillations. However, the interaction
of the wave with the shear also resulted in the transfer
of wave energy to the mean current. The vertically

integrated total energy of the oscillations decreased
in direct proportion to the frequency of oscillation.
This result is similar to the one found by Phillips (6)
in his study of the interaction of internal waves with a
mean shear. Another interesting result was implied by
actually looking at the vertical dependence of the total
energy. This showed that the farther away we looked from
the bottom boundary, the more rapidly the wave energy
was lost. This observation, coupled with the fact that
energy lost by the wave must be compensated for by an
equivalent gain by the mean current, would seem to indicate
that the steady current was being built up baroclinically.
(The larger increases in the velocity were occurring away
from the bottom boundary.) Again we see another example
of the peculiar property mentioned at the beginning of
the conclusion. Bottom-intensified oscillations seem
to be always associated with baroclinic motions having
larger velocities at the top. Another interesting point
about our solution for the interaction of topographic
waves with a shear current is the following. It is
related to wave character of our solutions. We recall
that our solution is wave-like even though the Rossby
number describing the interaction with the mean shear
was of the same order as the topographic parameter

(our basic restoring force for the waves). This is
unlike Phillips's solution which only showed wave character
in the limit of a weak shear compared to the basic re-
storing force of the internal waves, N^2 . Our results
bring to mind the remarkable results found by Rhines (12)
in his study of geostrophic turbulence in a β -plane.
He found that when the Rossby number describing the large-
scale motion was of order the topographic effect, the
flow patterns looked extraordinarily wave-like. His
calculations were two-dimensional while our results
are three-dimensional. Perhaps a more careful and com-
plete analysis of the simple interaction of a mean shear
with topographic oscillations can provide more physical
insight and shed some light onto the more complicated
problem of three-dimensional geostrophic turbulence
in a β -plane.

As a final remark we would like to suggest that an
experiment to generate bottom-intensified oscillations in
the laboratory should be carried out. It should be done
as an initial value problem. This should clarify some
of the ideas about the vertical decoupling of the motion
by topographic slopes. It should be done for the case
in which the Rossby number is of the same order as the
oscillations' frequency. Perhaps the results will show

that the motion close to the topography is a bottom-trapped oscillation while the interior motion is composed of drifting eddies originating from the initial decoupling of the motion by the topography. We would like to add that a paraboloidal bottom configuration is the simplest one to use. The normal modes over this configuration were found by Rhines (8). A sliced cylinder configuration will not lead to a simple model structure for the bottom-intensified waves. Unlike depth-independent topographic waves, bottom-intensified waves do not reflect simply at boundaries crossing constant-slope lines. The reason for this can be easily seen by looking at the dispersion curve in Fig. 2-4 , Chapter II. To conclude, the investigations carried out in this thesis seem to point to the result that the most important role of bottom-intensified motions is to release the interior of the ocean from the constraints imposed by topography.

Bibliography

1. Bretherton, F. P. (1966) The propagation of groups of internal gravity waves in a shear flow. Quart. J. R. Met. Soc., Vol. 92, No. 394, pp. 466-480.

2. Crease, J. (1962) Velocity measurements in the deep water of the western North Atlantic. J. Geophys. Res., Vol. 67, No. 8, pp. 3173-3176.

3. Holton, J. R. (1965) The influence of viscous boundary layers on transient motions in a stratified rotating fluid: Part II. J. Atmos. Sci., Vol. 22, No. 5, . pp. 535-540.

4. IGY Charts (1968) Oceanographic data from Crawford cruise 16, 1 Oct.-11 Dec., 1957 for the International Geophysical Year of 1957-58. Ref. No. 58-31, WHOI, 127 pages.

5. Morse, P. and H. Feshbach (1953) The Methods of Theoretical Physics, Vol. 1, McGraw Hill, New York, 997 pages.

6. Phillips, O. M. (1966) The Dynamics of the Upper Ocean, Cambridge University Press, 261 pages.

7. Rhines, P. B. (1971) A comment on the Aries observations. Submitted for publication to Proc. of Roy. Soc.

8. _____ (1970) Edge-, bottom-, and Rossby waves in a rotation stratified fluid. Geophys. Fluid Dyn., Vol. 1, pp. 273-302.

9. _____ (1971) Film stills on topographic oscillations. Submitted for publication to Rev. of Geophys. and Space Physics.

10. _____ (1970) A note on long period motions at Site D. Deep-Sea Research, Vol. 17.

11. _____ (1967) Ph.D. thesis, Cambridge University.

12. _____ (1971) Private communication

Bibliography (cont.)

13. _____ (1969) Slow oscillations in an ocean of varying depth, Pts. I, II. J. Fluid Mech., Vol. 37.

14. Schmitz, W. (1971) Private communication.

15. _____ (1971) Private communication.

16. Stommel, H. (1960) The Gulf Stream, University of California Press, Berkeley, 202 pages.

17. Swallow, J. C. (1971) The Aries current measurements in the western North Atlantic. Submitted for publication to Proc. of Roy. Soc.

18. Swallow, J. C., and L. V. Worthington (1969) Deep currents in the Labrador Sea. Deep-Sea Res., Vol. 16, pp. 77-84.

19. Thompson, R. (1971) Topographic Rossby waves at a site north of Gulf Stream. Deep-Sea Res., Vol. 18, pp. 1-19.

20. Walin, G. (1969) Some aspects of time-dependent motion of a stratified rotating fluid. J. Fluid Mech., Vol. 36, pp. 289-307.

Biographical Note

Alfredo Andres Suarez was born October 17, 1943 in Havana, Cuba, and came to this country in April, 1960. He is married to the former Katherine Kahler, and has a daughter, Carolyn Elizabeth, born July 6, 1971. He received his B.S. degree from Boston College in 1965, and his M.S. degree in Physics from the University of Illinois, Urbana, in 1967.